1999

Design and model verification of flat-sided polymer composite propane gas pressure vessels.

Justin James Gammage
University of Windsor

DESIGN AND MODEL VERIFICATION OF FLAT SIDED POLYMER COMPOSITE PROPANE GAS PRESSURE VESSELS

by

Justin James Gammage

A Thesis
Submitted to the College of Graduate Studies and Research
through the Department of Mechanical and Materials Engineering
in Partial Fulfillment of the Requirements for
the Degree of Master of Applied Science at the
University of Windsor

Windsor, Ontario, Canada

1999

Your file Votre référence
ISBN: 0-494-00122-4
Our file Notre référence
ISBN: 0-494-00122-4

888065

Committee Approval Page

Dedicated To:

Mom, Dad, Emilee

And

Angie B.

ACKNOWLEDGEMENTS

I would like to take this opportunity to thank my supervisor, Dr. Daniel Watt, for both his support and guidance throughout the research conducted in this thesis. His encouragement and wealth of knowledge contributed significantly to the progression of the research. Additionally, his example and dedication to research motivated my decision to further my academic studies to the Ph.D. level. For this I am truly grateful.

I would also like to thank Chrysler Canada and NSERC for their financial support to the project. Specifically I would like to acknowledge the contributions of Shawn Yates and Jim Lanigan from Chrysler Canada's Automotive Research Development Center. Shawn Yates' willingness "to go the extra mile" to support the establishment of a strong research partnership with the University of Windsor is recognized and greatly appreciated.

Doug Bain first conceptualized the entire research project through which the compilation of this thesis was possible. In addition, his tremendous knowledge and ambition, toward furthering development of the project, kept the project running full speed ahead. Of course, Doug's friendship and the many days we spent working (or just discussing the project at the Grad House) will be remembered as the best days in my life. I would like to thank Doug for these great times and most importantly for his lasting friendship.

Jacqueline and Lindsay Wright's contributions also deserve acknowledgment. Their assistance and knowledge allowed the completion of this thesis in a timely matter. Whether it involved their patience in tank construction or their reassuring encouragement, their friendship and contribution is greatly appreciated.

I could not conclude this acknowledgment page without thanking those closest to me. My parents, my sister Emilee and Mike deserve a sincere "thank-you" for their input, patience, love and understanding. Finally, the person that provided the drive to push toward the completion of this thesis, and motivated me through her love and caring, deserves a special thank-you. Thanks and love go out to Angie, for her love and friendship through the past, present and future.

ABSTRACT

Clean air legislation has fueled the development of alternatively fueled automobiles. As a result, automotive companies have looked for ways to increase the performance of these vehicles while attempting to bring down the price of this technology. In many cases, the fuel storage method plays a significant role in the achievement of these goals.

The development of a flat sided pressure vessel would allow for better use of the available fuel storage space on the automobile. Construction of the pressurized fuel tank out of lightweight and economical materials will further increase the performance levels and bring down the cost of the fuel system.

This thesis investigates the potential for the development of a flat sided, polymer composite pressure vessel. As part of the design approach, finite element analysis models, incorporating internal ribs for reinforcement against the bending of the flat walls, were constructed, analyzed and refined. Two final potential designs were constructed from fiberglass and pressure tested to validate the finite element analysis models.

Analysis of pressure testing data and sectioning of a prototype tank, revealed potential problems with the construction approach utilized. In comparing the experimental data with the predicted finite element analysis values, conclusive correlation could not be drawn. Indications, however, lead to the belief that direct water contact with the composite walls and manual filament winding of the tanks led to the poor results. Finally, the results and information gained in this research have advanced the possibility of future successful development of a flat sided, polymer composite pressure vessel.

TABLE OF CONTENTS

LIST OF FIGURES

LIST OF TABLES

Chapter 1

INTRODUCTION

1.1 Background

The industrial revolution of the early 20th century, fueled largely by the automobile and metal industry, led to a development of a largely transportation dependent North American society. Prior to the 1970's emissions controls were poor which resulted in significant pollution of the environment. The public's concern for the environment increased with the threat of smog, global warming and ozone depletion.

The automotive industry responded to society's concerns through research into alternatively fueled automobiles. Alternative fuel systems used today include electric power, hybrid fuel/electric power, compressed natural gas (CNG) and liquefied petroleum gas (LPG). Unfortunately, these technologies come at a greater cost to the consumer and usually result in lesser performance as related to gasoline.

Alternative fuel systems in automobiles are classified largely on emission performance. Typical designations today are categorized follows:

- Low Emissions Vehicle
- Ultra Low Emissions Vehicle

- Zero Emissions Vehicle

Arguments exist as to which fuel systems result in the release of the least total amount or life cycle emissions to the environment. For example, a zero emissions, electric powered vehicle may be supplied by power from a coal burning thermal electric generating system. In this case the pollution resulting from the generation of this power may in fact be worse then if the vehicle ran on regular gasoline.

Liquefied Petroleum Gas (LPG, principally propane) powered vehicles offer a reduction in emissions, little reduction of vehicle performance and a straightforward conversion from gasoline to LPG. Additionally, LPG fuel is readily available in many locations across North America. Even with the apparent advantages, several hurdles must be overcome before LPG can become a viable alternative to gasoline power.

Two of the greatest obstacles remaining are the increased cost of the LPG automotive fuel delivery system and the fuel tank, and a reduction in the vehicle driving range. In addition, the added weight of the required fuel system components reduces the performance of the vehicles. The fuel tank is necessarily heavier because it is a pressure vessel, whereas gasoline is stored at ambient pressure. So the source of these disadvantages lies quite heavily on the fuel storage methods currently employed on the vehicles.

The scope of the present research is to address these two primary issues through the development of a more economical, higher storage capacity LPG fuel tank. A less costly fuel tank would produce a more economic LPG fuel system. Additionally, a greater storage capacity for the fuel tank would result in an increase in the vehicle's driving range.

1.2 Concept

The goal of the research is to develop a cost effective, high storage volume pressure vessel. A primary design constraint is the size of the rectangular shaped envelope available on the vehicle for the fuel storage vessel. Designs focused on developing a fuel tank for a Dodge full size van. Dimensions for the storage space in this case measured 36"X23"X14" (914.4 mm X 584.2 mm X 355.6 mm).

Several possible design variations would make use of the available space for fuel storage. Multiple cylinders are currently used in various arrangements to provide fuel storage within the tank envelope. However, areas above and below the intersection areas between the cylinder are effectively wasted space. Figure 1 illustrates how effectively different arrangements utilize the available space.

The aspect ratio is the width to height ratio of the available space. From Figure 1, it is quite evident that a low aspect ratio results in a single or double cylinder arrangement, and a poor utilization of space. As the aspect ratio increases,

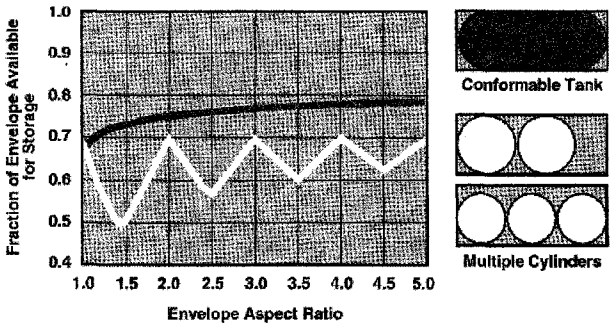

Figure 1. Volumetric efficiency of different tank designs (from Ref [10])

then more numerous cylinders would increase the space use efficiency. However, multiple connections between the cylinders would increase the complexity and cost of the system. A single rectangular, storage envelope conformable design would maximize space use efficiency, increasing the fuel storage capacity of the vehicle.

1.3 Design Considerations

Pressure vessels are typically cylindrically shaped. A thin walled spherical or cylindrical shape produces membrane loading of the walls. The resulting stress is solely tensile in the hoop and axial direction.

A flat walled pressure vessel has the tendency to bow outward under pressure. Although, the axial stress is not large, the bending forces generated by the pressure pushing the walls outward is significant. The resulting bending stresses act to force the walls out towards a cylindrical or spherical shape.

Computer modeling of pressurized flat plates and published equations for flat plates provided the foundation for the design process. The deflection of a flat plate varies with the square of the unsupported span length. Cutting down the unsupported span length, through reinforcement or wall segmentation, would be the key to reducing the deflection and stress in the vessel walls.

To utilize a flat walled pressure vessel, a method of reinforcing the walls from outward bowing had to be devised. Concepts such as utilizing a space frame around the tank and tie rods between flat walls were explored and were set aside. Two final concepts were arrived at and followed through by detailed analysis, and eventually by tank construction.

The first concept was a rectangular tank with internal walls formed by connecting modules. Bain's research [1] focus dealt primarily with developing a modular design. His design would allow for the flexibility of adding or subtracting modules to change the volume as required.

This thesis investigates a single shell tank design. Support against bending is obtained through the use of an internal ribbing system. Various rib configurations, based on preliminary finite element analysis (FEA) rib modeling, were compared for their effectiveness of reinforcement versus factors such as weight and volume losses.

Three final ribbed designs were arrived at through successive iterations of varying rib dimensions and spacing. The final designs utilize ribs running parallel to

each other across the width of the tanks. Two prototypes of the designs were constructed to validate the results of computer FEA with experimental results.

1.4 Material Selection

Two of the original design requirements were weight and cost reduction over the currently used storage vessel. To satisfy both objectives, material processing and properties were examined. A high production volume, economical construction process resulting in a lightweight product would serve as the ideal candidate method for making such a product.

The complexity of the internal cavity design in the single shell pressure vessel imposed significant constraints on the construction of the tank. The use of metals, such as aluminum would be possible through a multi-stage welding process. However, DaimlerChrysler had previously experienced problems with aluminum contaminants entering the fuel from the bi-products of the construction process. Additionally, a welding process would require significant tooling set-up costs if undertaken in production.

Polymer materials, with their inherent design flexibility, immediately appeared as promising candidates for the construction of the LPG tanks. In particular, fiber-reinforced polymer composites, have high specific strengths and can be utilized to produce almost any design shape. Material processing flexibility

through the use of polymers could diminish many limitations that might otherwise be realized with other materials.

The proposed tank utilizes a combination of unidirectionally wound E glass fiberglass ribs and a final bi-directional, fiberglass mat wrap over a thermoplastic, blow molded tank cavity. A blow molded tank liner is proposed to provide a form for over-wrapping and act as a fluid barrier for the fuel. The fiberglass unidirectional ribs and bi-directional mat over-wrap carry the majority of the stress resulting from pressure acting against the walls of the tank.

1.5 Prototype Construction

Prototype tanks were constructed to validate the performance predicted by computer models. Modeling of the tanks was performed in ALGOR, a finite element analysis software package. Prototype models were then constructed based on the design of the computer models.

Two prototype models were constructed but with sculpted polystyrene foam forms substituting for the blow molded tank liners. The foam was utilized to allow for low cost design flexibility and reduced construction times over other prototyping methods. Fiberglass and epoxy were then applied over the foam form, based on a pre-designed, specific lay-up procedure. After a minimum 36 hour cure time, the foam core was dissolved with acetone.

1.6 Prototype Validation

As a final step, both prototype tanks were tested to validate the models. A Sciemetric™ data acquisition system, using Gen200™ data acquisition software, was utilized to measure both the strains and displacements during the test. Results from the comparison of physical testing and computer results were used to assess the validity of the final full-scale tank designs.

Chapter 2

LITERATURE REVIEW

2.1 Introduction

Several design objectives for the development of a conformable liquefied petroleum gas (LPG) were laid out prior to undertaking research on the single cavity design. Most significantly, decisions involving material selection and potential future manufacturing techniques were made. Bain's thesis [1] describes the decision making process on material selection and the relative technologies quite extensively.

The design of a conformable pressure vessel is unique. Utilizing polymer composites to accomplish this task furthers the scientific contribution through innovative designs coupled with advanced material selection. Before the research was undertaken, an extensive review of literature was conducted to gain better understanding of the materials selected and the status of the current state of the art. In addition, the review provided insight into potential development concerns and various options to accommodate the manufacturing of a polymer composite, flat sided pressure vessel.

2.2 Polymers

Polymer selection is based largely on a component's material's performance requirements. As with any material, a polymer's performance is measured based on several parameters. In the case of the thermoplastic tank liner, performance must

allow for both chemical resistance to propane and good interaction with the composite over-wrap.

Many suitable monomers for polymerization exist. The polymer's resulting reactions with the monomers are categorized with respect to the polymerizing mechanism. Two categories of polymerizing reactions are common, addition and condensation. In either case the polymers formed by these reactions may be linear or cross-linked [2].

2.2.1 Thermoplastic Polymers

Within the thermoplastic group of polymers, there are basically two arrangements of polymer chains, amorphous and crystalline. Amorphous polymers, Figure 2a, have randomly orientated molecular chains. The tangled string-like structure of amorphous polymers generally results in high ductility and elongation. Crystalline structures, Figure 2b, contain regular chain arrangements resulting in a stronger and stiffer material.

To better understand the behavior of the two different molecular arrangements under load, the resulting molecular motion must be examined. When an amorphous structure is subject to load, the chains generally untangle and elongate with relative ease. However, some amorphous polymers such as pure polystyrene and poly(methyl methacrylate) (PMMA), form brittle structures due to their side groups. In the case

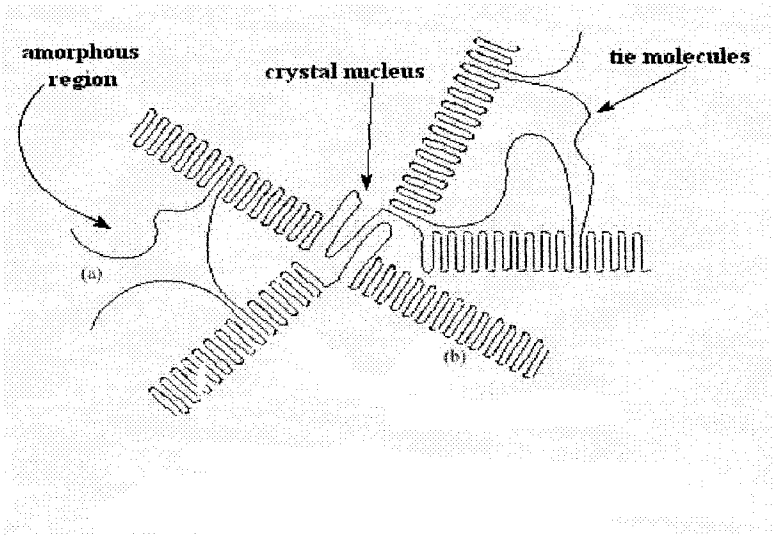

Figure 2. (a & b) Comparison of chain arrangements in thermoplastics

of a crystalline structure, it is much more difficult for the individual chains to move. The highly orientated arrays of molecular chains hold the molecules more closely together, resulting in restricted molecular motion.

In general, the performance of polymers can be related largely to the ease at which molecular chains can move. In addition to molecular arrangement, any factor that makes chain, or molecule, movement more difficult increases the strength of the material. Increasing the number or size of side groups, the molecular weight or adding stiff fillers can all increase the strength and reduce the ductility of a thermoplastic polymer.

2.2.2 Thermoset Polymers

Thermoset polymers behave similar in principle to thermoplastics as far as strengthening mechanisms are concerned. Like thermoplastics, the strength of a thermoset may be changed by factors such as side groups and molecular weight. The significant difference is that a thermoset has a structure that forms cross-linking between the molecular chains as shown in Figure 3.

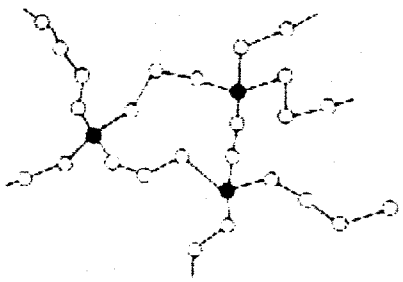

Figure 3. Cross-linked structure

Unlike thermoplastics, that on heating, may be formed into different shapes, a thermoset once cured will remain the same shape. The cross-linked structure prevents the movement of molecular chains, through the tying of all chains together into one lumped mass. When a thermoplastic is reheated, the absence of cross-linking allows the chain spacing to increase. This in turn makes molecular movement much easier, resulting in an easily reformed material.

Thermoset plastics often have higher moduli than amorphous thermoplastics. This may be attributed to the cross-linking. As load is applied to a thermoset

structure, the load is carried with little or no movement between polymer chains. This is a result of the cross-linking holding the chains rigidly together. As mentioned previously, an entire mass of polymer chains act together to carry the load.

The increase in moduli results in a loss of ductility or toughness in the material. As a result of the chains remaining tied together, movement between molecules will be constrained until the cross-links are broken. Once the load applied to the structure generates molecular shearing forces exceeding the strength of the cross-links, cross-links throughout the structure break. As a result, failures in thermosets occur immediately after yielding or result from fracture when impact or cyclic loads are applied. In either case, little or no warning is provided before catastrophic failure occurs.

In many cases, themosets such as epoxy or polyester resins are toughened with the use of inorganic fillers such as fiberglass or glass spheres [3]. Rigid particles or fibers, such as glass spheres or fiberglass, toughen the thermoset polymers through crack tip pinning and crack surface bridging mechanisms [3]. Pinning of the crack tip causes the crack wave to bow outward between the two rigid fillers, absorbing energy through line tension effects that form between the particles. Rigid particles also bridge the gap between the cracked surfaces, providing tension that acts to pull the crack closed as the crack front pushes through. These toughening principles, in addition to strengthening mechanisms effected through the use of inorganic fillers, are the fundamental principles on which composites have been developed.

2.3 Fiber Reinforced Composites

Composite materials are those made up of two or more components, consisting of two or more phases that do not change character when combined. This is distinct from alloys that mix when combined. In composites, particles or fibers are added as fillers, or reinforcement to polymers in order to change or enhance the performance behaviour of the polymer material. Composite materials in general are attracting increasingly more attention in industry as a result of the potential for creating more cost effective, higher stiffness and more complex shaped components.

Factors affecting the strength of the composite include the volume fraction of filler, the orientation of the filler in the matrix, and the size and the shape of the reinforcing fibers. In the vast majority of polymer applications, the composite is composed of a polymer matrix containing either reinforcing particles, or discontinuous or continuously wound fibers of fiberglass or carbon fiber. The strength of the matrix is significantly lower than that of the fiber; in the case of carbon fiber surrounded by a polymer matrix, the Young's modulus ratio of fiber:resin can be in the ranges of 50:1 to 100:1 [4].

For continuously wound fibers, the fibers can be considered to be so long that the effects of their ends can be ignored. When loads are applied to the block illustrated in Figure 4, it may be assumed that the entire block extends uniformly and as if the load created uniform stresses and strains within each individual component.

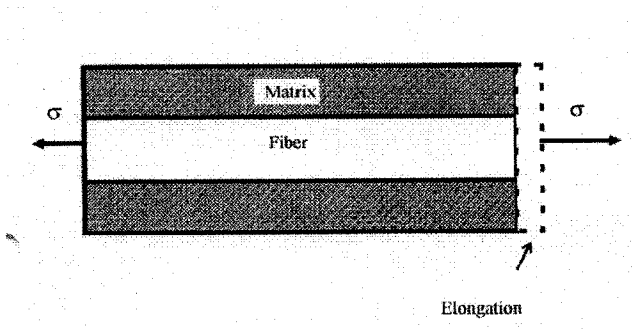

Figure 4. Strain behavior a continuos fiber reinforced composite

The stresses act parallel to the fiber direction, and the entire composite elongates equally in the direction of the applied stress. The axial strains are therefore $\varepsilon_f=\varepsilon_m=\varepsilon_c$, where the subscripts f, m and c denote fiber, matrix and composite respectively. From the assumptions of constant strain, and force equilibrium, the total applied stress carried by the composite times the total cross-sectional area of the composite, must be the sum of the stress in the fibers times the area of the fibers plus the stress in the matrix multiplied by cross-sectional area (Eq'n 2.1).

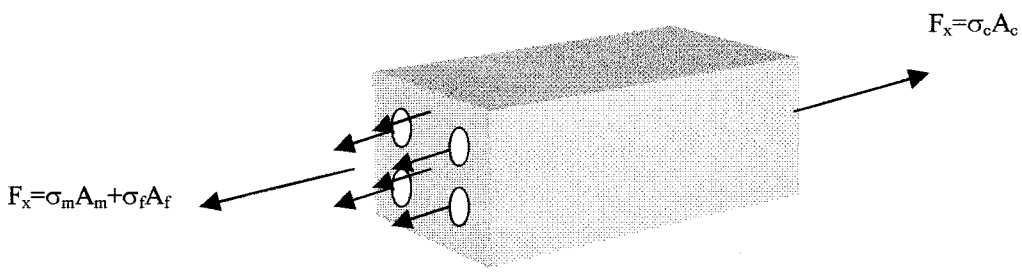

Figure 5. Tensile loading of continuous fiber reinforced composite

$$\Sigma F_x = \sigma_c A_c = \sigma_m A_m + \sigma_f A_f \qquad (2.1)$$

Dividing through by the area of the composite, gives the applied stress in terms of area ratios. Because the ratios of areas may be represented by the volume ratios, the relationship becomes:

$$v_m=A_m/A_c \ , \ v_f=A_f/A_c \qquad (2.2)$$

$$v_m=1-v_f \qquad (2.3)$$

$$\sigma_c=v_f\sigma_f+(1-v_f)\sigma_m \qquad (2.4)$$

Because the component strains are equal to the composite strain, then dividing through by the composite strain gives the effective modulus of the composite as in reference [2].

$$E_c= v_fE_f+(1-v_f)E_m$$

These equations indicate the relative ease with which the stresses throughout a continuously wound composite can be determined.

2.3.1 Critical Fiber Length

Discontinuities in a continuous reinforced composite are a concern. In locations where reinforcement continuity is broken, such as in seams or cuts, the stress transfer becomes a critical issue. However, a properly designed overlapping seam may maintain moduli of elasticity and strengths that approach 90% and 50% respectively, of their continuously wound counterparts [5]. The resulting mechanical characteristics depend on the effectiveness of load application to the fiber by transmission through the matrix.

According to shear lag theory [5], to determine the efficiency of stress transfer in a discontinuous composite, a critical fiber length, or overlapping length, is necessary for effective strengthening and stiffening of the composite material. In determining the critical fiber length, *lc*, three parameters in particular must be considered. These are the fiber diameter, the tensile strength of the fiber and the matrix fiber bond shear strength, τ_c. It is common practice to assume that the strength of the fiber/matrix interface is dependent on the shear strength of the matrix material, $\tau_m=\tau_c$.

Critical fiber length should be considered when developing joints, or overlapping seams in a multi-layer composite. The overlap length should be sufficient to allow for stress transfer through the matrix to reach that of the fiber strength in both layers. Effectively, once the fiber overlap exceeds the critical fiber length the effect of the seam is significantly reduced. This is best illustrated by comparing the stress distributions in various fiber lengths in Figure 6.

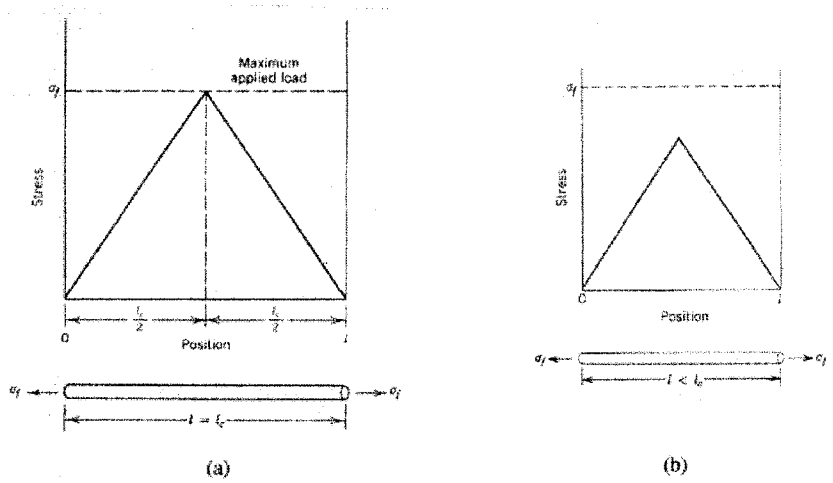

(a) (b)

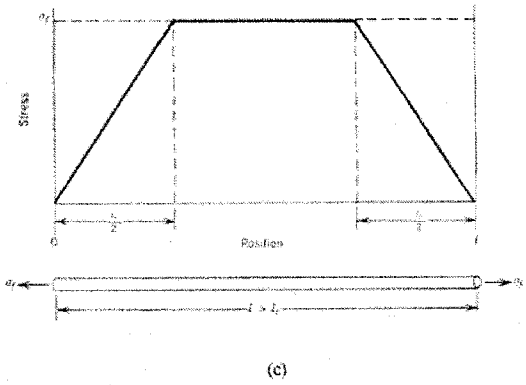

Figure 6. Stress distributions in fibers for different fiber lengths
(a) fiber length equal to critical length, (b) fiber length less than critical length, and (c) fiber length greater then the critical length. Fiber reinforced composite subjected to stress equal to that of the fiber strength.

The concept of Stress Transfer Length [6] is illustrated in Figure 6 (c). This length is the length over which the strain in the fiber builds up to the plateau or matrix value. If the system remains perfectly plastic, and the fiber does not slip at the interface the value is dependent only on the elastic constants of the fiber and the matrix. However, in Figure 6 (b), the length is less than that of the critical fiber length so the stress does not build up to the plateau value. If the fiber or overlap length is not at least that of the critical value, the fiber reinforcement is not being fully utilized to it's potential. The design of patterns for reinforcement should be conducted with this consideration in mind.

Three dimensional finite element models of fibers in a solid matrix do not show these types of stress gradients in stress along the fibers [7].

2.3.2 Polymeric Matrix

A polymeric matrix serves two purposes in a polymer composite. The first is to provide a mechanism of transferring the stress between adjacent fibers. A second role is that the polymer matrix serves as a protective barrier against chemical and mechanical attack on the fibers. Two main thermoset polymers, in addition to other thermoplastics and thermosets, are commonly used in the manufacture of polymer composites. Epoxy, polyesters or vinyl esters are used in many applications.

Epoxies are primarily used in high performance applications like aerospace or aircraft applications. Base materials for epoxy materials are low-molecular weight organic materials containing epoxide side groups [8]. Liquid resins containing the epoxide groups are then reacted with a curing agent to initiate the cross-linking polymeric reaction. Curing results in a solid polymeric material.

Principal advantages of epoxies over other thermosetting materials include low shrinkage during cure and excellent adhesion to a vast variety of fillers and fibers. Epoxies additionally possess a high chemical resistance to corrosive chemicals and solvents, which is useful in aerospace and automotive environments. The main disadvantage of epoxy is its relative high cost, high heat of reaction, and lengthy cure time over other conventional polymers.

There are 5 families of polyesters which can be used as the resin in fiberglass. They are prepared by the condensation polymerization of a dibasic acid (-C$\overset{O}{\underset{OH}{}}$) or

anhydride with a dihydric alcohol (-C - OH) to produce an unsaturated molecule with the ester group (- C – C – O - C-). Within any of these 5 families, the properties of the cured polymer can be changed from stiff to flexible by varying the type of alcohol used or by varying the fumaric/saturated acid ration. (REF 15)

To initiate the polymerization process in polyester, a catalyzing curing agent such as organic peroxide or aliphatic azo, is added to the liquid mixture. Polyester, polymerized to a cross-linked structure with styrene, transforms into a solid resin. The main advantage to polyester is its low cost relative to other polymeric matrices. Polyester properties, such as chemical resistance and strength, are lower than those of epoxy resins. Additionally, polyesters shrink considerably during the curing process. This effect is deleterious to both the performance and appearance of the composite parts.

In addition to thermosetting matrices, thermoplastic materials are reinforced with discontinuous fibers in many applications. Injection molding and blow molding processes have effectively utilized thermoplastics as the composite matrix in many applications. Due to the flow requirements of the thermoplastics in these cases, the fiber volume fraction is limited to approximately 30%. However, if the part is designed around these constraints, effective reinforcement is often achieved in these polymer composites.

2.4 Fiberglass Reinforced Composites

Fiberglass components have been used in performance applications for several decades. The marine industry was first introduced to fiberglass components in the mid 1960's for small production watercraft. Since the introduction to the marine industry, boats over 30.4 m (100') in length now have superstructures made entirely of fiberglass.

Use of fiberglass in the marine industry is only one of the examples of fiberglass use in manufacturing. Currently, the manufacture of pressure vessels with fiberglass filament winding over metal cores remains one of the most widely accepted methods of construction for these high performance components.

Fiberglass reinforcements in a polymeric matrix take many forms. Chopped fibers are used economically in many applications that require high production rates with relatively good performance. Higher performance components typically use woven or stitched mat and the highest performance components utilize continuous filament wound fiberglass.

Two different fiberglass materials are common in industry. The most commonly used in industry is E-glass, with prices typically about the same per kilogram as common plastics [2]. In addition, both S-glass, with higher specific strengths, and C-glass, a more chemical resistant fiberglass, are commercially available to meet higher performance requirements.

Fiberglass composite strength, as in the case of most fiber-reinforced composites, is orthotropic. The result of this is that a component's strength is highly dependent on fiber orientation. A composite designed with fibers running parallel to the load, utilizes the specific strength of the material to its full potential. The specific strength is a measure of the ultimate strength over the density of the material. This ratio is highest when the strength is measured in the direction of the fibers. As the angle of the fiber reinforcement direction varies with the load, the strength of the composite drops off drastically to its minimum at the orthogonal. This results from high fiber strength in the axial direction of the fibers. Any deviation from the axis of the fiber length results in significant reductions in strength. The modulus of the fibers approaches that of the matrix in the off axis direction, resulting in the load being carried primarily by the matrix. Figure 7 illustrates this effect graphically for an aligned carbon fiber reinforcement example.

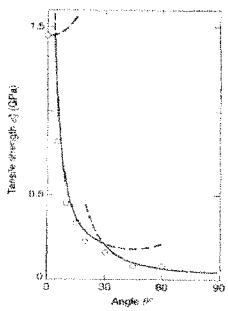

Figure 7. Angular dependence of tensile strength in an aligned composite (from Ref [6])

An additional factor that effects the strength of a fiber reinforced composite is the volume fraction of the fibers over that of the reinforcing matrix. As an example,

for a continuously reinforced composite the following rule of mixtures was developed:

$$E_c = v_f E_f + (1 - v_f) E_m$$

It is quite apparent that since the modulus of fiberglass is much greater than that of the matrix, the strength is strongly but linearly dependent on v_f, the volume fraction of the fibers. Mallick [8] illustrates this point in the following graph, Figure 8.

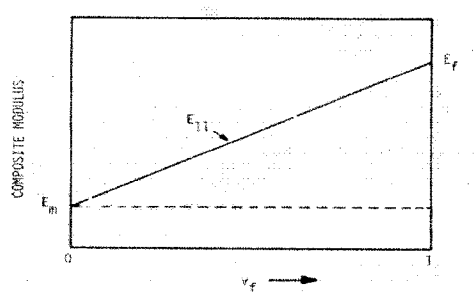

Figure 8. Composite strength vs. fiber volume fraction (from Ref [8])

2.4.2 Other Fiber Reinforcements

Of the fiber reinforcements commercially available, fiberglass is by far the most economical. This is especially the case when E-glass fiberglass is used in the composite with the polymeric matrix. There are, however, other materials available for the fiber reinforcement in composites. Two of the more common alternatives are carbon fiber and Dupont's Kevlar.

2.4.2 A) Carbon Fiber

Carbon fibers are available in various tensile moduli ranges. The moduli may range from 207 GPa to 517 GPa ($30x10^6$ to $75x10^6$ psi) depending on the desired properties. Typically, the lower modulus materials offer higher tensile strengths, lower specific gravities and higher elongation to failure.

Carbon fiber use is primarily limited by its significantly higher cost compared with fiberglass. In addition, the manufacturing process utilized with carbon fiber reinforced composites are typically more stringent then those employed with the fiberglass counterparts. Carbon fibers do, however, have many advantages over other composite reinforcements.

Some of advantages of carbon fibers are exceptionally high specific tensile and modulus strength ratios, very low coefficient of linear thermal expansion and high fatigue strength. Two of the most significant disadvantages are poor impact resistance and high electrical conductivity, a problem that is experienced in carbon fiber composite compressed natural gas storage cylinders. Static charges that accumulate in the carbon fiber reinforced walls, arc across the interior of the cylinder, eroding the composite walls.

Carbon fibers are manufactured from two different starting materials, either textile or pitch. The manufacturing process, associated with each of the precursors is more complex then fiberglass, which may be attributed to its higher cost. Of the

textile precursors, polyacrylonitrile (PAN) is the most common. Pitch, on the other hand, is a by-product of petroleum refining or coal coking and is therefore a lower cost alternative to PAN.

The starting point for the manufacture of carbon fiber from PAN is wet spinning, followed by stretching the polymer filaments drawn from the PAN solution, at elevated temperature. Filaments are then stabilized by heating in air at 220°C. Next the stabilized PAN filaments are carbonized by heating and stretching in an inert atmosphere at 1000°C. The resulting fibers produced are high strength, low modulus fibers. High modulus carbon or graphite fibers are produced through graphitization by further heating the fibers to 2000°C.

The manufacture of carbon fibers from pitch differs primarily in the preliminary steps. Carbon fibers, arranged in an aromatic, ring like pattern in the staring precursor, are transformed into long chain like structure through heating to 300°C. Pitch filaments spun from the highly viscous solution formed during heating, referred to as the mesophase, are passed through a spinnet. While passing through the spinnet die, the filaments are heated, aligning the molecules in the filament direction. Following that freezing of the filments locks the arrangement in position and subsequent reheating to between 250-400°C, in oxygen, stabilizes the filaments. The remainder of the process, involving carbonization and graphitization, is very similar to that described for the PAN filaments.

The cost and post-production processing of the carbon fibers limits their use to primarily military and high performance products. One of the primary processing problems is the successful wetting of the fibers with the polymeric sizing on the fibers. Increasing the number of filaments in a strand of tow, reduces the cost, but results in furthering the difficulty of fiber wetting. As a result, the higher cost of carbon fiber reinforced composites is not related exclusively to higher material cost, but also to increased processing costs.

2.4.2 B) Kevlar 49 Fibers

Kevlar 49 fibers have the lowest specific gravity and highest specific strength ratio of all the fibers commercially available. In addition, Kevlar is the only organic fiber commercially used for reinforcement in structural components [5]. Kevlar 49 composites are employed in military and marine applications, and are used to produce the light-weight, bullet proof vests used in law enforcement.

Kevlar 49 is a highly crystalline aromatic polyamide fiber containing the repeating amide C≡N found in acylonitrile and an aromatic ring. The presence of the aromatic ring results in higher chain stiffness and better chemical stability over acrylonitrile.

The acidic solution precursor from which the filaments are wound is proprietary. In the filament drawing process, the Kevlar molecules become highly aligned in the drawn direction. The hydrogen bonds formed between the chains serve

to hold the chains together, but do not support much load as the hydrogen bonds are quite easily broken.

One of the clear advantages of Kevlar 49 over other fibers is its non-catastrophic failure mode. The stress-strain behavior of Kevlar composites is linear, however, fracture is proceeded by fiber fragmentation and splintering. In addition, a high degree of yielding is present on the compression side in bending, an advantageous property when compressive stresses are a concern. Like carbon fiber, a main disadvantage is the increased cost of Kevlar reinforced composites.

2.5 Manufacturing Techniques

Although the materials used for reinforcing fibers play a significant role in a composites performance, another, almost equally important, consideration is the manufacturing method. Two primary factors affect the properties of the composite, the strength of the materials employed and the volume fraction of the reinforcing fibers. The varying strengths of different fibers and matrices were discussed in the previous sections. This section investigates different manufacturing techniques, and how they differ in terms of processing limitations and the effect on the fiber volume fraction in the composites.

2.5.1 Hand Lay-up

Hand lay-up is one of the most straightforward methods of manufacturing composite. For this reason, hand-lay up techniques are employed to manufacture products that typically do not require high performance. This manufacturing technique also proves to be useful for manufacturing single part prototypes or for customized, individual components. The key advantage to hand-lay up manufacturing is the relative low tooling cost required for construction of the desired part.

Hand lay-up usually requires a form or a mold as a starting point. The form serves as a base on which to wrap, or lay-up, the composite into the desired shape. A common lay-up technique employed involves building up a part by layering plies of reinforcing mat fabric onto the form until the desired thickness is achieved. As each ply, or layer, of mat is laid onto the form, the ply is wetted with the polymeric matrix. Rollers are rolled over the mat to ensure that the ply is completely wet and infused with polymer before laying down the next layer. The process is repeated with each successive ply until the composite construction is complete.

One of the main limitations to a hand lay-up is the low attainable fiber volume fraction. Typically, in a hand-lay up process, more resin than necessary is applied to ensure the fibers are completely wet with the matrix. The resulting excess resin, decreases the overall fiber volume fraction, lowering the composites performance, while increasing the weight of the component. As a consequence, hand lay-up

techniques are not used in conjunction with high performance reinforcing fibers, such as carbon or Kevlar 49, as they can not be used to their full potential with this construction method.

2.5.2 Filament Winding

In a filament winding process, continuous winding takes place on a rotating mandrel to produce hollow parts, generally cylindrical or spherical in shape. During winding, a continuous band of filament fibers, impregnated with resin, are wound onto the mandrel under tension. Curing then takes place, producing the final part.

As filaments, or fibers, are wound onto the mandrel, the tension applied to the fibers squeezes the preceeding layers of windings together. Excess resin is forced to the surface of the part, resulting in a high fiber volume fraction in the interior of the composite.

A typical filament winding process, shown in Figure 9, first starts by pulling the fibers from creels through a resin impregnating bath. Tension in the filaments is controlled by fiber guides or scissor bars located between the creels and the resin bath. As filaments exit the bath, the resin impregnated fiber is pulled through a wiping device that removes excess resin, controlling the resin coating thickness. The wiping device usually uses a set of squeeze rollers to remove the excess resin. However, in some cases, the individual filaments are pulled through a narrow orifice to squeeze out the resin. The latter method provides somewhat better control over the

resin contents, but fibers are more susceptible to friction damage with this wiping technique.

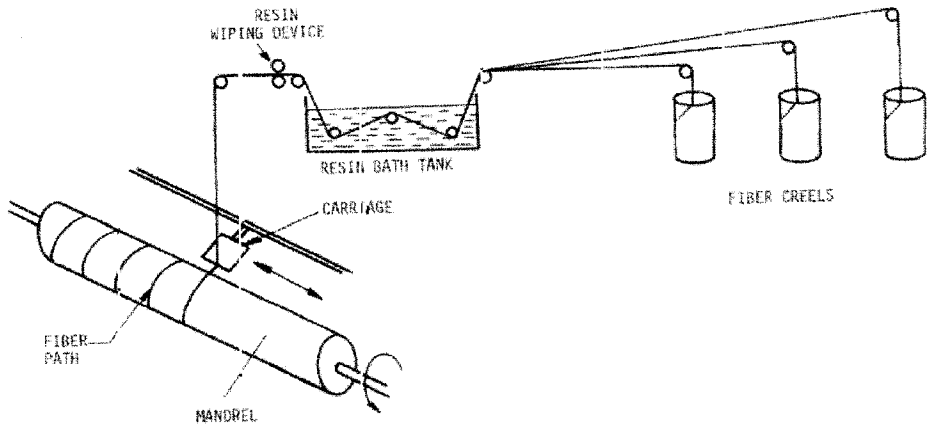

Figure 9. Common filament winding apparatus (from Ref [5])

Once the filaments exit the wiping device, they are banded together before being wound onto the mandrel. Winding the fibers may be accomplished through different methods and winding patterns. The most common method is having a moving carriage, guiding fibers onto the rotating mandrel longitudinally. This winding approach is referred to as helical winding.

In recent years, the winding technology has allowed for deliberate uneven distribution of fibers through multi-axes feeding eyes. In these cases, a fiber guiding eye places the fibers specifically on certain locations of the mandrel requiring varying thickness. The multi-axis freedom of this type of winding opens up opportunities for winding more complex shaped parts and has increased the flexibility of the process.

Filament winding processes are used to manufacture automotive drive shafts, spherical pressure vessels, conical rocket motor cases and piping. In addition, filament winding processes are used to manufacture continuous reinforced sheet molding compounds such as XMC. As a result of the attainable high fiber volume fraction, and the continuous, directional reinforcement with filament winding, this method is employed in constructions using both fiberglass and high performance fiber reinforcement.

2.5.3 Bag Molding

Bag molding processes are used extensively in the aerospace industry. In these applications, the importance of composite performance far outweighs production rates. Bag molding processes result in high fiber volume fractions, and are therefore used extensively with carbon or Kevlar reinforcing fibers.

The bag molding process starts with a pre-epoxy-impregnated laminate that is partially cured. Typically this "pre-preg" contains approximately 42% resin. Individual pre-preg plies will then be layed in their appropriate position in the bag molding process.

The walls of the mold are coated with a layer of Teflon to prevent the laminate from sticking. A porous release cloth and layers of bleeder cloth are placed below and on top of the pre-impregnated laminate in the next step (see Figure 10). The bleeder cloths are used absorb the excess resin that will flow out of the laminate

during the bag molding process. Finally, the lay-up is covered with another sheet of Teflon coated fabric separator, a caul plate and a thin vacuum bag.

Once the assembly is complete, see Figure 10, it is placed in an autoclave, and pressure is applied to consolidate the individual pre-impregnated plies. The applied pressure forces the plies together, squeezing out excess resin and entrapped voids of air or volatiles to the bleeder cloths. Heat from the autoclave first decreases the viscosity, aiding the flow of resin to the bleeder cloth, and later increases the degree of cure in the partially cured epoxy.

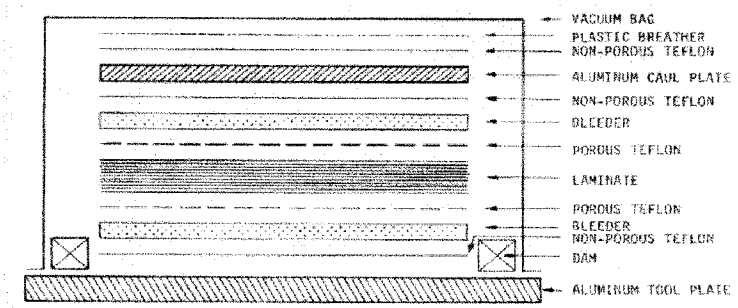

Figure 10. Depiction of layers in bag molding process (from Ref [5])

The resulting composite has a high fiber volume fraction, and therefore utilizes the fiber reinforcement to its potential. A bag molding process provides superior composite performance, however, it is a more costly method of producing composite parts. For this reason, the process is limited to applications where composite performance is a critical aspect of the design.

2.5.4 Coupling Agents

In addition to enhancing a composites performance through utilizing more advanced manufacturing techniques, chemical additives may also be used which can result in improved performance. Coupling agents are used to improve the fiber/matrix interfacial shear strength and to further protect the fibers from deleterious chemical exposure.

Without a coupling agent the stress transfer is highly dependent on the mechanical locking between the matrix and the fibers. This mechanical locking results from residual stresses that arise from the contraction of the polymer matrix onto the fibers during curing. During periods of high temperature variation or rapid strain, the residual stress from the contraction onto the fibers may be relieved, weakening the mechanical interlock.

A coupling agent mixed into the resin, or applied to the fibers before resin impregnation, forms a chemical coupling between the fiber and the polymeric matrix. So in addition to the mechanical interlocking, the strength is increased through the chemical bonding between the reinforcing fibers and the matrix.

The chemistry of the coupling agent varies with the resin used and the type of reinforcing fiber. This is largely due to the need to ensure that the coupling agents are chemically matched to the intended materials. Through proper use, coupling

agents improve the properties of the composite and may aid in the wet-out during composite construction.

2.6 Flat Sided Pressure Vessels

Pressure vessels are utilized primarily for storage or transport of compressed fuels or gases. In automotive applications, compressed alternative fuels require the use of specifically designed pressure vessels. These pressure vessels are designed to meet specific requirements.

DaimlerChrysler's commercial alternative fuels program includes the use of two compressed fuels, liquefied petroleum gas (LPG) and compressed natural gas (CNG). These systems include pressure vessels that contain pressures of 1.73 MPa (250 psi) and 24.8 MPa (3600 psi) respectively. The major challenges to improve the fuel storage in the propane program include:

- Simplification of the installation
- Reducing the weight of the fuel tank
- Increasing the capacity of the fuel tank, while staying within the existing storage envelope of the gasoline tank
- Reduction of the tank cost
- Conformance to corrosion, safety and environmental test resistance requirements of pressure vessels [9]

Improvements have been made to simplify the installation of the tanks. Modifications to the tank designs allowed for the incorporation of mounting brackets that would match existing locations used for gasoline tanks. Conformance to

corrosion and environmental test resistance requirements are met with proper material or coating selection.

The greatest challenge facing the industry involves the design limitations of the tanks themselves. An abundance of literature on spherical and cylindrical pressure vessels may easily be found. However, literature on flat-sided pressure vessels is quite rare.

In an attempt to evaluate the current state of the art, extensive literature searches were conducted on flat-sided pressure vessels. All literature located on flat-sided pressure vessels was held internally at DaimlerChrysler. To date, only three sources of literature could be located on flat-sided pressure vessels.

2.6.1 Thiokol's Conformable Approach

Since Thiokol Corporation began in 1982, the company has gained experience in pressure vessel design, testing and production. Currently, Thiokol's triple cell LPG tank is recognized as one of the industry leaders in conformable pressurized fuel storage by DaimlerChrysler [9].

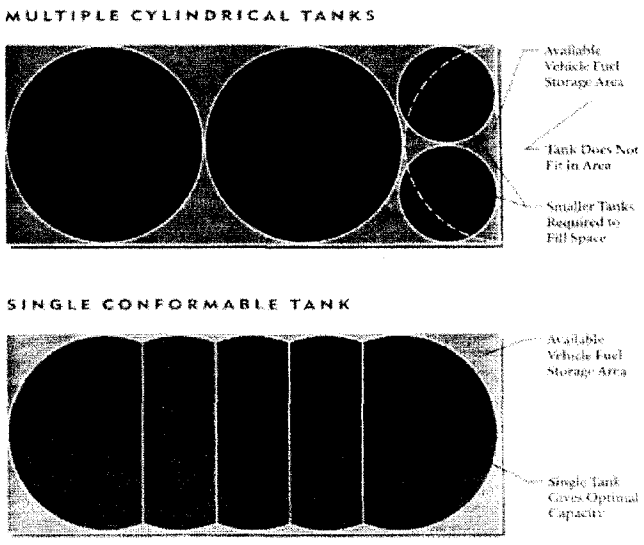

Figure 11. Thiokol Conformable Tank
(from Ref [13])

Thiokol's current commercial, conformable, LPG tank is manufactured by an aluminum extrusion process. Two aluminum "D" shaped tubes, and a rectangular shaped tube, are extruded and then welded together in an automated welding process. More or less hemispherical aluminum end caps are welded onto the ends of the assembly to complete the construction of the pressure vessel. Thiokol's tank, Figure 11, takes advantage of the bending strength of cylindrical pressure vessels, while utilizing space that would otherwise be wasted with intersecting cylinders. Compared to cylindrical vessels up to 40% more fuel storage [10] may be utilized, over cylindrical vessels, with more conformable designs.

It is quite clear, by examination of Figure 11, that a significant amount of wasted space in the first diagram is utilized by Thiokol's design, as shown in the bottom figure. This 34.1 kg (75 lb.) tank, with a 113 L (29.9 gal. (US)) capacity, replaced the previous 59.1 kg (130 lb.), 106 L (28.0 gal. (US)) tank at a considerable increase in storage space. An additional factor worth consideration is the weight savings gained with the use of the Thiokol tank.

Although the performance of this tank is significantly better than conventional propane tanks, problems do exist. One of the greatest drawbacks with the Thiokol tank is cost. The manufacturing process for these tanks is costly, and the added costs are in turn passed on to the consumer. A second concern is contamination of the fuel from welding bi-products left over from the tank construction.

Through a partnership between Thiokol and the National Renewable Energy Laboratory of the U.S. Department of Energy, research on injection molded, conformable LPG tanks has been conducted. The potential of such a process, in terms of manufacturing and reduced cost was a main factor in the consideration of an injection molding process. It was hoped that significant cost savings could be realized by molding the part in one piece, or utilizing economical polymeric joining processes between modules.

Bain's literature review investigates Thiokol's polymer conformable LPG tank quite extensively. His work carefully examines Thiokol's approach and problems that lay behind their approach to this problem's solution. Repeating his work in detail would prove to be redundant since the work of both this thesis and his are based on the same project.

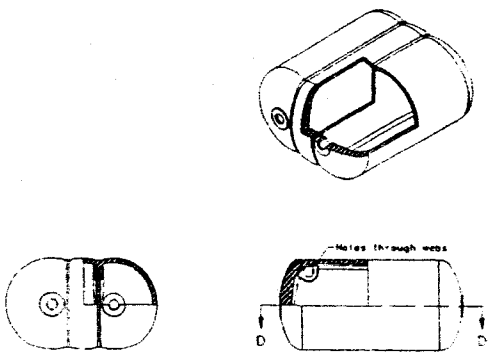

Figure 12. Thiokol's Intermediate Tank Design (from Ref [10])
(note similarities to the aluminum conformable tank)

Thiokol's approach basically involved using existing technologies developed on the aluminum conformable tank and transferring it to a polymeric material, shown if Figure 12. As a consequence of this approach, excess material was used to make up for the reduced modulus of

polymeric modulus over aluminum. To carry the stresses within the vessel, the resulting tanks were heavy and inefficient in the use of the available storage volume.

In addition to this deleterious effect, Thiokol experienced several problems with the injection molding process, including core shifting during the molding cycle. As well, high shrinkage stresses were produced in the polymer when cooling over the sand core inserts.

An important consideration in the design of polymeric parts is design around the material. To take advantage of a polymer, a part must be designed to account for the orthotropic behavior mentioned earlier in the literature review. Thiokol recognized this problem through examination of the material after testing took place. Tanks were injected molded in a manner that resulted in reinforcement running perpendicular to the highest, circumferential stresses in the part. In addition the effects of weld lines, resulting from the intersection of polymer flow fronts during molding, were significant. As a result, a significant deterioration in the strength of the polymeric material was experienced.

The results of their efforts identified the difficulties associated with their development approach. In addition, these difficulties served to affirm the importance of design around the material, when using polymers.

2.6.2 Witte van Moort Shape Conformable Tank

A conformable LPG tank is under development for the European market at Witt van Moort. Only a brief internal report could be located on the companies conformable tank development. The shape of the tank resembles the double "D" shape of the Thiokol tank. One unique feature of this tank is shown in Figure 13.

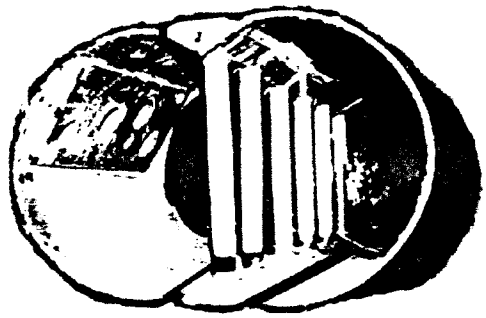

Figure 13. Reproduction of photograph of Wit van Moort conformable LPG tank (from Ref [14])

This tank originates from a standard, cylindrical tank. The tank is reformed, by hydraulically compressing opposite sides inward, to achieve flat sides on the top and bottom of Figure 13. Following the compression of the tank, these upper and lower walls are strengthened with pull bars that span the distance between them. The pull bars are threaded and sealed against leakage with backing plates on the exterior of the cylinder.

Prototypes of a 57 liter version of this design have been successfully tested. Failure in the tested tanks occurred first in the pull bars that reinforce the upper and lower flat walls of the tanks. Three tank tests have established burst strengths of 10, 10 and 11.5 MPa (1489, 1489 and 1700 psi).

No additional information on the weight or manufacturing material of the tanks was available at the time of writing. However, the tank material is clearly metallic. These tanks do illustrate an alternative, yet somewhat similar approach, to Thiokol's current commercial tank.

2.6.3 Modular Polymer Composite LPG Tank

The single cavity, polymer composite LPG tank, the focus of this thesis, was developed in conjunction with a modular design. Bain's research into the development of a modular, polymer composite LPG tank, laid out the foundation of the project's research. In addition to the development of the modular tank design, Bain's research addressed detailed design concerns such as minimum edge radii determination and the effect of using elliptically shaped walls in place of perfectly flat walls.

Research into the area of minimum radii of intersecting corners played an important role in establishing design criteria for the single cavity tank. The goal was to minimize the compressive stresses along the tank edges, while preserving as much storage volume as possible. Bain's modeling of corners revealed that, with span sizes in his design, corner radii less than 63.5 mm (2.5") produced compressive stresses greater than were permitted in bi-directional mat.

In addition to corner modeling, further modeling of flat plates revealed the advantages of adding slight curvature to the tank. Simply adding a small amount of

curvature to a flat plate resulted in a substantial increase in the rigidity of the tank. His work suggested that in areas where bending stresses were significant, adding slight curvature would significantly reduce the bending stress.

Prototype construction utilized thermoformed ABS polymer modules. After thermoforming the individual parts that made up the modular shape, the parts were bonded together forming the modules. The goal of this approach was to simulate the presence of internal, blow molded, inner liners making up each module.

Construction of thermoforming molds started from a plaster plug, shaped to the design of the prototype. A fiberglass mold was formed by overlaying the plug with a polyester, fiberglass composite. The mold was then removed from the plug and sectioned to form the required, individual module molds. Numerous ABS thermoformed modules were successfully and accurately formed in the mold made from this unique manufacturing process.

With ABS module construction complete, only the installation of fuel transfer rails and joining of the modules remained prior to over-wrapping. The tank construction was completed with an over-wrap of 9 plies of 24oz fiberglass mat. Three individual patterns were utilized for the plies of the fiberglass mat. Pattern design prevented the overlapping of multiple seams, which in turn would have served as points of weakness in the tank.

Pressure testing of the tank revealed the need for a continuous thermoplastic liner. During pressure testing, the bond between the thermoformed liner and the composite wall deteriorated at a lower than expected pressure. Speculation into the root cause of this effect, and the general failure of the tank, led to the following hypothesis. During pressure testing, the bonds that sealed the thermoformed joints in the internal modules were thought to have leaked. As a result, pressurized water entered the region between the composite wall and the thermoplastic liner. Pressure from the water acting between the composite and the inner modules would force the walls apart, effectively eliminating the strengthening effect of the interior walls. The phenomenon was audible during pressure testing, as loud popping noises, corresponding to significant increases in strains and deflections in the walls, were heard.

The result of this mode of failure was unfortunate, as it did not test the load carrying ability of the composite walls. An impermeable liner, such as that formed by blow molding, would alleviate this problem and allow for a better validation of the design. Experimental results were obtained in parallel to results from the experimental testing of the single cavity designs described in this thesis.

Chapter 3

CALCULATIONS

Early in the original development stages of the project, general stress calculations were performed to gain a better understanding of related solid mechanics. These calculations provided exposure to areas of design requiring significant consideration. Bending stresses, in particular appeared to be the greatest obstacle to overcome in the design of the single cavity, conformable LPG tank.

3.1 Comparison of Stress Distributions in Flat Plates and Cylinders

Prior to applying to the Natural Science and Engineering Research Council of Canada for funding, Bain performed preliminary analyses to determine the feasibility of constructing a polymer composite, flat sided pressure vessel [1]. Calculations were based on two simplified, different assumptions.

The first calculations assumed the walls of a rectangular shaped, 914 mm x 584 mm x 355 mm (36"x23"x14") box, were perfectly rigid. Normal forces in the walls were calculated by multiplying the 1.725 MPa (250 psi) pressure by the area of the walls. In-plane stresses in the vertical walls were determined by sectioning the tank across the horizontal mid-plane of the tank. In-plane stresses in the other walls were similarly calculated by sectioning the tank along other mid-planes. According to Bain's results [1], the normal stresses in the walls, up to the calculated maximum

of 152 MPa in the vertical walls, could be safely born by 4 mm thick carbon fiber cloth[≠1] composite walls.

A second assumption was based on fixing the edges of the rectangular walls in space and allowing the walls to deflect outward due to the 250 psi pressure. Deflections at wall mid-points were calculated for different materials based on published equations for the deflection of a simply supported flat plate subjected to a uniform pressure. Calculations of the deflection were based on different material properties and thickness. The most acceptable results, 8mm deflection with a 10mm thick wall, were obtained in the smallest 23"x14" end walls and the 36"x14" side walls of the tank using properties of unidirectional carbon fiber reinforced walls. These calculations illustrated the clear relationship between the unsupported span length[≠2] and the magnitude of the deflection [1].

In thin walled cylinders tensile stress is uniformly distributed through the wall thickness. Only tensile stresses form in the walls of a pressure vessel, resulting in tensile membrane loading. This tensile loading best utilized the highly orthotropic, high tensile strength properties of fiber reinforced composites. In the case of a flat plate, the tensile and compressive stresses that develop across the cross-section result

[≠1] Based on published property values for carbon fiber mat in an epoxy matrix.
[≠2] In the acceptable cases the unsupported span length was 14" ; increasing it to 23" significantly increased the deflection.

in bending. Only the portion of the cross-section under tensile stress takes advantage of the high strength properties of the fiber reinforcement.

3.2 Changing the Second Moment of Area

The bending stress resulting from pressure acting on a flat plate was developed in the preceding section. Two obvious methods of decreasing the stress acting in the plate are to reduce the bending moment or increase the second moment of area. Reducing the moment may be accomplished by reducing the area of the unsupported span the pressure is acting on. This approach was utilized in the design of the modular tank.

Increasing the second moment of area of flat plates is the other method of decreasing the bending stress. The second moment of area, I, may be increased through a variety of methods. One method is increasing the thickness of the plate. The second moment of area, I, changes proportional to the cube of the thickness, h. In comparison to the base dimension, changing the thickness of the plate will have the greatest effect on the second moment of area. One obvious effect of thickening the plate results in an overall increase in the weight of the material. Additionally, if walls were thickened around a rectangular shaped container, a reduction in the interior volume would occur.

A more effective, alternative approach to increasing the second moment of area is the use of ribs. Ribs effectively stiffen the plate more weight efficiently than thickening the plate. Mathematically this is shown by the development of the following equations.

As a simple illustration, consider a one-dimensional plate with unit depth as shown in Figure 14.

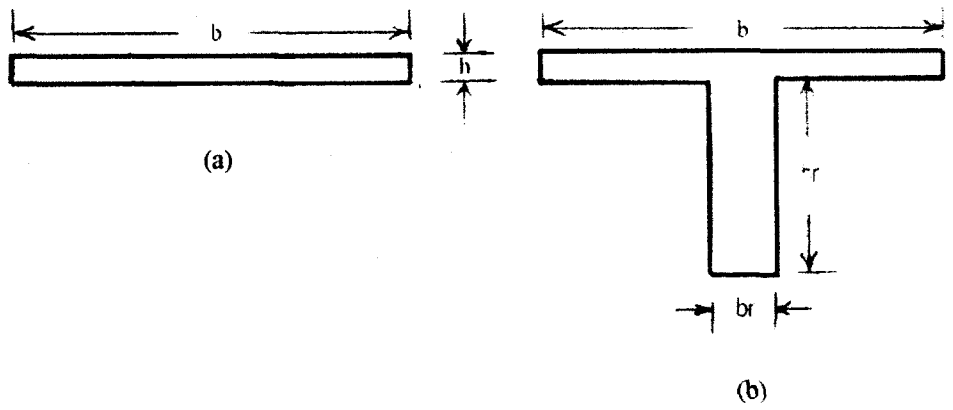

Figure 14. (a) Simple flat plate, (b) Same flat plate with rib

The second moment of area for a simple flat plate is given by:

$$I = \frac{1}{12} bh^3$$

Now as consider the same flat plate that incorporates a single rib in the center of the span as shown in Figure 14 (b). Using the parallel axis theorem, the second moment of are is first calculated separately for the flat plate and the rib.

$$I_p = \frac{1}{12} bh^3 \; I_r = \frac{1}{12} b_r h_r^3$$

The area centroid is calculated and simplified to:

$$y_c = \left[\frac{bh^2}{2} + \frac{b_r h_r^2}{2} + b_r h_r h \right] \times \frac{1}{bh + b_r h_r}$$

The value of y_c is then substituted into the parallel axis theorem:

$$I_{total} = I + I_r + bh\left(\frac{h_r}{2} + h - y_c\right)^2 + b_r h_r \left(\frac{h}{2} - y_c\right)^2$$

Since all terms in the above equation are positive, the second moment of area will increase.

To illustrate the significance of the addition of ribs, consider a plate with ribs spaced 127 mm (5") apart, compared with a plate with no rib reinforcement. In this case assume that the thickness of the plate, h, equals 12.7 mm (0.5") inches and the plate base, b, equals 127 mm (5") inches. The assumed rib dimensions will have a base, b_r, equal to 1 inch and a height, h_r, equal to 76 mm (3").

In the case of the simple, 12.7 mm x 127 mm (0.5"x5") flat plate, the result of the calculation of the mass moment of inertia is 2164 mm^4 (0.052 $inch^4$). Incorporating the 76 mm x 25.4 mm (3"x1") rib yields a second moment of area of 2.69E6 mm^4 (6.478 $inch^4$). The rib results in an increase of the second moment of area by a factor of 124.8. Bending stress in the same plate would therefore be

reduced by a factor of almost 125 due to the inverse linear relationship of the two variables.

As a further comparison, consider a rectangular plate with the same cross-sectional area as the total cross-sectional area of the rib-stiffened plate. Keeping the base constant at 127 mm (5"), the required thickness, or h, would be 27.9 mm (1.1"). Calculation of the second moment of area for this plate would result in 2.305E5 mm^4 (0.554 in^4). Therefore, the reinforcing rib described increases the second moment of area by a factor of 11.7 without increasing the weight of the plate, or decreasing the internal volume of the tank.

Concepts learned from these preliminary calculations provided the fundamental background for the development of a single cavity, flat walled pressure vessel. As a consequence, the decision to use ribs as reinforcement served as the starting point for subsequent designs of the tank.

Chapter 4

COMPUTER MODELING

4.1 Introduction

With preliminary calculation results complete, the next progressive step in the project was computer modeling. The computer modeling began through simple models of flat plates with reinforcing ribs. Use of an FEA package was invaluable in quickly modeling various designs that included many variations in material properties and dimensions.

The Finite Element Analysis package used for all computer modeling was ALGOR. Previous experience on this commercially available and widely used software was gained through a fourth year computer aided design course by this author. Familiarity with the software enabled modeling to commence immediately, with little or no time required gaining familiarity with the software. In addition, ALGOR's meshing features reduced modeling time, allowing for the efficient development of multiple designs under consideration.

ALGOR is an implicit Finite Element Analysis package. The package originated from Public Domain software in the 1960's with its first static processing module SAP0. Later the module was upgraded with a second module, SAP1, through developments at Berkley in California. The second module permitted the modal analysis of components in addition to the static stress analysis available with SAP0.

Following introductory flat plate modeling of rib reinforcement, modeling was carried over to the development of proposed complete tank designs. The development of the tanks became an iterative process of varying rib spacing and design. The designs used symmetrical modeling wherever possible, with appropriate boundary constraints applied, to reduce processing time.

4.2 Flat Plate Modeling

S-glass, fiberglass composite flat plates were modeled in ALGOR to take advantage of the ease with which material properties could be changed within the package. Values for the modulus of elasticity, thickness, density and coefficient of thermal expansion for elements are assigned within the Decoder module of the ALGOR package. These values are assigned to elements based on element colour and group number. Once a model had been meshed, assigning elements specific colours or groups was quite easily accomplished through the use of an update tool within the SuperDraw module of the software.

In the case of flat plate modeling this proved to be an invaluable tool in the efficient modeling of various designs. Through the use of plate elements, models only required re-meshing if rib spacing or depth were changed. The remaining parameters under consideration were easily changed without ever reworking the actual model.

Wire frames of the upper flat plates and ribs were first constructed within the SuperDraw module. After the wire frames were constructed, the frames were meshed to create the surfaces of the models. Following meshing, the upper plate was assigned a specific colour and group numbers. The same procedure was repeated separately for the ribs with a different colour and group number assigned. Within the decoder, values for the modulus of elasticity, thickness and pressure were assigned to both components individually in imperial units. As a result, numerous models were quickly run with varying rib thickness and material properties. An example of one of the flat plate models is shown in Figure 15.

Displacement of 1/2" Fibreglass Plate Reinforced with
1/2" X 4" Polypropylene Rib

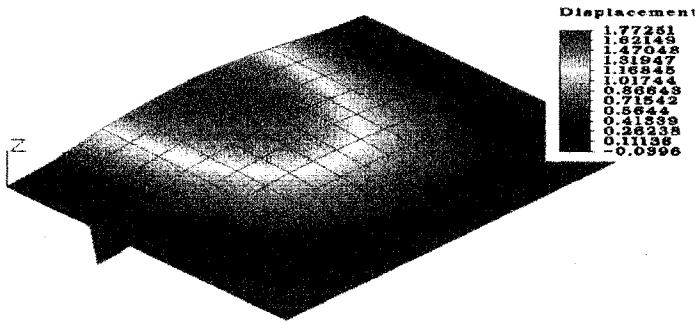

Figure 15. Example of Flat Plate Model
(displacement in inches; plate pressurized at 250 psi.)

Initially, the concept of using a thermoplastic for the ribs was investigated. Models of flat plates with ribs assigned properties of polypropylene were modeled to

determine the feasibility of this material for rib reinforcement. The results of numerous models revealed that effective reinforcement could not be obtained with polypropylene. This determination was based on the consideration that the thickness of the polypropylene would be have to be much greater than current commercial blow or injection molding constraints would permit.

The modeling also raised another issue, in terms of strengths achievable with thermoplastics. Even with the use of a reinforced thermoplastic in the ribs, problems with processing would be unavoidable. If a thermoplastic containing up to 40% volume glass fiber were utilized, the effect of all the glass reinforcement would not be realized. It was anticipated that if the tanks were blow or injection molded, with rib construction incorporated into the processing, fiber orientation would become a problem. Thiokol had already experienced similar problems on a much simpler prototype, where mold filling is concerned. With a single mold filling process, forming both the walls and ribs, proper axial fiber orientation in the ribs would be difficult if not impossible. If axial orientation could not be achieved, the presence of fiber reinforcement would not provide any significant advantage in the rib properties. In addition, material strength in the ribs could not be accurately modeled due to the unpredictable fiber orientation.

Investigation and computer modeling of filament wound, fiber-glass ribs indicated required stiffness could be achieved with filament wound ribs. Unidirectional fibers have the highest strengths of the various fiber orientations. The

fact that the ribs are subjected to tensile forces, ribs wound in the direction of the stress would provide high specific strengths required for effective reinforcement.

4.3 Tank Design

Results obtained through modeling of flat plates played a significant role in decisions made in the initial tank design. It was determined that the ribs would be most effective running in parallel spanning across the 584 mm (23") width of the tank. As a result, rib spacing could be increased significantly more than in the other direction, while still maintaining the same value for unsupported wall area.

Navier's bending equation for flat plates [11] under a uniform load also confirms that bending is dependent on the ratio of the longest side over the shortest side of a rectangular, flat plate. The following equations, for maximum bending at the center of the plate, developed by Navier illustrate this point.

$$deflection(\max) = \frac{16 p_o a^4}{\pi^6 D} \phi(\rho) \qquad (4.1)$$

where

$$D = \frac{EI}{(1-\upsilon^2)} \qquad (4.2)$$

$$\rho = \frac{a}{b} \qquad (4.3)$$

$$\phi(\rho) = \frac{(-1)^{\frac{m+n-2}{2}}}{mn(m^2 + n^2\rho^2)} \qquad (4.4)$$

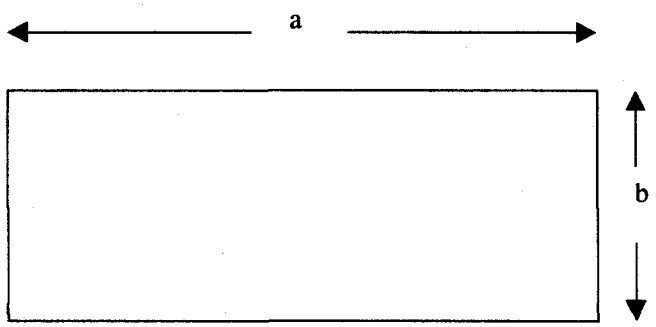

Figure 16. Locations of dimensions used in Navier's bending equation

Values of *m* and *n* are based on the number of terms taken in the rapidly converging, double trigonometric series Navier used to develop the equations. The uniformly distributed load is represented by p_o. Consider a simple case where m and n both equal 1. The resulting dependence of $\phi(\rho)$ on the ratio of a over b is tabulated below.

ρ	1/3	1/2	1	2	3
$\phi(\rho)$	0.8100	0.6400	0.2500	0.0400	0.0100

Table 1. Dependence of $\phi(\rho)$ on ρ

Through observation of the results in Table 1, it is clear that increasing the ratio of a over b results in a decrease in $\phi(\rho)$. As a result the maximum deflection is decreased most significantly by keeping the value of the 'b' dimension small in comparison to the dimension of 'a'. This illustrates why reinforcement was more effective running across the top and bottom spans of the tank in the shortest distance, due to the greater significance of the smaller dimension in the resulting bending.

One concern in the design of the rib structure was fuel drainage across the bottom of the tank. Ribs running across the bottom of the tank would trap fuel when the fuel level, in the tank, dropped below the height of the ribs. Fuel trapped between the ribs would effectively be unusable, particularly in a liquid withdrawal system. To alleviate this problem, Watt [14] proposed steps, rather then ribs, be utilized on the bottom of the tank. The presence of a step would serve to maintain the increase in the area moment of inertia, over a flat bottom, due to significance of the step height in the calculation. Like ribs, steps filament wound with fiberglass, would also effectively reduce the bending stress while permitting fuel drainage across the tank bottom. The original concept of the stepped tank design in shown in Figure 17.

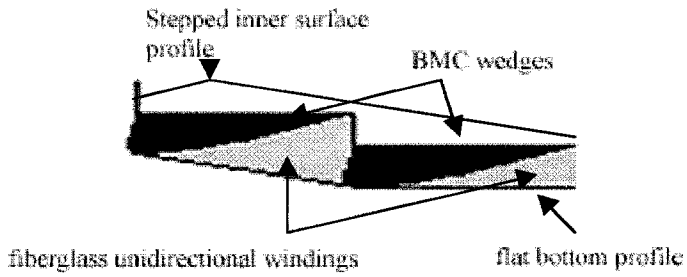

Figure 17 Concept sketch of proposed step profile

Originally, bulk molding compound, BMC, filling wedges were proposed to fill the areas between adjacent steps and the filament winding. It was thought that filament wound fiberglass on the tank bottom would fill out flush with the previous step profile. A concern was that when the filament winding ended, an abrupt drop would be present between the end of the winding and the next step. To smooth the transition from the filament windings to the next step, filling wedges would be used.

Triangular wedges would butt up against the filament winding and taper down to the next step. The net effect would be a smooth continuous transition between steps.

Smooth, convex transitions were desired as a result of selecting a fiberglass composite as the construction material. As a general rule, fiberglass cannot be wound or wrapped onto concave curves. Wrapping onto a concave surface with fiberglass mat can result in delamination between layers when the surface is subjected to opposing bending stresses.

Preliminary tank designs and the consideration of the volume of filament winding within the ribs, eliminated the need for filling wedges. After modeling the initial tank designs, it became apparent that a greater number of ribs would be required than initially anticipated. In an attempt to increase the effect of rib reinforcement, rib depth was increased significantly. The resulting rib depths varied between 76.2 and 101.6 mm (3 and 4") with typical widths of 25.4 mm (1"). With this increase in the volume of the filament winding in the ribs, the question as to where it would go on the bottom of the tank was raised. The tank bottom step height was less than the depth of the ribs, and so the filament winding material would have to taper out across the bottom of the tank. As the step height was reduced to maximize internal volume, the width of the volume the filament winding required to taper out was increased. It was soon determined that it would not be worthwhile having filling wedges since a more desirable transition could be achieved by evenly tapering out the fibers across the steps during winding.

4.4 Computer Modeling

With preliminary tank models completed, final designs were made that incorporated the concepts learned from the previous design iterations. Designs were now at a point that approached the set requirements for deflection and allowable stresses. The goal for the maximum allowable deflection at operating pressure was no more than 3.17 mm (0.125"). In addition, the maximum tensile and compressive stresses were limited to 138 MPa (20ksi) and 69 MPa (10ksi) respectively. The stress values were based on published fiberglass composite strengths of 552 MPa (80ksi) in tension and 276 MPa (40ksi) in compression. Using a design factor of 4 resulted in the previously mentioned design limits.

On previous step designs, the maximum deflection occurred on the bottom at the center of the tank bottom. It was anticipated that this would be the location of maximum deflection. The step depths were less than those of the ribs, as a result the area moment of inertia was lower on the bottom of the tank. Modeling, previously performed by Bain, indicated that adding slight curvature to a flat plate reduced the deflection of the plate under pressure. As a result of his findings, the concept of adding slight curvature to the bottom tank wall was included in the final designs.

An illustrative progression of the remaining tank designs, to the originally proposed prototype design is located within APPENDIX I. Within the appendix

finite element analysis results for deflection and stress are plotted out. In addition, the models are described, including assumptions and discussions of results.

4.4.1 Step/Rib Design of First Design

This first, full-scale dimension design, was the first model to incorporate both a step profile and curvature on the bottom of the tank. Rib depth in this tank was 101.6 mm (4") and rib spacing varied between steps 1 and 2 and steps 2 and 3. In a previous design the location of maximum deflection was at the center of the tank bottom. In an attempt to reduce this deflection, the rib spacing was decreased closer to the center of the tank and increased further from the center. The spacing between steps 1 and 2 was 76.2 mm (3"), between steps 2 and 3 this spacing was increased to 101.6 mm (4"). In addition the step heights of the first two steps is 76.2 mm (3"), the remaining step height is 50.8 mm (2"). Exterior wall thickness was 12.7 mm (0.5"). Curvature on the bottom of the tank resulted in a 25.4 mm (1") change in the elevation of the bottom profile, from the center of the tank to where the tank bottom met the side wall. The deflection results from modeling this design are presented in Figure 18.

Material properties assigned in the model accounted for the unidirectional wound ribs and steps,

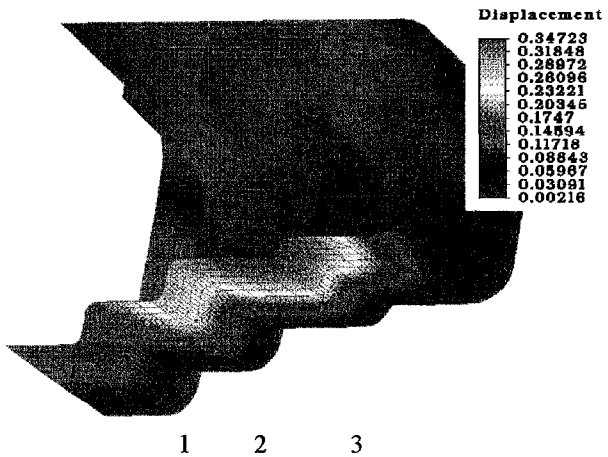

Figure 18. FEA Results of First Tank Design
(displacement in inches at 250 psi)

and bi-directional mat on the tank walls. In an attempt to confirm that published strengths of bi-directional mat could be attained in the proposed construction process, tensile testing was conducted. The results of the tensile tests indicated that the attainable strength values were significantly lower than those published. As a result, the modulus of elasticity used in bi-directional mat walls was assumed to be 10.3 GPa ($1.5x10^6$ psi), reduced from the previous value of 20.7 GPa ($3.0x10^6$psi). In addition, the modulus for the unidirectional ribs was reduced to a conservative estimate of 27.6 GPa ($4.0x10^6$psi), half of the published value.

Results of the computer modeling reveal a shift in the location of maximum deflection from the center of the bottom of the tank, to the location with the shortest step height and largest unsupported span. Further examination of the tank in its deflected state indicates that the step 3 actually twisted downward. This buckling effect and reduction of the area moment of inertia were contributing factors to the transfer of the maximum deflection to this location.

Stress values for the majority of the tank remained within the allowable value of 138 MPa (20ksi). Higher stress values were concentrated at the corner locations of the intersection between the third step and the tank side wall. This was a result of a high bending stress that developed from the excessive deflection at the center of the tank on the third step.

4.4.2 Step/Rib FEA of Design II

Results from the previous step design revealed defections that were considerably higher than the acceptable 3.17mm (0.125") deflection. In an effort to reduce this problem, an additional rib and corresponding step were added. Material property values were maintained for the ribs and the outer walls in the analysis. Rib dimensions remained the 25.4mm x 101.6 mm (1"x4") values of the previous model. In addition, to reducing the rib spacing, the step height of the steps was reduced. The purpose of this was to minimize the loss of volume resulting from the presence of the steps. In this design, the step height was a constant 50.8 mm (2") for all four steps.

Analysis results of the second prototype once again revealed the significance that even a slight difference in unsupported span length plays. In this model the steps with the greatest deflection, had unsupported spans that were only 12.7 mm (0.5") longer than the remaining steps. The maximum deflection, however, was reduced by 2.54 mm (0.1") in this second model over the predecessor. In Design II, the second step, the location of greatest deflection, also appeared to twist when the model was examined in the deformed state.

Stresses in the Design II were considerably lower than in the first. This was a result of the reduction in the bending stresses from the decreased values of deflection. In this case the highest stresses were concentrated on the sharp corners at the steps.

Unlike the first model, fillets were not added to the transition areas between steps. However, the resulting stress concentrations, although above allowable values, were still approaching the acceptable limit of 138 MPa (20 ksi).

4.4.3 Step/Rib Design of First Prototype Design

Results from the second design iteration, revealed that the designs were approaching values that were within the acceptable limits. One important omission in the computer modeling was realized. This was the consideration of the dispersion of filament winding across the steps on the bottom of the tank. An intermediate model, utilizing the previous, second tank design, accounted for the presence of unidirectional winding on the bottom of the tank. The results from this model revealed displacement and stress values that bordered the acceptable design criteria.

The designs were now at the point where the concept tanks had potential for prototype models. Consideration into the prototype construction methods became a factor in the design of the subsequent models. As a result, computer modeling was based on both full and half dimension scale size for the prototypes. The half dimension scale refers to the fact that all geometrical dimensions are reduced by half. This results in areas being ¼ of the full-scale counterpart, and volumes of 1/8 the full-scale values. It was hoped that through experimental model verification of FEA predictions of half scale prototype deflections, that the designs could be easily carried to the full scale with confidence.

Volume loss remained a concern associated with the step profile on the bottom of the tank. To further reduce the amount of volume lost due to the presence of the steps, the step height was reduced to 25.4 mm (1") on the full-scale design or 12.7 mm (0.5") on the half dimension scale design. The half scale results, located in APPENDIX I, assume filament wound exterior walls of 8.89 mm (0.35") thickness and 20.3 mm x 50.8 mm (0.8"x 2") ribs spaced close to 50.8 mm (2") apart. The exterior dimensions of the half scale tank were taken as 457mm x 292mm x 178mm (18"X11.5"X7").

Results from the analysis appeared very promising on the half scale design. Here the deflections were well within the acceptable limits. The maximum deflection in the tank was 1.06 mm (0.040"), a value much less then the maximum 3.17 mm (0.125") constraint. In addition the values for stress were less then the 138 MPa (20ksi) limit even in the areas of stress concentration within the tank.

4.4.4 Step/Rib FEA of Final Prototype Design

The final prototype design model is identical to the previous model with two major exceptions. The first is that the modulus of the fiberglass bi-directional over-wrap, 10.3 GPa ($1.5x10^6$ psi), is utilized on the exterior walls, rather than the modulus for unidirectional winding of 20.7 GPa ($4.0x10^6$psi). In addition, the wall and rib thickness values were exact half scales of the proposed full-scale tank design.

Deflection results for this final, half dimension scale design are illustrated in Figure 19. In all cases, deflection and stress results were well within the acceptable limits set early in the design phase. These results, arrived at through conservative estimation of material properties, indicated that this design would be suitable for prototype construction.

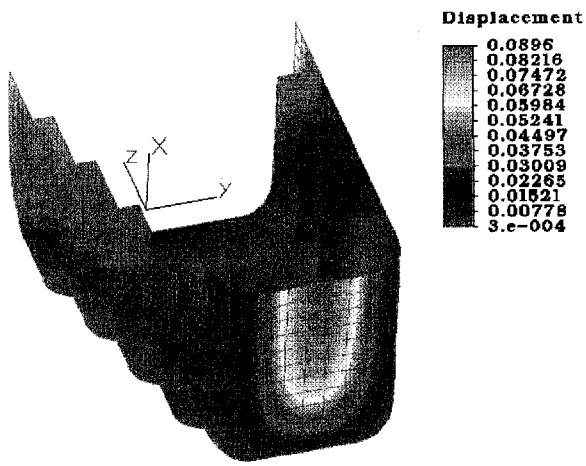

Figure 19. Deflection prediction on half scale design of Final Prototype at 250psi (dimensions in inches)

In addition to modeling the tank at half-scale dimensions, the design was modeled at the proposed full-scale size. Predictions for stress and deflection on the full-scale model were acceptably within the design requirements. The one location that possessed deflections higher than acceptable is the red area of Figure 19, which could be corrected by adding slight curvature to the wall.

Based on the FEA results, it was predicted that this final half scale prototype design would serve as a good starting point for prototype construction. The experimentally tested prototype would serve to check the fidelity of the computer models and give a measure of confidence in FEA performance predictions for subsequent designs.

Part way through the construction of the stepped prototype, but before testing it a second half scale prototype design was developed. This second model was essentially identical to the step design, with the exception that the profile of the tank bottom had only one step, rather than the four steps on the proceeding model.

Careful consideration into how the over-wrap would be dispersed across the steps on the first prototype design led to the development of this design. As a result of the windings spreading uniformly across the step profile, the necessity of the steps was questioned. If the tank bottom was covered with a 12.7 mm (0.5") layer of filament wound fiberglass, suitable reinforcement was expected through the increase in material properties and thickness.

Results of these considerations, and the desire to investigate the effects of the two tank profiles, lead to the decision to commence construction on this second prototype design. Successful prototyping of this second model would allow for model validation of the different approach in the design of the bottom steps. With the inherent increase in volume of this design, the second design, if successful, would prove more advantageous.

Chapter 5

MATERIAL TESTING

5.1 Purpose of Testing

Material testing was conducted to provide insight into attainable material properties. The polymer composite pressure vessels constructed as described in this thesis, resulted in a final composite material whose actual properties were not known. But the design of the tanks needed representative property values to estimate the performance capability of the tanks as simulated in FEA. Therefore test comparisons were made using methods that attempted to mimic those used in the actual tank construction.

5.2 Shear Lap Test

Shear Lap testing was based on the ASTM Designation D 1002-94 description of a shear test for measuring bond strength. In the case of the design and construction of the modular cell tanks [1] the bond strength between the thermoplastic liner and composite over-wrap would be important. If the bond strength was not sufficiently strong, then there was a concern that the composite walls could pull away from the liners In the modular tank design, internal thermoplastic walls served as the reinforcement against deflection. Shear movement of the module walls, in contact with the composite, might also result in additional torsion placed on the internal

reinforcing walls. Adequate bond strengths between the thermoplastic and the composite over-wrap would reduce this effect and aid in the reinforcement.

In the case of the single cavity design discussed in this thesis, the proposed ribs were to be wound under enough tension to ensure that the ribs would remain in contact with the liner. Additionally, the internal pressure acting from within the liner would force it against the surfaces of the composite walls.

Shear lap tests were performed to determine the significance of variation in the adhesion of three thermoplastics with a fiberglass-epoxy matrix. The results, illustrated in Table 2, revealed that the bond strengths varied significantly between the three materials tested. (SEE APPENDIX II for detailed analysis)

Shear Lap Test of ABS/EPOXY Bond

Shear Area				Failure	Failure Shear
ABS #	b (inches)	w (inches)	A (inches	Load (lbs)	Stress (PSI)
A1	1.59	1.178	1.87302	498	265.881
A2	1.58	1.172	1.85176	Nil	Nil
A3	1.55	1.165	1.80575	510	282.431
A4	1.57	1.182	1.85574	507	273.206

Average Failure Stress
273.8 PSI

Shear Lap Test of High Density Polyethylene/EPOXY Bond

Shear Area				Failure	Failure Shear
HDPE	b (inches)	w (inches)	A (inches	Load (lbs)	Stress (PSI)
H1	1.31	0.995	1.30345	66	50.635
H2	1.29	1.025	1.32225	Nil	Nil
H3	1.33	1.012	1.34596	Nil	Nil
H4	1.28	0.983	1.25824	Nil	Nil

Average Failure Stress
50.6 PSI

Shear Lap Test of High Impact Polystyrene/EPOXY Bond

Shear Area				Failure	Failure Shear	Failure Tensile
HIPS	b (inches)	w (inches)	A (inches	Load (lbs)	Stress (PSI)	Stress (PSI)
HP1	1.13	0.987	1.110375	236	212.541	1700.326
HP2	1.13	0.991	1.114875	240	215.271	Nil
HP3	1.12	0.993	1.115139	180	161.415	1291.319
HP4	1.13	1.012	1.14356	248	216.867	1734.933
HP5	1.13	0.996	1.121496	215	191.708	1533.666
HP6	1.13	0.983	1.11079	240	216.062	1728.500

Average Exceeded Shear Stress
202.3 PSI

Note: The shear stresses actually exceed these values. Failure occurred across the cross-section of the HIPS. Values stated in Failure Shear Stress are maximum values attained before failure in the ABS occurred.

Table 2. Shear-lap bond failure stress tests

From the results shown in Table 2, it appears that the strength of the bond between the ABS and epoxy was the strongest of the three materials tested. However, it is important to note that the high-impact polystyrene, HIPS, failed across the cross-section of the HIPS material. Failure did not occur at the bond location. As a result, the bond strengths of the HIPS-epoxy interface are expected to exceed the values shown in the graphical representation. The testing did reveal that, due to the variation in bond strengths, significant testing would be required to find a material suitable for use with an epoxy composite.

5.3 Effects of Various Lay-up Techniques on Tensile Strength

Preliminary tensile testing of fiberglass-epoxy samples revealed that the attainable strengths were much less than those published. The results, from this preliminary testing dictated the use of these lower values of elastic modulus in computer modeling.

Methods to improve the composite strengths were investigated. Scanning electron microscopy revealed that a possible cause for the reduction in strength was a lower than expected volume fraction of glass fibers in the epoxy matrix. An additional potential problem of coupling difficulties between the fibers and the matrix was considered. In an attempt to improve on both the coupling and fiber volume fraction, two approaches were taken.

The first approach investigated the effect of varying the fiber impregnation method. Three methods of impregnating the fibers with the epoxy were utilized. The first method (1) was the traditional method of laying down a bi-directional, fiberglass ply, soaking the ply with epoxy and rolling the epoxy into the mat. After the mat was soaked, the next fiberglass ply was added using the same procedure. A second method (2), essentially the same as the first, involved rolling the epoxy into the mat with considerably more pressure.

A final method (3) utilized a "bagging" technique to impregnate the fibers with epoxy. Each ply was first laid down then covered with epoxy. Next a polyethylene bag was placed over the epoxy covered, fiberglass ply. Rolling occurred with the bag placed between the roller and the fiberglass ply. The author has observed that with this barrier in place, epoxy was forced sideways through the fibers, rather then upward, to the surface of the composite, as in the case of the usual methods of laying down fiberglass.

The second approach utilized a coupling agent added to the epoxy during preparation. A coupling agent, Titanium [V Tetraksis(2,2-BIS(2-Propenyloxy)Methyl-1-Butanolato-0) adduct with 2 moles (D[TR]oecyl Phosph[TOD]Hydrogen), was supplied by Kenrich Petrochemicals Inc. When mixed with the epoxy, the color changed to a florescent yellow.

In laying up the samples containing the coupling agent, the same three methods of varying the lay up technique were used. Test results are shown in Figures AVII 2 and 3 in APPENDIX II. Mean values of the results are summarized for comparison in Table 3.

Modulus of Elasticity Values

	No Coupling Agent		Coupling Agent	
Method	Mean	Std. Deviation	Mean	Std. Deviation
1	12.7 GPa	0.46 GPa	10.2 GPa	1.9 GPa
2	15.1 GPa	1.4 GPa	12.7 GPa	2.0 GPa
3	17.4 GPa	4.0 GPa	16.6 GPa	3.3 GPa

Ultimate Strength Values

	No Coupling Agent		Coupling Agent	
Method	Mean	Std. Deviation	Mean	Std. Deviation
1	187 MPa	39 MPa	193 MPa	40 MPa
2	217 MPa	24 MPa	232 MPa	23 MPa
3	234 MPa	33 MPa	252 MPa	25 MPa

Table 3. Comparison of Tensile Testing Results

Method 1- Conventional impregnation method
Method 2- High pressure impregnation method
Method 3- Bagging impregnation method

The results of the testing show that both the ultimate strength and modulus values increased through the use of the alternative impregnating methods. Applying more pressure while rolling epoxy into the fiberglass, as in method 2, increased the strength of the composite. The strength was further increased if the bagging technique, designated method 3, was used.

The use of the coupling agent resulted in an increase of the ultimate tensile strength, in all impregnation methods, over the epoxy without the coupling agent. Samples without the coupling agent, however, had higher modulus values. The lower modulus of the samples with the coupling agent may be explained by higher strains, or greater elongation to failure, that resulted in testing these samples.

Chapter 6

PROTOTYPE CONSTRUCTION

6.1 Introduction

With a final design proposed for construction, research focused on the development of a construction method. As part of Bain's approach [1] to the modular prototype design, thermoforming molds were constructed from a molding plug of the design geometry. Problems with the construction of the plug and the long construction time raised issues in the consideration of construction method for the single shell design described in this thesis. Flexibility in modifying the design and rapid prototyping of subsequent designs was desired.

Investigation into prototyping methods for fiberglass composites revealed that an alternative approach might be suitable. This method is used frequently by people constructing models, such as model airplanes and cars, as a hobby. Polystyrene foam blocks are first sculpted to the desired shape. A composite over-wrap is then applied over the sculpted foam form. After the resin cures, the inner core is dissolved with mineral spirits or acetone, resulting in the formation of a hollow shell of the final desired shape. In addition to the use of foam in the construction of hobby models, foam is used in the construction of plugs in the marine industry [12], due to its rapid prototyping and dimensional stability properties. Polystyrene foam cores also serve as a rigid working surface for over-wrapping. The use of a dissolvable inner core

became the approach utilized in the construction of the prototype composite tanks described in the present work.

6.2 Construction of Foam Cores for Composite Over-wrap

High density, building insulation foam was selected as the material for construction of the inner cores. Slabs of 50.8 mm (2") thick sheets were rough sized to approximate dimensions, glued together and stacked to form a rectangular block. The dimensions of the block measured approximately 330 mm x 508 mm x 203 mm (13"x20"x8"). After waiting for the predetermined set-up time recommended by the manufacturer of the glue, the plug was cut using a band saw to the 292 mm x 457 mm x 178 mm (11.5"x18"x7") outer dimensions of the half scale design. Problems with the 50.8 mm (2") foam slabs sliding on each other were experienced when the ribs were cut into the foam plug. It appeared that the glue did not properly set up, and little shear stress was required to break the bond between the adjoining slabs. To prevent the sliding of the glued foam sections, nails were randomly placed between the layers to prevent the sliding motion.

Final finishing and sculpting of the foam cores was accomplished with hand tools such as sculpting saws and sanding blocks. Figure 20 shows some of the tools used in addition to the foam core for the first prototype design as it was under construction. Two half-scale prototype designs, and an eventual third tank which was full scale, in two dimensions, were constructed in this manner. The exception of the

full-scale design was that it utilized 101.6 mm (4") thick blocks, rather then 50.8 mm (2") blocks used on the half scale designs.

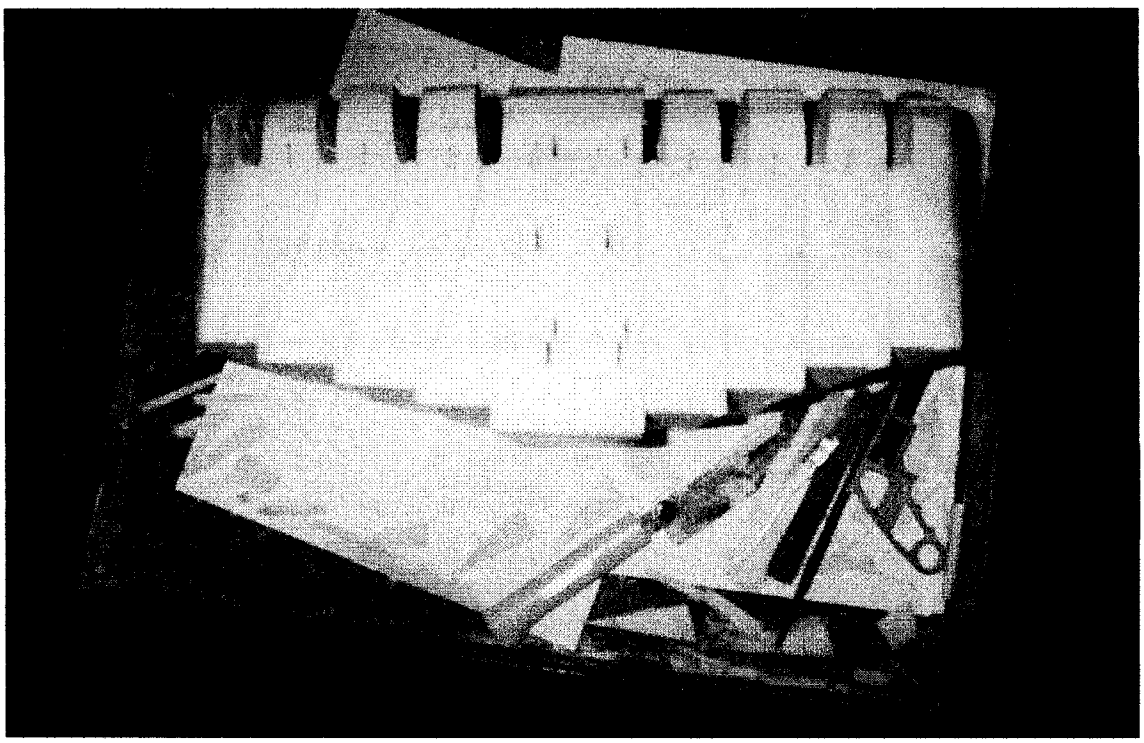

Figure 20. Foam core for prototype 1 under construction
(additional construction views may be found in Appendix II)

6.3 Pressurizing Ports

Consideration into the method of pressure testing resulted in the design of pressurizing ports for incorporation into the prototypes. One of the concerns of pressurizing the tanks was the presence of trapped air in the tanks. As a result the pressurizing ports required placement in a location that allowed for complete venting of the air trapped between ribs. It was determined that placing the ports on one of the end walls would allow for free venting of air, through the center of the tank, to the

highest location, preventing entrapment between ribs. This is best described by considering the illustration of Figure 21.

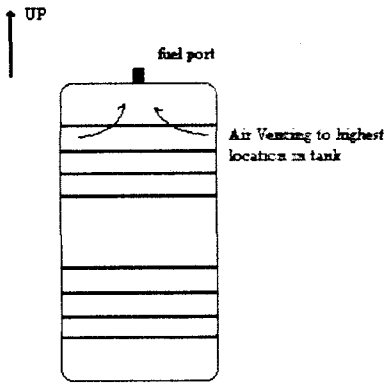

Figure 21. Illustration of air venting to highest location in the tank

As backing to the fluid transfer nipple, a 6.35 mm x 63.5 mm x 152.4 mm (0.25"x2.5"x6") steel plates was utilized which would be incorporated inside the composite cover. This avoids problems which occur in attempting to thread pressure ports into the composite over-wrap. The steel plates would be pressed flat against the composite wall as pressure was applied. This backing plate eliminated the risk of having the nipple pull out of the tank composite walls during pressure testing. The nipples were first threaded, then welded, through the center of the plate. As an additional step, air release holes were drilled into the side of the nipples that protruded into the tank to prevent air entrapment when filling the prototypes with water. Each pressurizing plate was then counter sunk into the foam plug at an end wall. As a final step, the core was covered with an epoxy coating to protect the foam and bond the steel plates to the foam cores.

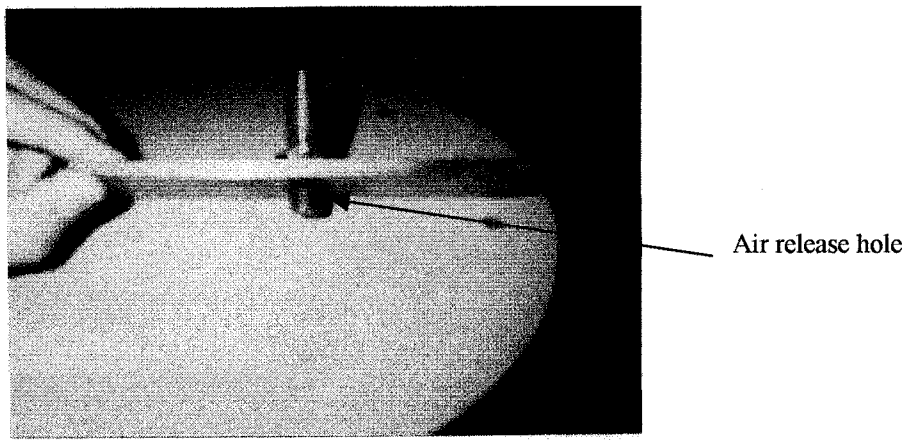

Figure 22. Pressurizing plate used on prototype tanks

6.4.1 Lay-up Procedure and Materials

The use of a polystyrene core dictated the use of epoxy for the polymeric matrix used with the fiberglass reinforcement. The epoxy manufacture's representative assured the author that the cured epoxy would not dissolve in acetone. Polyester would not be a suitable matrix for use with this manufacturing approach due to poor resistance to the acetone used to dissolve the foam core. To allow for more flexibility in the lay-up of subsequent patterns during construction, an epoxy with a one-hour pot life was used. Longer pot-life proved useful in allowing time for the adjustment of fiberglass layers as they were applied.

Composite over-wrapping of the single shell design was a two-stage process. Filament wound ribs were first wrapped followed by a bi-directional mat over-wrap over the entire tank. One area of the concern was the location where the filament windings from the ribs met the mat over-wrap. Ribs integrated into the wall

prevented the formation of high bending stresses that would otherwise lead to failure in the flat walls of the tank. Separation of the ribs from the walls would most certainly lead to failure. As a result precautions were taken to ensure that the ribs were adequately tied to the walls, as discussed in the next section.

6.4.2 Filament Winding

Filament winding the tanks required the construction of a filament winder. Construction of the filament winder was kept as simple as possible. The main objective of the winding device was to provide a method of continuous wet out of the fibers, as they were pulled through the apparatus. Originally, the filament winder consisted of a tube with multiple bends filled with epoxy. The tubes were supported with a simple plywood stand.

The first version of the filament winder used 25.4 mm (1") diameter clear PVC tubing. Problems were first experienced trying to thread the fiberglass tow through the 838 mm (33") long tube. Once the fibers were threaded through the tube, the first prototype tank was readied for filament winding. In order to tie the ribs into the flat walls, thin fiberglass mat was tucked into the rib grooves prior to filament winding. The mat ran up the sides of the ribs and onto the surface of the foam core where the fiberglass mat would be placed. Periodically, at approximately every 12.7 mm (0.25") increase in rib depth, an additional layer of mat was placed into the ribs and wound over with tow. Flaps of fiberglass mat, resulting from the excess exiting

the ribs, spread out over the top surface of the foam plug. The flaps were later laid up and joined with the general fiberglass outer wall, ensuring that the ribs would remain tied to the walls. The method of tying the ribs to the walls is better illustrated in Figure 23.

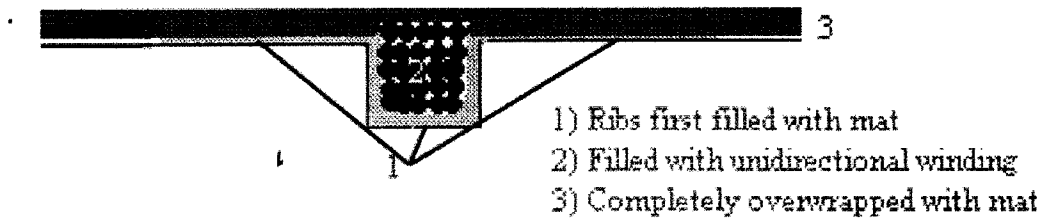

Figure 23. Illustration of method of tying ribs to walls

The first attempt to filament wind glass onto the ribs with the winding apparatus was unsuccessful. When the clear tubing was filled with epoxy, the viscosity of the liquid polymer generated shear stresses so great that it was impossible to pull the tow through the tube. After two revisions, 50.8 mm (2") tube with one U bend was used successfully in the winding apparatus. A photograph of prototype 1, in the filament winding stages is shown in Figure 24.

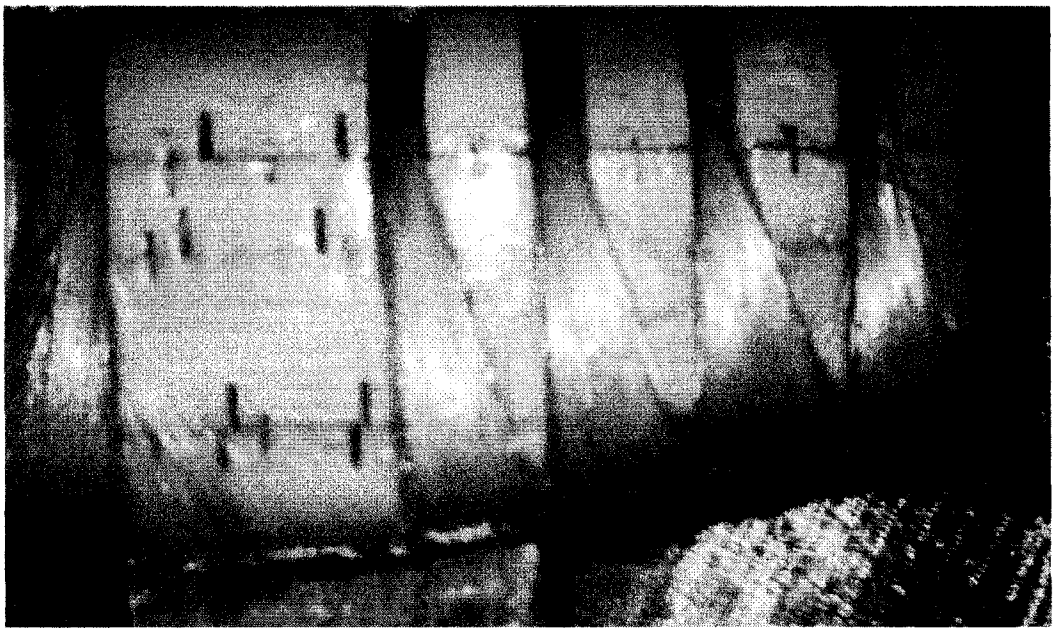

Figure 24. Prototype 1 During Filament Winding

6.4.2 a) Exotherms

Once the filament winder was modified and used successfully, filament winding became quite efficient. During the second attempt at winding the ribs on the first prototype, a significant problem occurred. Once an approximately 8 mm thickness of tow was wound into the ribs an exotherm occurred.

Prior to prototype construction, the possibility of developing an exotherm during the lay-up procedure was recognized. The term exotherm, used in the composites industry, refers to the exothermic curing reaction of the epoxy. However, the reaction can be controlled provided that the rate of external heat loss is sufficient to match the amount of heat generated. To control this, epoxy layers are applied in multiple stages when thick parts are laid up. The epoxy supplier recommended that

no more than between a 8.4 mm to 12.7 mm (0.33" to 0.5") thickness be applied during each stage of the lay-up schedule.

Even though the thickness of the tow at the stage the exotherm occurred was not greater than the allowable value, one consideration was not taken into account. Material utilized for the foam plug is the same foam rated at a R2000 insulation value. The insulating properties of the foam prevented the heat loss necessary to keep the exothermic reaction controlled. Trapped heat raised the temperature further increasing the rate of reaction. The unstable reaction occurred until the epoxy was completely polymerized in its cross-linked state. Heat generated by the exotherm resulted in the deformation of the foam core, so that construction on prototype one ceased. Attention then focused on the construction of a similar prototype 2 and the completely new design of a third and final full scale prototype.

6.5 Pattern Designs for Bi-directional Mat Over-wrap

Locations of seams, or discontinuities, in the bi-directional fiberglass mat over-wrap are locations of weakness in the tank. In the design of patterns for the fiberglass mat over-wrap, careful consideration was given into the locations of seams on each ply of fiberglass. It was the goal to ensure that, within a quarter inch of over-wrap, no seams would lay on top of each other. Additionally, patterns allowed for some overlapping by having the same layer fold back on itself at the seams. The

24oz fiberglass mat used had a predicted thickness of approximately 1.58 mm (0.0625"), when completely wet-out with epoxy. Four plies would result in a wall thickness of 6.35 mm (0.25"), five plies were expected to result in a thickness of 7.94 mm (0.3125"). Five plies would provide for a more conservatively constructed tank.

Five different patterns were designed, one pattern per ply. As a result of the pattern designs, no seam lay on top of another, within five plies of fiberglass mat. The ply designs are laid out in Appendix III, and are numbered in order of lay-up schedule. During tank construction, a small hole cut in the fiberglass mat allowed for the presence of the pressurizing nipple on the one end wall of the tank.

6.6 Lay-up of Second Prototype Design

The second, 457 mm x 292 mm x 178 mm (18"x11.5"x7"), prototype foam core was filament wound at a significantly slower rate then the first prototype design. Special care was made to ensure that the depth of the uncured tow windings never exceeded 6.35 mm (0.25"). Between each 6.35 mm deep winding, a layer of thin, fiberglass body repair mat was placed into the ribs to ensure the ribs were effectively tied to the exterior walls. As result of the 1 ½ hour time required for partial curing of the epoxy before subsequent windings, the total time for filament winding was slightly over 12 hours.

Over-wrapping of the exterior walls was conducted in two stages. The first stage involved the lay-up of the first two plies, immediately after filament winding of the ribs was completed. The reason for the timing was to maximize cross-link density in the epoxy between the last filament windings and the wall fiberglass mat. If the epoxy in the ribs partially cured, the cross-link density between the epoxy in the ribs and the first layers of mat would be reduced. Laying the first layer of fiberglass mat on the ribs before the epoxy cured, allowed for complete cross-linking between the epoxy in the fiberglass mat and toe. The remaining three layers were then over-wrapped resulting in an approximate total wrapping time of 16 hours.

6.7 Full Scale Third Prototype

Following the destruction of the first prototype from the exotherm experienced during filament winding, a third and final prototype, based on full scale dimensions, was developed. As a result, two of the three dimensions were set to those of a full-scale design. The resulting dimensions resulted in internal tank dimensions of 559 mm x 559 mm x 305 mm (22"x22"x12"). Considering a 12.7 mm (0.5") over-wrap on all the walls and an approximate additional 25.4 mm (1") thickness of excess tow, resulting from shallower ribs on the bottom of the tank, exterior dimensions of 584 mm x 584 mm x 343 mm (23"x23"x13.5"), were expected.

6.7.1 FEA Modeling of the Third Prototype

As the foam core for the third prototype was being constructed, a finite element analysis of the proposed design was modeled. This design was based largely on the fact that earlier models, with conservative assumptions for material properties and frequent rib spacing, were overbuilt. Additionally, having experimental results of a full-scale dimension design would validate models at full-scale dimensions. Concerns over the uncertainties of similtude on smaller scale models, would also be addressed by testing the behavior of the full-scale design.

The loss of volume resulting from the step profile on the bottom of the tank remained a concern. As a result the steps were eliminated in the design of the bottom of the tank. In place of the steps, 25.4 mm (1") deep ribs were used across the bottom span of the tank. Rib depths were 76.2 mm (3") on the side and top walls of the tank. The rib thickness was 25.4 mm (1") around the entire rib, in all three ribs. On the bottom of the tank, the excess filament winding was dispersed across the bottom surface as effectively as possible. Any uneven profiles on the bottom of the tank would be corrected through the use of rectangular cut, fiberglass mat patches between the rib windings. It was also hoped that the thicker walls on the bottom of the tank would account for the loss of rigidity from the shallower ribs compared with the top wall. The first two ribs were spaced 127 mm (5") apart, with the third placed 203 mm (8") from the other two. The spacing between the last rib was increased to model

the deflections of the area in which the 190.5 mm (7.5") fuel port was proposed to be located on a production tank.

An example of finite element analysis of deflections shown in Figure 25 for this tank design revealed significantly high deflections on the largest unsupported span. This span was on the end walls, or the non-ribbed side of the tank with the 559 mm x 305 mm (23"x12") dimensions. Stress concentrations, shown in Figure 26, were located at the rib corners between the large lower wall and side wall were also of concern. However, the stresses in the rest of the tank appeared to lie within the set limit of 20ksi in the remainder of the tank. As a result of the computer models, an additional, 2" deep, diagonal rib on the end wall was incorporated into the construction of the foam core in an attempt to reduce the deflection.

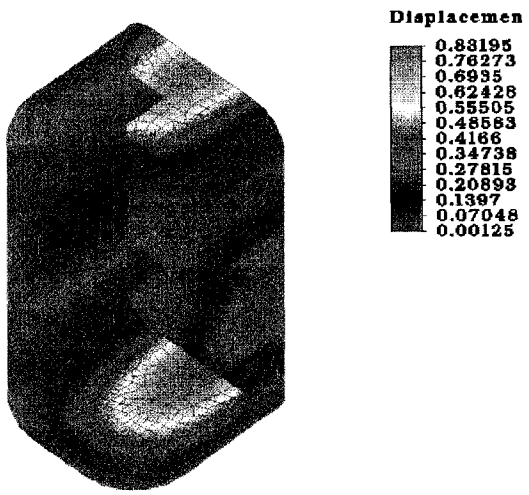

Figure 25. Deflection predictions on third prototype design proposed (displacements in inches at 250 psi)

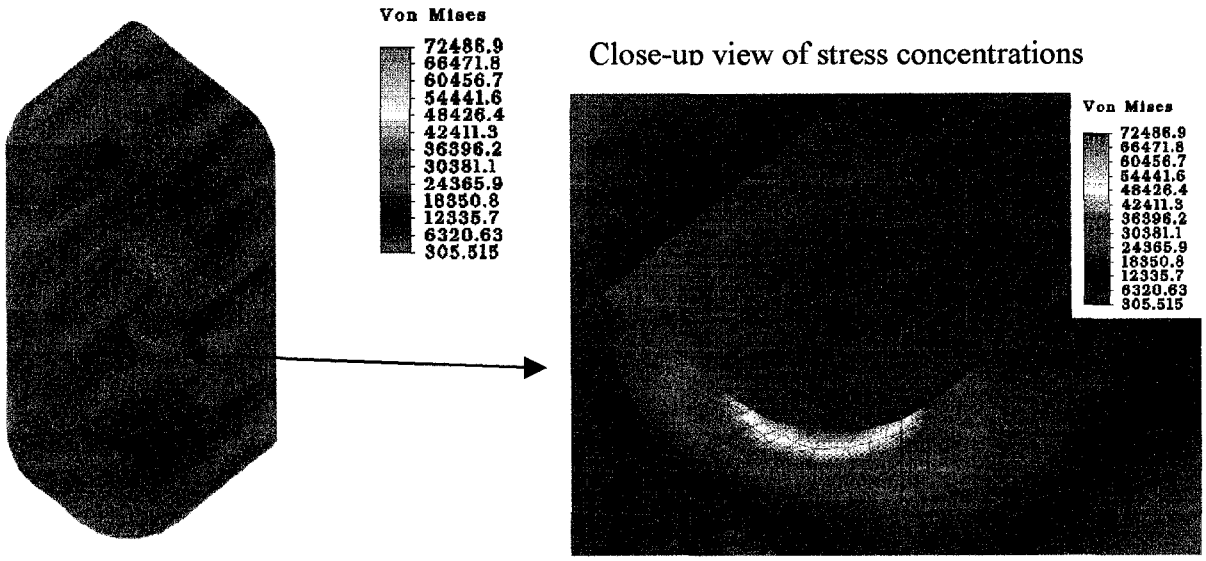

Figure 26. Stress concentrations at rib corners between large lower wall and side wall (Stresses in psi at 250 psi internal pressure)

6.7.2 Construction of the Third Prototype

Once the final prototype foam core construction was completed, the construction procedure followed the same sequence as that of the second prototype. As a result of the thicker ribs, heavier weight mat was used to tie the ribs into the walls of the tank. Filament winding of the ribs took place over a 24 hour time period. After the completion of rib winding, rectangular patches were laid-up, in stages, on the bottom of the tank. In total, nine layers of fiberglass were required to smoothen out the transitions between the overflow of filament windings on the bottom ribs of the tank.

The patterns for the bi-directional mat over-wrap of the third prototype utilized scaled up designs of those used on the ½ scale prototype. The first two

fiberglass layers, patterns 1 and 2, were laid onto the tank following the application of the last patching layer. The remaining 7 plies of the fiberglass were applied in two final stages, 4 hours apart. Tank over-wrapping, including winding the ribs, required approximately 40 hours to complete.

6.8 Removal of the Foam Cores

Prior to implementing the use of the prototype construction with dissolvable foam cores, simple experiments were conducted. Results from these experiments, involving dissolving polystyrene blocks, confirmed the feasibility of the proposed prototype construction method

The smaller, second prototype, required significantly less acetone to dissolve the inner core than the larger, third prototype. Acetone was used only after the epoxy had cured for a minimum of 36 hours. The minimum recommended cure time was based on information obtained through a supplier representative. In addition, the supplier confirmed that epoxy would be resistant to the acetone used to remove the foam.

While dissolving foam in the preliminary, simple experiments, an important observation was made. Acetone added to the foam would be absorbed until the foam was completely dissolved. Once the foam was dissolved, no additional acetone was absorbed and the excess formed a puddle. This information proved useful in

determining when the foam core was dissolved. In both tanks, acetone was added to the tanks until the addition of further acetone could be poured back out of the tank. Prior to attempting to pour out the contents of the tank, the tank was rolled around and held at various orientations. This ensured that acetone had time to react with the polystyrene foam and all interior surfaces were exposed to acetone. In the case of the small prototype tank, 1.5 liters of acetone was used to dissolve the foam out of the 20.9 liter interior volume. The larger tank required over 4 liters of acetone to dissolve the foam out of the 83.4 liter interior tank volume.

6.9 Prototype Weights

In addition to the tank volumes, the weight of the tanks was another important consideration in the development of prototypes. The second prototype weighed in at approximately 11.8 kg (26lb). Considering the 20.9 L volume of the prototype, the calculation of the tank volume to weight factor resulted in 1.77 L/kg. In the case of the third prototype, the tank weighed just under 48.2 kg (106lb). Similar calculations into the volume over the weight ratio, resulted in 1.73 L/kg. In comparison, the Thiokol tank provides a volume over weight ratio of 3.02 L/kg.

Chapter 7

DEVELOPMENT OF A PRESSURE TESTING SYSTEM

7.1 Objectives

A significant portion of model validation required the development and set-up of experimental apparatus. Testing equipment was required to provide a means of pressure testing the prototype tanks. Additionally, a Data Acquisition System, DAS, was required for the acquisition of experimental strain and displacement values obtained during testing. As a final step, a location for testing was selected with consideration of a means of containing any explosion that might occur as a result of pressure testing.

7.2 Pressure Testing Apparatus

The tank designs were based on a pressure design factor of four. As a result, the validation of any tanks required that tanks could successfully hold a 6.9 MPa (1000 psi) pressure without failure. The method of pressurizing fluid therefore had to be capable of pressurizing water to a minimum 6.9 MPa (1000 psi) pressure. To accomplish this, a dual cylinder arrangement, illustrated in Figure 27, was used.

The cylinder arrangement utilized a 50.8 mm (2") diameter cylinder, with a 152.4 mm (6") stroke, and a second 25.4 mm (1") diameter, 305 mm (12") stroke cylinder from a previous project. A mobile hydraulic power pack, comprising a fluid

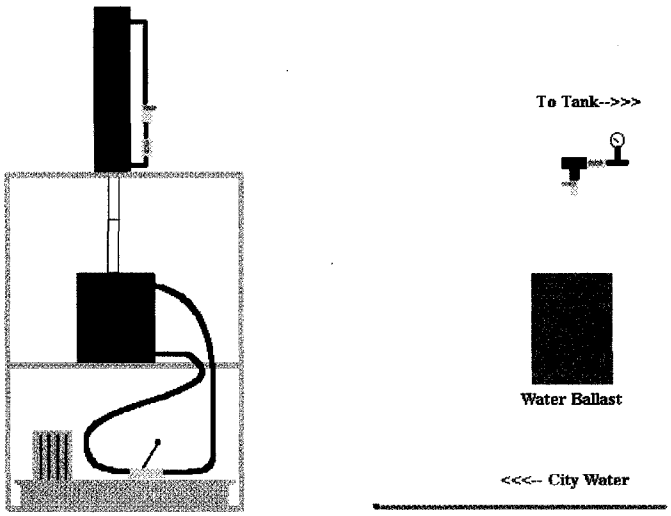

Figure 27. Conceptualized design of pressure testing apparatus

reservoir, a pump and a hand operated 3-way valve, where incorporated into the design of a stand that supported the hydraulic equipment. Modification to the design was required to convert the existing hydraulic, polymer forming apparatus into one suitable for pressure testing.

As a first step, the hydraulic lines were removed from the smaller 25.4 mm (1") diameter cylinder and reconnected to the larger 50.8 mm (2") diameter cylinder. This operation allowed the apparatus to develop the largest possible pressure the hydraulic pump was capable of producing. Simple hand calculations indicate the

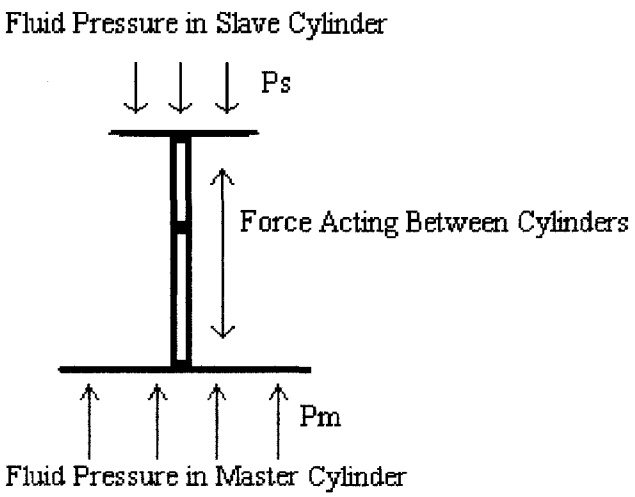

Figure 28. Forces acting in a dual cylinder arrangement

validity of this approach. Setting the forces acting on each cylinder equal to each other and balancing forces:

$$Fm = Fs$$
$$PmAm = PsAs$$
$$\frac{Pm\pi dm^2}{4} = \frac{Ps\pi ds^2}{4}$$
$$Ps = Pm\frac{dm^2}{ds^2}$$

Where *dm* and *ds* are the diameters of the master and slave cylinder respectively

The resulting equation illustrates that, assuming pressure in the master cylinder is held constant, the pressure in the slave cylinder is elevated by increasing the ratio of master cylinder diameter over slave cylinder diameter.

A remaining concern in the development of the pressure testing apparatus, was the method of filling the slave cylinder with water. Any method selected had to ensure that air was not drawn into the cylinder chamber. Additionally, the volume of water in the 25.4 mm (1") diameter cylinder could provide was limited to 0.077 L (4.7 in^3), a volume significantly less than that of the tanks. This is a result of the small diameter of the 25.4 mm (1") cylinder and the limited 152 mm (6") stroke of the 50.8 mm (2") diameter cylinder.

To solve this problem, a system of hoses and valves were arranged in a manner that permitted the recharging of the slave cylinder while pressure was maintained in the tank being tested. Once an entire stroke of the slave cylinder forced

water into the tank, pressurizing the fluid, the line to the tank was closed off with a gate valve. A second gate valve was opened while the slave cylinder stroke returned to its starting position. As the cylinder moved back up, water in a ballast tank was drawn up into the cylinder, in a manner similar to the operation of a medical syringe. The valve to the ballast tank was then closed and the tank valve re-opened to allow for the next pressurizing cycle. The process could be repeated as many times as necessary to pressurize to failure pressure, or to the limits of the pressure testing apparatus.

Originally, it was proposed that the prototype tanks be filled by multiple cycling of the pressure testing equipment in the manner described above. However, the arrangement could only provide water at a rate of 0.003 L/s (0.22 in^3/s)$^{\neq}$. To increase the rate at which fluid could be added the design was further revised. This revision utilized one additional valve to take advantage of the available city water pressure. The third valve permitted the attachment of a city line (garden hose) to the pressure testing equipment. With appropriate valve positions set, the prototypes could be quickly filled with city water. Additionally, the set-up allowed for integral filling of the ballast tank, and if more suitable, elimination of the need of the additional water ballast. The fact that apparatus was designed so city water could be utilized, in addition to a ballast tank, made the apparatus more efficient for the initial tank filling.

In addition, to valve modification and line rearrangements, a pressure gauge and bleeder where added to the apparatus. The pressure gauge operated from 800 kPa to 20.7 MPa (150 to 3000 PSI), and a check valve was added to the separate line to the pressure gauge. The check valve served to record the maximum pressure attained, in the prototype tank, in the event of tank failure. Finally, the bleeder valve allowed for the manual release of pressure from the prototype tank and pressurized lines when testing was completed.

7.3 The Data Acquisition System

As part of the experimental set-up, a Data Acquisition System, DAS, was required for the acquisition of experimentally measured values. Two physical measurements were required to provide for data correlation of the computer models. ALGOR FEA software capably provides predictions of deflection, stress and strain in analysis models. Devices for the measurement of deflection and strain are commercially available. Stresses could be predicted, from measurements of strain, using available material property estimations.

7.3.1 Sciemetric System 200 Upgrade

The Sciemetric System 200, used for the acquisition of data, is based on an

---

* Based on a measure average 21 second time for one 6" stroke

industrial style, modular chassis. The chassis itself contains an integral power supply with three individual modules. An integrating A/D converter module, Sciemetric model 231, provides signal conditioning and provides an internal instrumentation amplifier for voltage ranges from 10mV to 10V. Attached in series to the A/D converter module is a 32-channel expansion module and a bridge/strain gauge conditioning module.

Upgrading of the data acquisition system was required on the model 206A, bridge/strain gauge board. The original system was set up with two of the eight available bridge circuits utilized. To expand the board to its full 8-channel capability, three 120 Ohm precision resistors were added to each bridge for completion of the quarter bridge circuitry. In addition to modifications to the 206A board, jumpers between five channels were added to the 32-channel expansion module board.

7.3.2 Quarter Bridge Circuit

Revisions to the 206A board utilized a quarter bridge configuration, with 3, 120 Ohm, precision resistors on each bridge circuit. The final completion resistor for the bridge was the 120 Ohm strain gauge used for the measurement. The voltage output, due to any change of resistance in the strain gauge, was the resulting measurable quantity with this bridge configuration.

Although a separate area for the completion resistors was available on each of the "baseball-diamond" bridge channels, reduction in the number of resistors was accomplished through common use of the right arm of the bridge. Only the first bridge used three resistors to complete the circuits. Since essentially the resistance only changes in the left arm, assuming that R_1 is the strain gauge, the right arm effectively only provides a reference voltage. The reference voltage is the same for all right arms of subsequent bridges, so jumpers running between the right arms of the bridges were utilized. Utilizing this approach resulted in eliminating the need of 14 precision resistors.

The quarter-bridge design also uses a three wire, measurement configuration. Two of the wires running to the strain gauge supply power to the gauge, while the third is utilized as the signal wire. The signal from the gauges was then passed through the 32-channel expansion module to the integrating A/D converter module. The signal was then supplied to the data acquisition software via a PC interface card.

7.3.3 Linear Voltage Potentiometers

Linear voltage potentiometers were used for measurement of deflection. The potentiometers used for acquisition had a maximum 152.4 mm (6") stroke. Integration of the deflection measurements with the potentiometers required further modification to the 32-channel expansion module.

Linear potentiometers work on different operating principles than strain gauges. The potentiometer body is a long axial coil of resistance wire. In most cases the potentiometer coil has one end at ground and the other at a constant supply voltage (say +10V). The measurement arm, brushes against the coils at some point to short out the remainder of the coil at that point along the length of the coil. When the potentiometer arm is fully withdrawn the signal voltage is that of the ground value, typically 0 volts. As the arm is pushed further into the coil, the voltage signal increases linearly until it reaches that of the supply voltage when it is at the end of the stroke.

One advantageous feature of the bridge/strain conditioning module, was that it had it's own internal power supply. This eliminated the need for a separate power supply for use with the potentiometers. To fully integrate the circuitry, 5-channels on the 32-channel expansion module were wired for use with linear potentiometers.

Wiring required that the individual channels all be grounded to provide a reference voltage for the processing of the return signal. To accomplish this, one channel was grounded to the ground location from the power supply on the bridge/strain conditioning module. The remaining channels were grounded together via jumpers running between channel locations. Additional channels could be easily added, through running additional jumpers referenced to the same ground.

A feed line, from the bridge/strain conditioning module power supply, was used to power the potentiometers. The power supply, as mentioned earlier, was capable of providing up to a 10 volt, supply voltage. The use of the 10 volt power supply made the conversion of voltage to the displacement easy. Due to the linear behavior of the potentiometers, the displacement was calculated as 15.2 mm (0.6") per volt.

7.3.4 Data Acquisition Software

The use of software for data acquisition was limited to DOS based packages. This was due to the fact that the Sciemetric™ data acquisition system interfaced with an IBM XT™ computer. Software had previously been loaded onto the computer for data acquisition.

Sciemetric Gen200™, DOS-based, data acquisition software was used for measurement of the data from the acquisition. Due to unfamiliarity with the software and the absence of user manuals, considerable time was required to learn how to effectively use the system for data acquisition. As a consequence, a complete, step by step, operating procedure has been developed for future reference to new users of the equipment. The manual does not go into the specific details on the fundamentals of the software, rather, it will walk the user through the steps necessary to acquire experimental data. Contents of the operating procedure are included in Appendix IV, for reference.

7.3.5 Debugging the Data Acquisition System

To ensure that data would be properly attained during experimental testing, a mock sample was tested to reveal any existing errors or problems. One concern was the possibility of errors occurring from strain gauge heating as a result of the applied voltage. To determine the effect on errors resulting from heating, a sample with both a non-glued (only taped) and a glued strain gauge was tested. The results showed that drift, in the reference values of strain, did occur only in the first two minutes of powering the gauges. However, the drift leveled out to constant reference values in the case of both gauges.

The results of this test did reveal one potential problem. Although strain gauge heating did not pose a significant problem to errors resulting from drift, it did cause an additional problem. One gauge got so hot that the foil on the gauge burned, resulting in the destruction of the gauge. This was the taped gauge which had no heat sink for heat transfer. An additional concern, was that the power drawn from the bridge module, to power both the potentiometers and strain gauges, was reaching maximum capacity. To alleviate both problems, the supply voltage to the bridge circuits was reduced from 10 volts to 5volts. This not only reduced the power heating the gauges, see Table 4, but also assured that sufficient power would be available to power the potentiometers at 10 volts.

Excitation Voltage	Gauge Power (milliwatts)
0.1	0.003
0.2	0.010
0.5	0.063
1.0	0.250
2.0	1.000
3.0	2.250
4.0	4.000
5.0	6.250
10.0	25.000

Table 4. Comparison of gauge power vs. excitation voltage

7.4 Instrumentation of the Prototype

Instrumentation of the prototypes involved the attachment of strain gauges and associated soldering of wires to the strain gauge terminals. Locations for the strain gauges were based on locations of maximum stress in the computer models. To reduce the effect of localized strains, due to the nature of fiberglass, longer, 6.35 mm (0.25"), strain gauges were used to obtain a better, average of strains in the locations investigated.

The installation of strain gauges required five steps. As a first step, the area of strain gauge application was rough sanded and cleaned. This was done in an attempt to get a better bond between the gauges and bonding surface. Next, the strain gauges

were carefully removed from their individual packages. The bonding agent, polyester cement, was then mixed in small quantities, and placed on the bonding surface. Strain gauges were picked up with 3-M™ scotch tape, sticking to the top surface of the gauge, and placing them down on the glue covered bonding surface of the tank. Air pockets were carefully squeezed out to ensure that the bonding surface was free of voids.

Once the bonding agent had cured for several hours, the tape covering the top of the gauges was removed. Wires[≠] for the strain gauges were then soldered onto the connection terminals of the gauges. As a final step, gauges and wires were covered with a coating of epoxy that served as a protective layer and an additional bonding agent.

Final instrumentation included running 6.1 m (20') wire lengths from the data acquisition system to the elevated testing location. Each bridge required an individual wire, so eight of the eleven 6.1 m (20') wires were required for the strain gauges. Because the potentiometers could all run on a common power supply, only one 6.1 m (20') feed wire was needed for the potentiometer power location. The return signal from each potentiometer arm required 1 wire strand. In an effort to utilize all three strands in each wire, individual strands from each wire were used for each potentiometer. The first three potentiometers utilized three strands in one 6.1 m

[≠] Wire used was three strand. 24 gauge, silver-plated insulated wire.

(20') wire length, the remaining two utilized two of the three strands in one additional wire.

7.5 Selection of Pressure Testing Location

Careful consideration into safety was given in the selection and construction of an appropriate pressure testing location. Due to the expected high failure pressures, a location that would contain any explosive forces was desired. A location formerly used to conduct river mechanics experimental research was chosen for testing. Within the river mechanics laboratory, an elevated erosion channel sat unused and completely drained. The rectangular shaped channel had 25.4 mm (1") thick plexiglass on the side and bottom walls supported by relatively heavy steel angle iron and I-beam sections. The clear plexiglass would be useful in observing the test, while providing significant protection against projectiles in the event of catastrophic failure of the experimental tanks.

To isolate any damage to one location of the channel, additional precautions were taken. The channel was significantly longer then required; in addition, the ends of the channel had gates and other apparatus that appeared to be susceptible to damage. As an extra precaution, sand bags where stacked across the width of the channel, effectively forming a rectangular barricaded volume in which the testing would take place. Finally, a top ceiling of three plies of plywood, weighed down with

additional sandbags, was used to prevent damage to anything above the pressure testing location.

7.6 Final Details

With all construction, or modification of experimental apparatus complete, only a few remaining tasks required completion. Once the tanks were placed in the testing location, strain gauge wires from the tanks were soldered to those running to the data acquisition system. After the process of filling tanks with water was completed, the tanks were carefully positioned for pressure testing. Care was taken to ensure that the tanks were supported in a manner that did not restrict the deflection of the walls under pressure. In the case of both single cavity designs testing, the tanks were place inverted onto the wall containing the pressurizing port. Wood blocks, placed at the location of minimal deflection on the fuel port wall, supported the tanks and provided space for the routing of pressure lines to the tank.

With all fittings and wiring in place, the remaining potentiometers were easily placed in the proper locations. Rigid retort stands were used as fixtures for the potentiometers. The instruments were carefully placed in the measured center of the five available walls. In locating the devices, the ends of the potentiometer arms were placed against the tank walls, providing an initial displacement. This compressed the internal spring of the potentiometer. The resulting reaction force, between the tip of

the potentiometer arm and the tank wall, ensured that the contact was maintained at all times during pressure testing.

Chapter 8

PRESSURE TESTING OF THE TANKS: GENERAL RESULTS

8.1 Introduction

With the final details in the experimental set-up complete, pressure testing could commence. Both prototypes were tested in an identical manner. After filling the tanks with water, the data acquisition system was turned on to allow strain gauges to heat to the equilibrium value.

8.2 Testing Prototype 2

The second prototype was pressure tested a total of three times. This was due largely to problems with the experimental set-up, and significantly lower then expected failure pressures.

8.2.1 Test 1

During the first test, it became apparent that the operating range of the pressure gauge would not be suitable. The original pressure gauge selected operated between 800 kPa and 20.7 MPa (150 and 3000 psi). A gauge that read a 6.9 MPa (1000 psi) value was desired because successful validation of the prototype, with a design factor of 4, required that a 6.9 MPa (1000 psi) pressure be held. At the time of

purchasing pressure test equipment, the next closest gauge operated between 345 kPa and 5.5 MPa (50 and 800 psi), which was not sufficient to test the tanks at 6.9 MPa.

After filling the prototype, the data acquisition systems was set to acquisition mode to record the reference values at no internal pressure. Internal pressure was first applied by city water pressure. While pressurizing the tank to city pressure, occasional cracking of the epoxy matrix was audible. Once the tank reached city water pressure, the tank was held at this pressure while the slave cylinder was being filled with a water charge. During this time the crackling of the matrix, heard earlier, ceased. At this point, the pressure gauge did not read any value (ie. $p<800$ kPa).

With the cylinder filled with water, the hydraulic pump powering the master cylinder was turned on. Direction of cylinder motion was controlled by a single, three way, manual control valve. Three positions were available, a neutral position, one that forced upward movement (used for charging the cylinder) and one forced downward motion (pressurizing stroke).

The slave cylinder was gradually lowered, pressurizing the prototype. During the first test the cylinders were slowly lowered, by toggling the control valve. It was hoped that by slowly increasing pressure, impact loading of the brittle epoxy matrix would be reduced. Throughout lowering the cylinder during the first stroke, crackling of the matrix was audible. When the cylinder reached the bottom of the stroke, the pressure line to the prototype was shut off to allow for recharging of the slave

cylinder. Once the cylinder was ready to provide a second stroke, the valve to the prototype line was reopened. At this time a much louder "snap" was heard. The pressure gauge still failed to register the pressure in the line. Observing the prototype, through the plexiglass walls, a small trickle of water was apparent on the bottom wall of the tank. The loud snapping noise, and the visible appearance of water, led to the belief that the tank failed. Pressure in the lines was bled off to allow for visual inspection.

Visual inspection revealed that source of the water was for the most part, microscopic. The area at which the leak source was located, could be traced back from the water trickle. However, once the water was wiped off, the source of the leak was not visible. Inspection of the remainder of the tank indicated that the structure was intact, and that the only source of leakage was at the source previously mentioned.

8.2.2 Test 2

After visual inspection revealed no signs of structural damage on the prototype, the pressure gauge was temporarily replaced with a second gauge. This gauge operated between 0 and 690 kPa (100 psi). It was believed that the pressure at which the leak appeared, in the first test, was significantly below the 1.04 MPa (150 psi) lower indicator limit of the first gauge. Once city water pressure was applied, the second gauge read a constant 379 kPa (55 psi). Pressure was applied in increments

resulting in pressures of 621, 655 and 690 kPa (90, 95 and 100 psi). The corresponding position of the cylinder at 690 kPa (100 psi) pressure was the bottom of the pressurizing stroke.

Interestingly, after the cylinder was recharged with water, the valve to the pressure line was reopened. At this time, the gauge that was previously maintaining a 690 kPa (100 psi) reading, spiked to the upper limit peg on the pressure gauge dial. This indicated that some sort of shock loading occurred as a result of the recharging method.

The trickle of water re-appeared around the 690 kPa (100 psi) pressure. Limits of the pressure gauge forced the testing to end when the 690 kPa (100 psi) pressure was attained. It is also important to note that significantly less crackling was audible during the second test.

8.2.3 Test 3

The final test of the second prototype design occurred after testing of the modular tank built by Doug Bain was completed. Prior testing of both the single cavity and modular tank design revealed failure by leaking of water through micro-cracks in the epoxy matrix. This appeared to be inevitable without the use of an impermeable liner. It was later confirmed in the textbook by Callister [6] that liners are used in polymer composite pressure vessel to prevent leakage through the micro-

cracks that typically develop. The unfortunate problem, with the present tests is that they did not allow for determination of the actual load bearing abilities of the composite outer wall.

In an attempt to better estimate the capabilities, or the maximum failure pressure strength of the composite walls, a more aggressive pressurizing schedule was used. Rather then slowly pressurizing the tanks by toggling the pressure up slowly, the pressure was applied through continuous strokes of the cylinder. In this case, the first stroke raised the pressure from 380 kPa to 690 kPa (55 to 100 psi), the second from 660 to 795 kPa (100 to 115 psi), third from 794 to 931 kPa (115 to 135 psi), the fourth to 1 MPa (145 psi) and the final three strokes re-pressurized to a maximum of 1.03 MPa (150 psi). With each increment, the amount of water seeping out of the tank increased. Finally, between the fourth and fifth stroke, an additional leak developed around the pressurizing nipple on the tank. At this point the amount of water added could not overcome the volume lost and pressures higher than 1.03 MPa (150 psi) could not be attained.

Visual observation of the tank, during testing, revealed that the amount of water leaking out of the tank increased significantly after the 931 kPa (135 psi) pressure was attained. Water appeared to almost "gurgle" out of the same location the original leak was detected. In addition, a significant leak at the pressurizing port was clearly visible when the tank was observed at 1.03 MPa (150 psi). Crackling of the composite matrix became audible again after the 794 kPa (115 psi) pressure was

reached. Crackling of the matrix continued to occur until the 1.03 MPa (150 psi) maximum pressure was attained. It is important to note that no further loud snapping noises, with the same intensity of the first, were heard at any time during the last test.

Following pressure testing, the areas that leakage occurred were marked. Wiring was disconnected and water was drained from the tank. The tank was then sectioned using a band saw to inspect the interior for damage or defects that may be present.

8.3 Testing Prototype 3

Like the second prototype, the third prototype was pressure tested a total of three times. As in the second prototype, water leaked out through the walls via apparent micro-cracks in the composite matrix. In this case, however, water seepage through the walls began during the filling process, at a pressure lower than the city water pressure of 414 kPa (60 psi).

8.3.1 Test 1

The first pressure test occurred after visual inspection of the water seepage source had been conducted. Investigation into the source revealed that the water was leaking out through the walls at a tank corner. The exact source was not directly visible. Leakage points could only be traced back to the source by following the path

of the water trickle. Through further inspection, it appeared that water permeated through a 9 mm^2 (3 x 3 mm) area of the tank. This determination was made through wiping the location dry and observing the water permeate back to the surface.

Pressure testing commenced with the initiation of data acquisition at ambient pressure. As in previous testing, results attained at the ambient pressure would be used as the reference values. After approximately 1 minute, the tank was pressurized to city water pressure, in this case 414 kPa (60 psi).

Immediately following pressurization, significant crackling in the composite walls was audible. After a few seconds the crackling ceased, however inspection of the real time strain plots revealed that strains were gradually increasing. Pressure test equipment was then readied for the first pressurizing stroke.

The first pressurizing stroke increased the pressure in the tank to 483 kPa (70 psi). At this point, water began to exit through the micro-cracks at a much faster rate. A fine, fountain like spray began to shoot out of the source of leakage. Spray from this micro fountain, reached an approximate 25 mm (1") height before it began to fall downward.

Subsequent pressurizing strokes did not serve to increase the pressure in the tank. During each stroke, the 483 kPa (70 psi) pressure could not be exceeded. On the fourth stroke, a clearly audible, loud "pop" could be heard. Due to the intensity of

the noise, it was believed that a failure had occurred. One additional stroke was applied and before testing stopped.

After pressure was bled out of the tank, the tank was visually inspected for damage. Other than the source at which water the water was trickling out, no problems were visible on the exterior of the tank. The decision was then made to conduct a second pressure test.

8.3.2 Test 2

After reactivating the data acquisition system to obtain measurements for the reference position, the tank was once again pressurized to city water pressure. During this time, no crackling noises were heard upon pressurization to city water pressure. However water continued to slowly trickle out from the same tank corner.

The first pressurization stroke increased the pressure to 483 kPa (70 psi). As in the first test, water sprayed out of the corner at a much faster rate, forming the fountain like spray. No further noises were heard in the tank.

Numerous, additional pressurizing cycles were utilized to pressurize the tank to 621 kPa (90 psi). During this time, problems with the pressure gauge configuration became apparent. A communication error resulted in confusion in the order of valve positioning during a pressurizing cycle. As a consequence, pressure that built up in

the main line, was released into the tank. The check valve used in parallel with the pressure gauge, held the pressure that resulted from the spike. During the next stroke, the pressure did not increase above the reading on the gauge. At this point it was determined that accurate measurement of pressure from future cycles could not be made. Pressure testing was stopped and the tank was depressurized and once again visually inspected for damage.

8.3.3 Test 3

Prior to starting the next test, the check valve in the pressure gauge configuration was removed. All indications from prior testing suggested that the existing testing apparatus would not be able to pressurize the tank to a pressure that would result in catastrophic failure. The test limit appeared to be when the rate at which water could be supplied by the equipment was exceeded by the rate at which water was lost through the micro-cracks and/or other leaks. It did not therefore appear that a check valve would be useful for recording burst pressure. Without the check valve, the gauge could read current pressure, not just the highest pressures obtained during cycling.

As in all prior tests, the data acquisition system was turned on to allow for measurement of reference conditions. Testing was once again initiated by pressurizing the tank to city water pressure, 414 kPa (60 psi). The pressurizing

cylinders were continuously cycled to increase the pressure in the tank. After approximately 12 minutes, a pressure of 655 kPa (95 psi) was attained.

Immediately after the 655 kPa (95 psi) pressure was attained, a loud bang bellowed from the tank. Observation of the pressure gauge, however, did not reveal any drop in pressure as would emanate from catastrophic failure. The pressurization cycles continued until a maximum 828 to 856 kPa (120-124 psi) pressure was attained.

The pressure appeared to be limited to 856 kPa (124 psi). At this point, the height of the fountain like spray from the corner leak increased and fanned out in a wider radius. Between each cycle, the pressure would typically reduce 20.7 to 34.5 kPa (3-5 psi), as a result of the water loss from the cracks and a leak that formed around the filling nipple. On the eighth re-pressurizing stroke to 828 kPa (120 psi) a further noise was heard. This noise, significantly lower than the earlier bang, sounded more like the "pop" heard during the first test.

After fourteen additional pressurizing strokes did not result in any increase in pressure, testing was stopped. In this instance the data acquisition system was left on to record the relaxation of the tank through de-pressurization. Once the pressure fell below the 345 kPa (50 psi) lower limit on the gauge, the remaining pressure was bled out of the tank, concluding pressure testing of the third prototype.

Chapter 9

ANALYSIS OF EXPERIMENTAL PRESSURE TESTING DATA

Following the conclusion of pressure testing, the data recorded on the data acquisition system was processed. This involved configuring the data acquisition output files to account for voltage conversions and reference data taken at the zero load condition. Finally, data was displayed as graphs to provide a better visual representation of the measurements in question.

9.1 Updating the FEA Models

In addition to data processing, models of the prototypes constructed were re-analyzed in ALGOR's finite element analysis software. Validation of the computer models, with experimental results, required that the FEA models resembled the two constructed prototypes as closely as possible. Models had to account for areas on the tank that were thicker than predicted in original modeling, and the addition of a horizontal diagonal rib in the third prototype.

As a result of the addition of the diagonal rib, the Finite Element Analysis model of prototype 3 had to be reworked. Once the model wire frame was modified to include the diagonal rib, the model was re-meshed. Following meshing, the process of assigning material properties to the elements, as described earlier, was repeated. However, in this case, the addition of patching on the bottom, and wider

than anticipated strips of overflowed filament winding on the prototype, was incorporated into the final FEA model.

In addition to revising the models to include varying material properties, the models were analyzed under different load cases. Originally, all modeling performed used 1.725 MPa (250 psi) as the internal pressure. As part of the final simulation, the resulting models were analyzed at pressures for which experimental data was available. The revised, final FEA modeling results can be found in APPENDIX V.

9.2 Results-Prototype Two

Analysis of pressure testing results included both investigation into experimentally attained results and comparison of these with the results obtained by finite element analysis.

9.2.1 Data Acquisition Results

The second prototype was pressure tested three individual times. During each test, the data acquisition system was utilized to measure both strains and displacements resulting from the test. The potential for catastrophic failure, resulting from the aggressive pressurizing schedule used in the third test, was a concern. As a precaution potentiometers, susceptible to damage, were removed during the test.

Displacement data is therefore only available for the first two pressure tests of the second prototype design.

Strain Gauge positions are indicated in the following figures. Figure 29 shows the locations of the strain gauges on the interior wall. Figure 30 reveals the locations of gauges on the exterior of the tank. FEA predicted principal strains are shown in Figures 29 and 30. Principal strains were utilized with the assumption that these strains will act in the hoop direction. This was verified through investigating strains in off-principal directions using the FEA models. Due to the insignificance of strains in other than this principle direction, strains compared with experimental data were approximated with the maximum or minimum principal values, depending on the load direction.

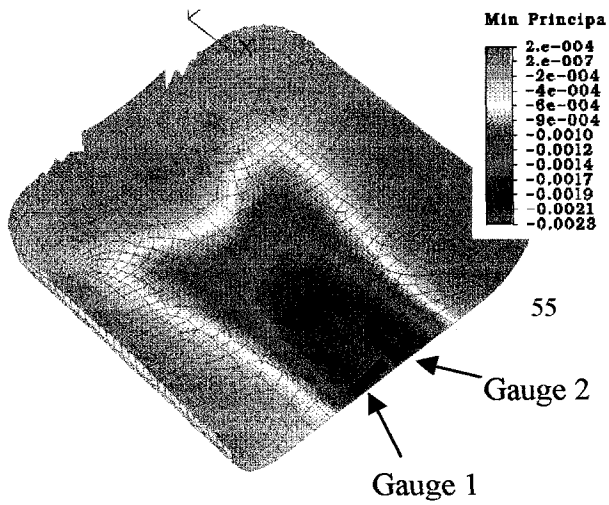

Figure 29. Illustration of the predicted principal strain results on the interior wall at 380 kPa (55 psi)
(Black lines, orientated in the strain gauge direction, show location of gauges)

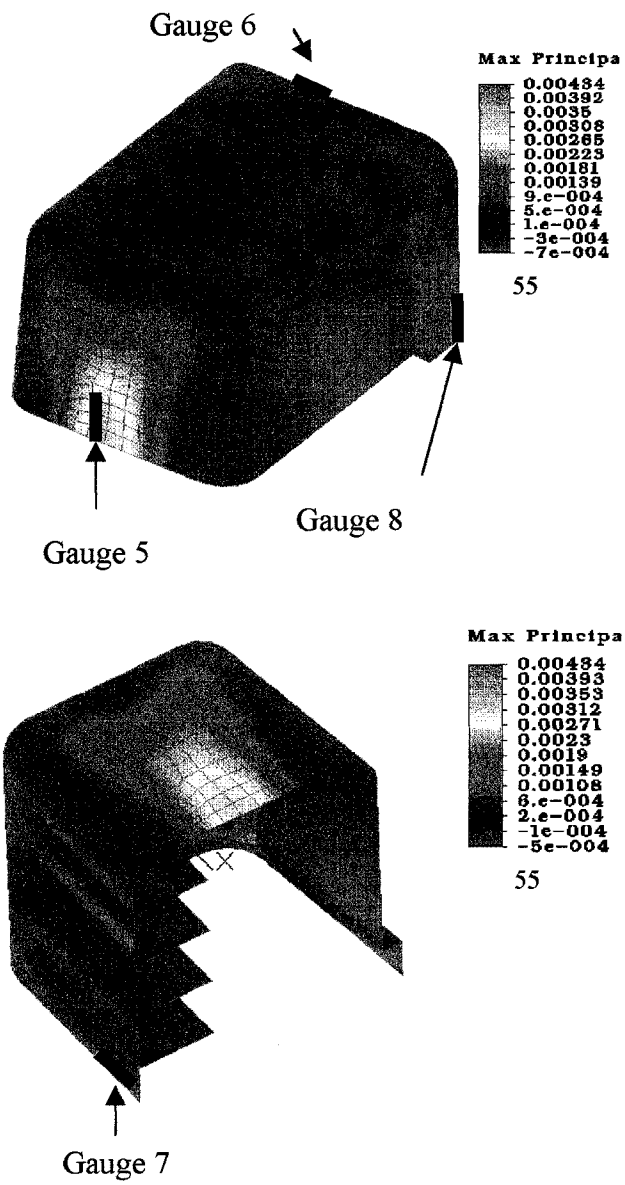

Figure 30. Illustration of the FEA principal strain results on the exterior walls at 380 kPa (55 psi)
(Black lines, orientated in the strain gauge direction, show location of gauges)

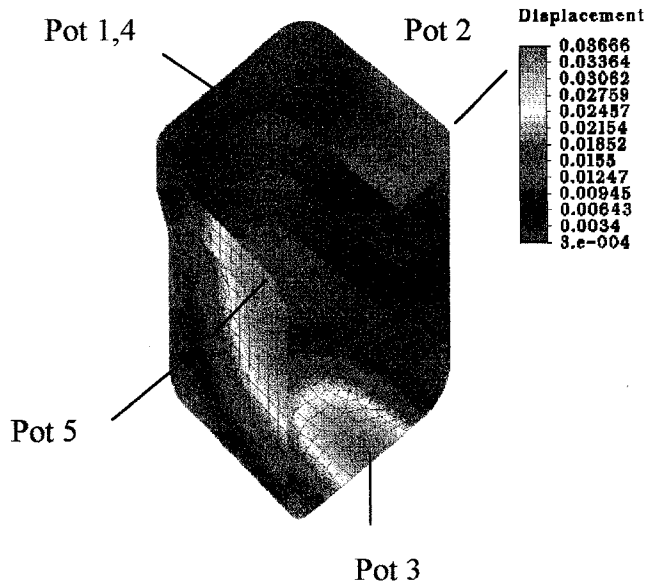

Figure 31. FEA predicted displacement (inches) results for prototype 2 at 380 kPa (55 psi) showing locations of potentiometer arms. Potentiometers 1 and 4, positioned on opposing walls, are shown together because of the tank symmetry which results in the same FEA predictions for both side walls.

Through analysis of the data, differences in both the strains and displacements between subsequent tests are visible. The first notable difference is the increase in the magnitudes of the values during each successive test. Figure 32 graphically illustrates this result. Please note that in the following comparisons the absolute values of strain were used. Strains on gauges 2, 3 and 6 were compressive.

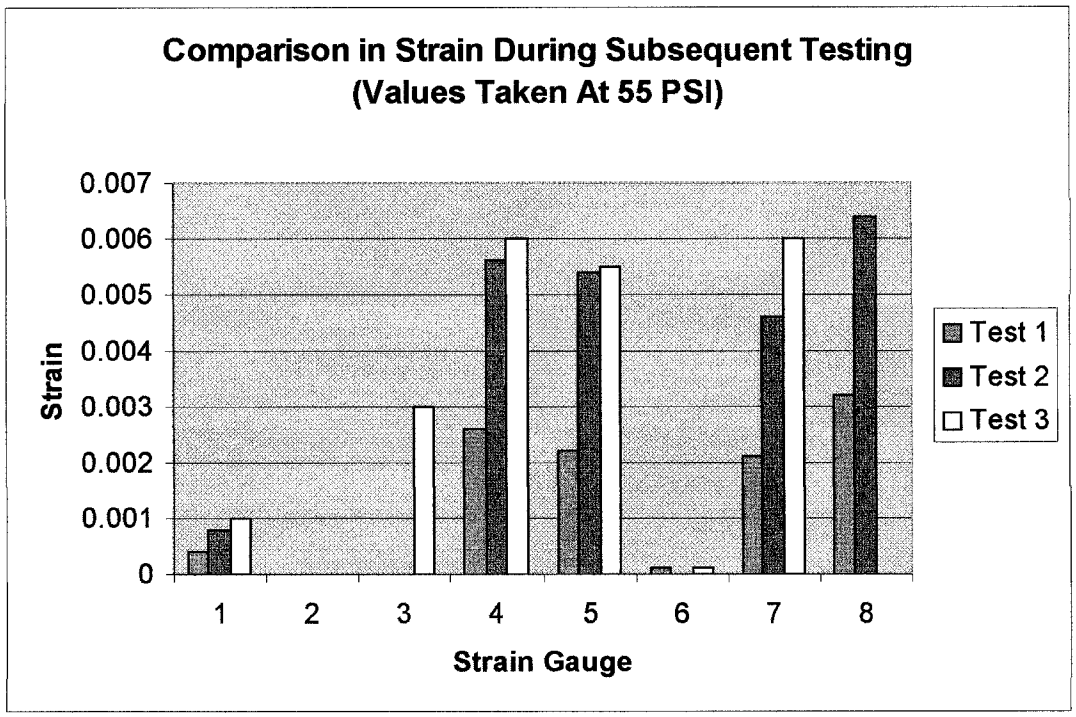

Figure 32. Comparison in strain during subsequent testing of prototype 2

Strain plots for the three pressure tests are located in Figures 33 thru 35. Through observation of the strain plots, the increase in magnitude, at corresponding pressures between the plots is notable.

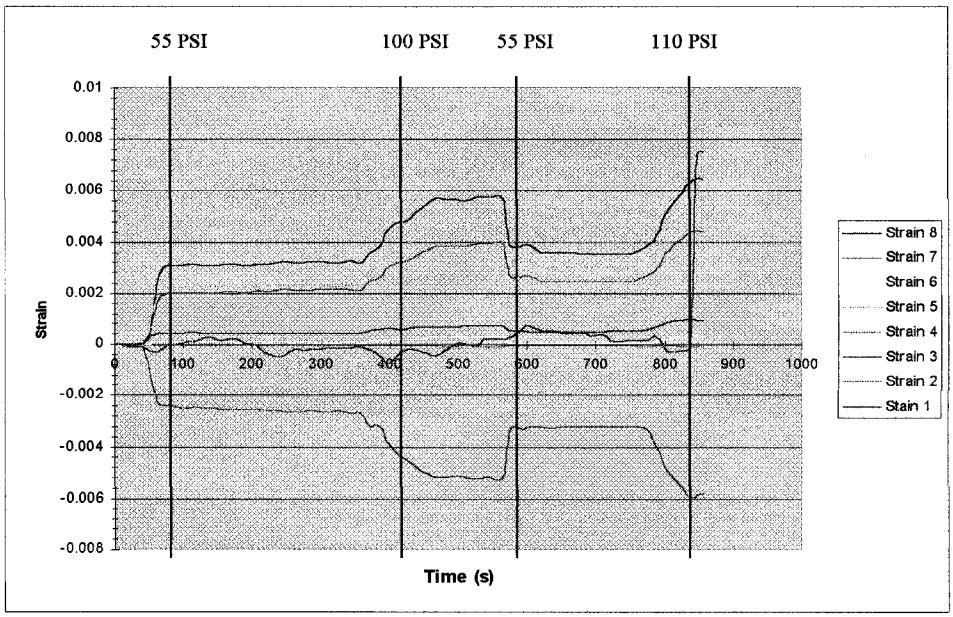

Figure 33. Strain plots for first pressure test of prototype 2

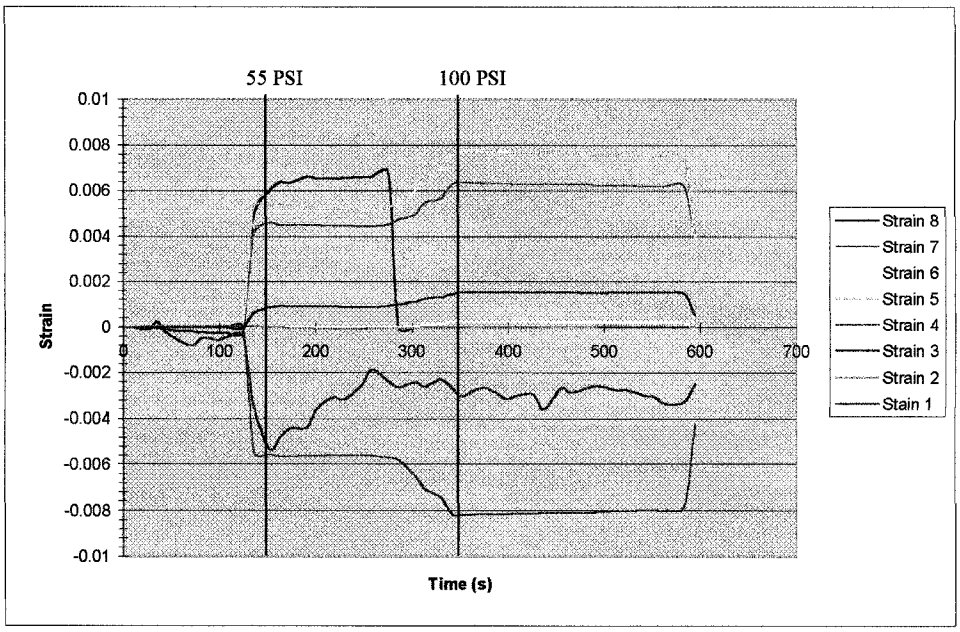

Figure 34. Strain plots for second pressure test of prototype 2

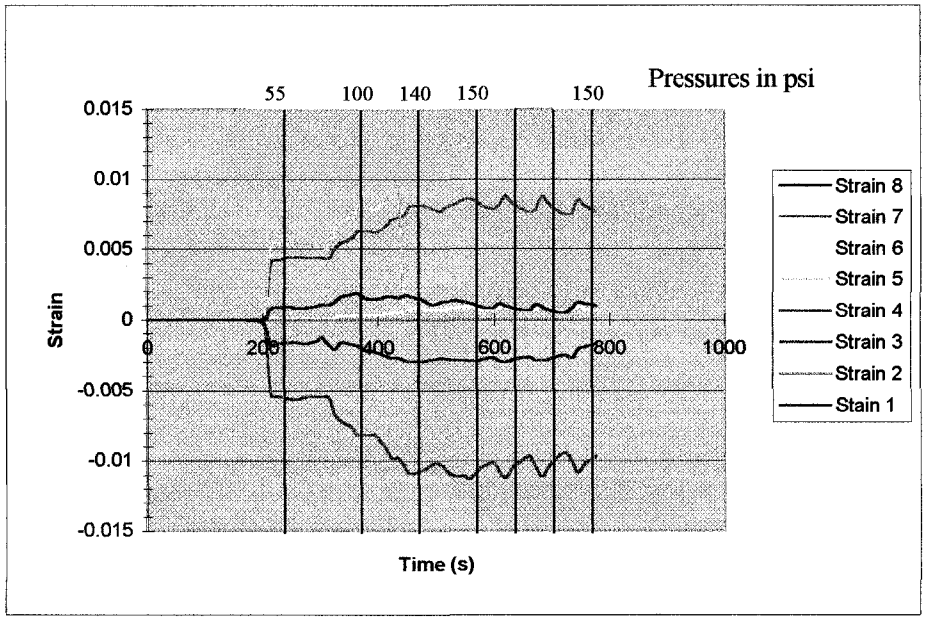

Figure 35. Strain plots for third pressure test of prototype 2

Displacement plots behave similarly to the plots of strains. An increase in deflection, between corresponding pressures, is clear. Displacement plots for the first two tests are shown in Figures 36 and 37.

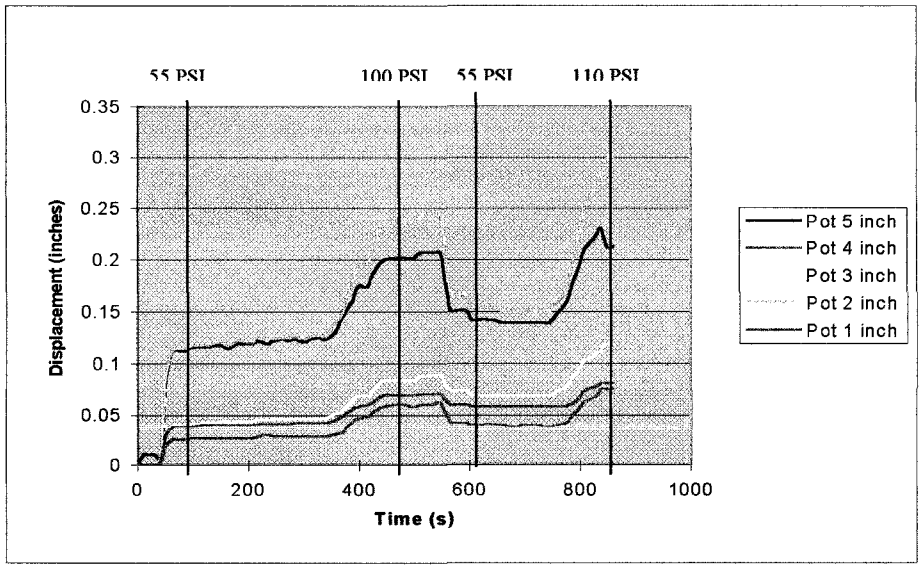

Figure 36. Displacement plots for pressure test 1 of prototype 1

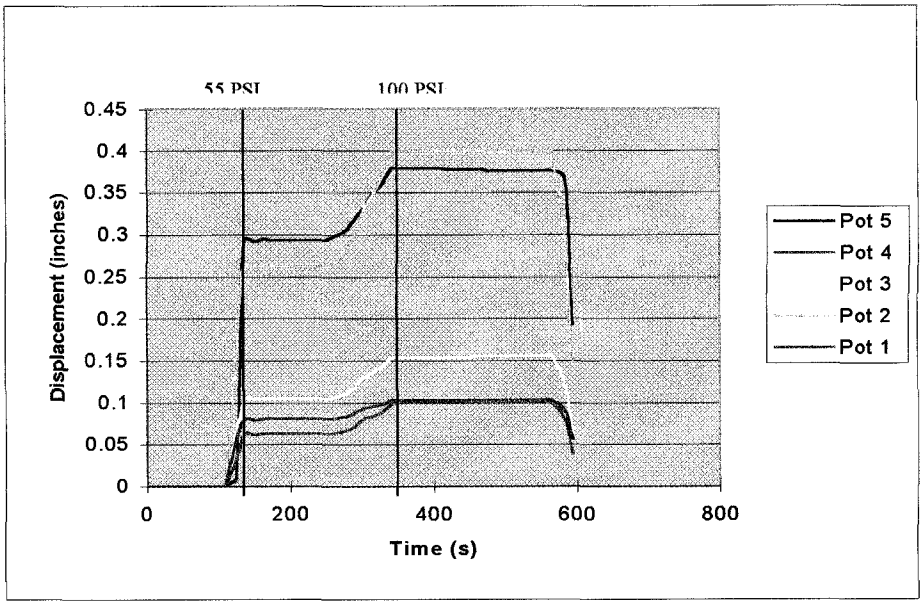

Figure 37. Displacement plots for pressure test 2 of prototype 2

9.2.2 Comparison between Experimental and Predicted Values

Experimental results were compared to those predicted by finite element analysis. This was done in an attempt to determine the extent of correlation with the accuracy of computer model predictions. Results read from the strain plots of the three tests from prototype 2, were tabulated with those obtained from the finite element analysis results. Values for both displacement and strain were compared at 55, 100 and 150 psi. Results of the comparisons are located within APPENDIX VI, an example, shown at 55 psi, is presented in Figure 38.

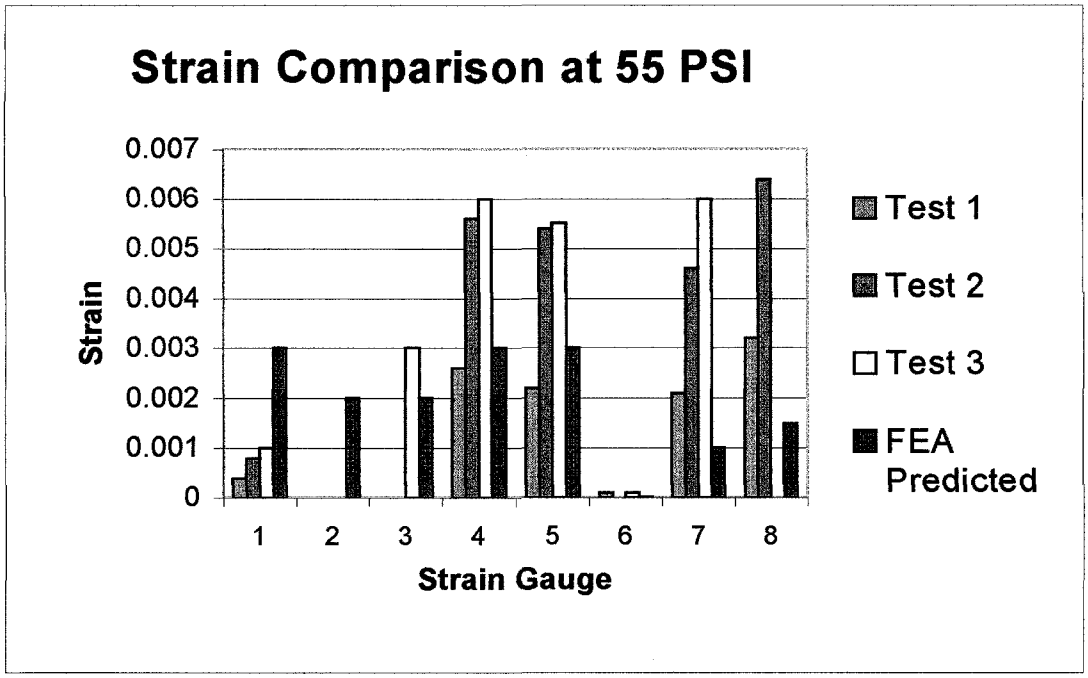

(a)

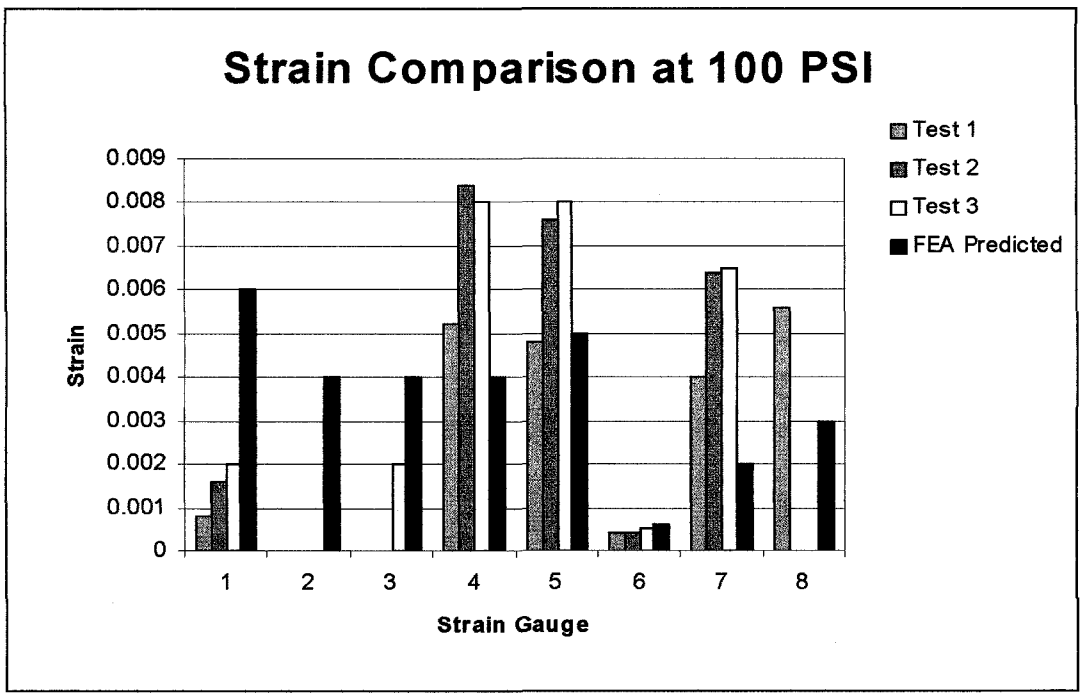

(b)

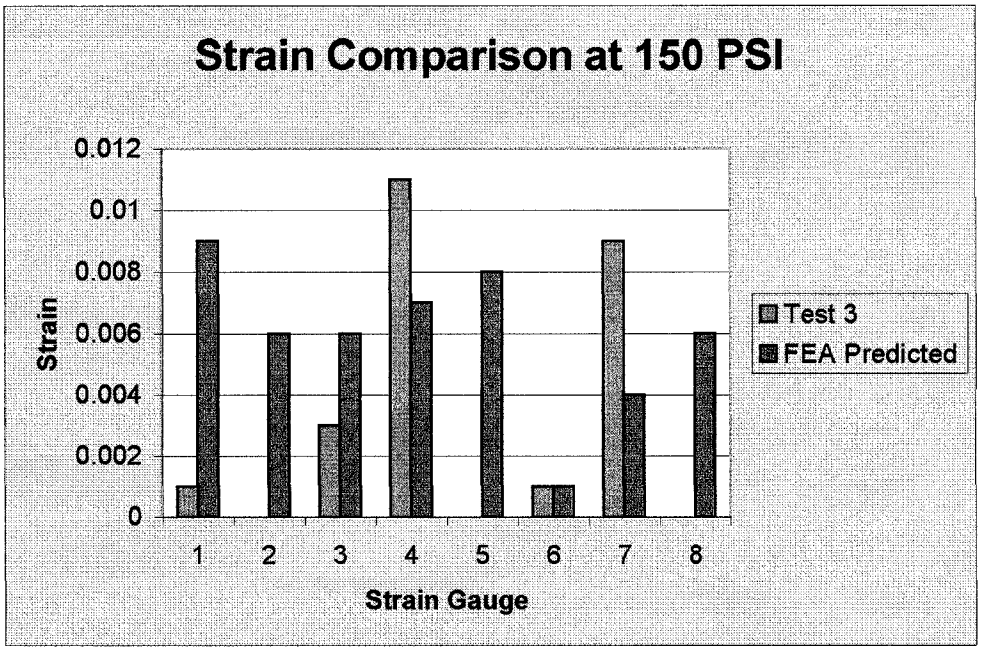

(c)

Figure 38. Comparisons of experimental with predicted results for prototype 2

Examination of the comparison plots in Figure 38, shows little correlation in the magnitudes of the predicted vs. experimental values, except for strain gauges 4 and 6. In these latter cases, the predicted values were reasonably close to those experimentally attained in the first test run. The other strain gauges show no correlation with the predicted values. The remaining test runs also showed little correlation at all measurement locations.

Interestingly, the comparison between experimental and predicted values of displacement yielded similar results, except that the measured displacements were all much higher than the predicted values. The closest correlation in data could be found in the displacement values measured by potentiometer 3 in the first test run. Potentiometer 3 was located on the same end wall as strain gauge 5. As in the case of

the strain comparisons, correlation could only be drawn when predicted values were compared with results from the first test. Displacement comparisons can also be found within APPENDIX VI. Figure 39 a and b illustrate the results graphically at 380 kPa (55 psi) and 690 kPa (100 psi) pressure.

Comparison of Figures 36 and 37 also show that on the second test, the displacement values at 380 kPa (55 psi) are essentially the displacements attained at 690 kPa (100 psi) in the first test run. This can be interpreted as indicating that the displacements are controlled by local, permanent damage events such as fiber breaking or pull out or epoxy cracking.

This behaviour is also seen in the strain gauge results (Figures 33, 34, 35) for test runs 1 and 2. Test run 3 produces strain levels more or less equal to test run 2 for the same pressure as in test run 2. There are no displacement values available for comparison in test run 3. The sudden drop in individual strain gauge output could indicate a detached strain gauge, or one which exceeded the gauge's strain capacity, therefore giving infinite resistance. Observation of the strain plots for the third test, reveal that strains drop off, after the maximum value is attained, between strokes of the cylinders.

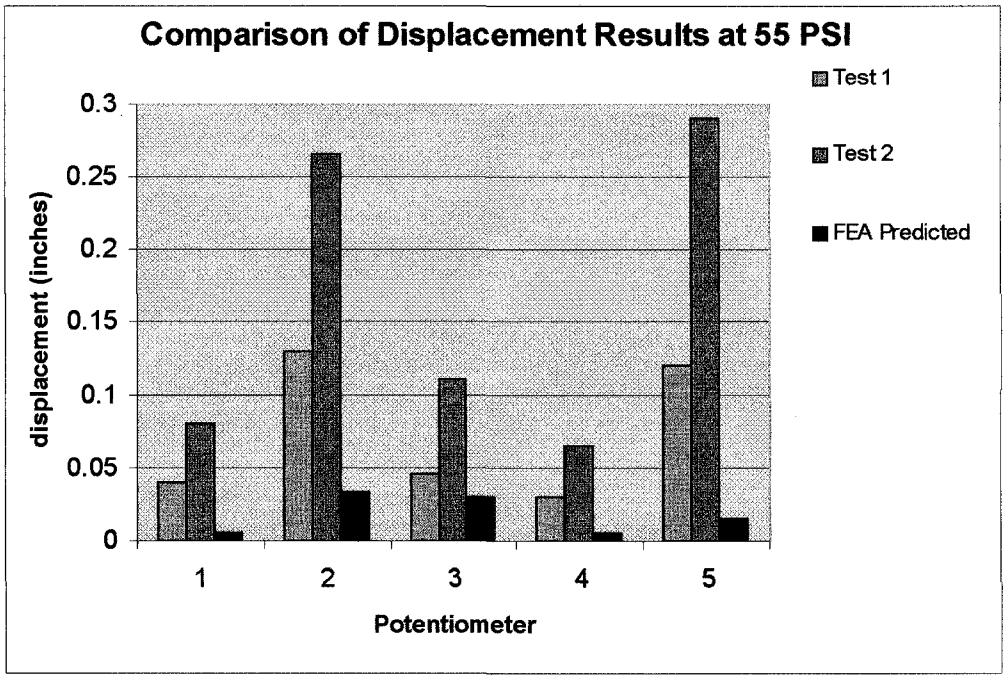

(a)

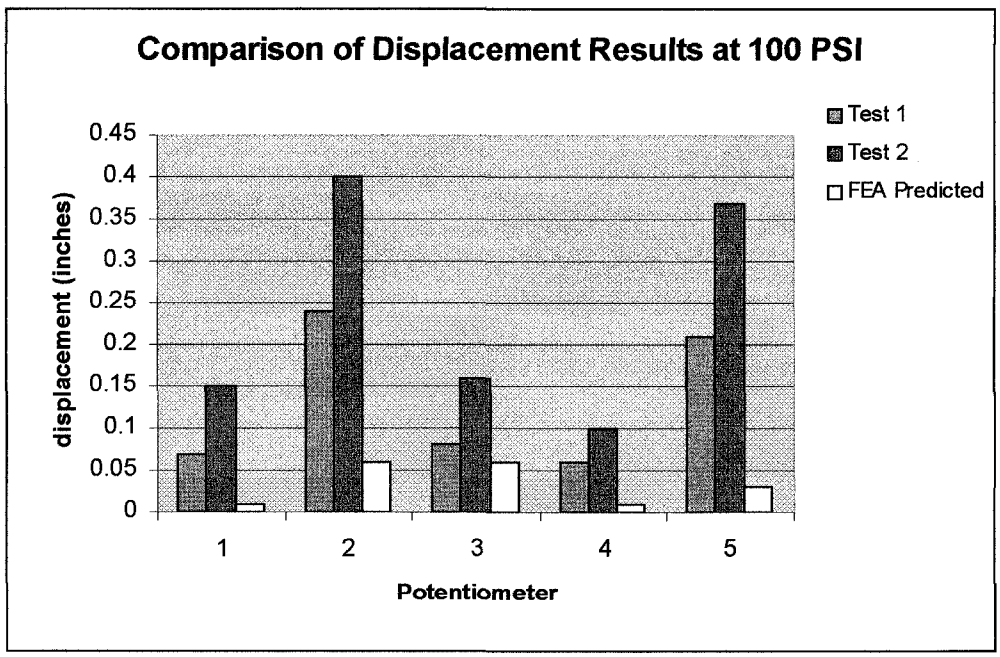

(b)

Figure 39. Comparisons of experimental vs. predicted displacement results for prototype 2

9.2.3 Summary of Prototype 2 Results

Data correlation with FEA predictions appears to exist only in measurements taken on the end wall of the tank. This correlation, however, is apparent only for those readings obtained during the first pressure test run. The end walls on the tank, are the only walls without the filament winding reinforcement.

9.3 Results-Prototype Three

The data acquisition system was used in a similar matter as in the testing of prototype two. However, upon viewing the data files generated by the GEN200 software, it was apparent that the potentiometers were not functioning properly during the tests on prototype 3. Subsequent investigation revealed that an electrical short, resulting from accidentally grounding one of the power supply wires, blew the fuse controlling the channels used for the potentiometers As a result experimental measurements of displacement were not attained for prototype 3.

9.3.1 Data Acquisition Results

Strain gauge positions are marked on the following figures. Figure 40 (a) looks down on the top of the tank, while Figure 40 (b) looks up at the bottom of the tank. As a reminder, the 3" deep ribs run across the top and down the sides of the tank. The bottom wall utilizes a 1" deep rib, with excess filament winding spreading

out on the bottom of either side of the rib. Principal strains were used as comparison values. Of the output options available for strain in ALGOR, the principal values were the most suitable for validation purposes. Experimental strain plots from the three tests are shown in Figures 41, 42 and 43.

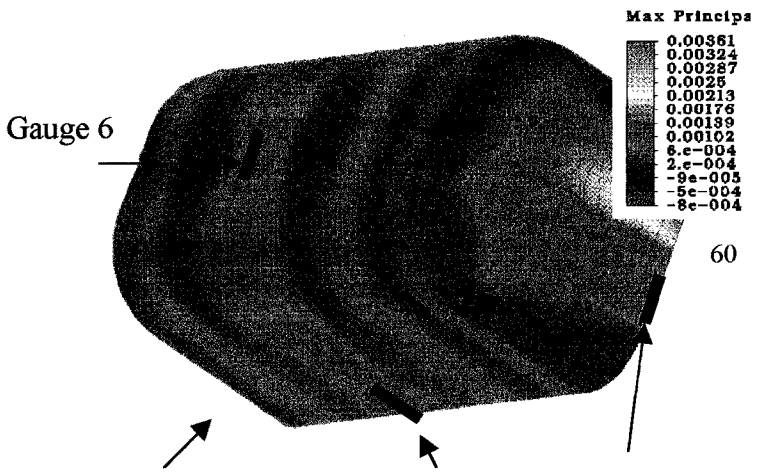

(a)

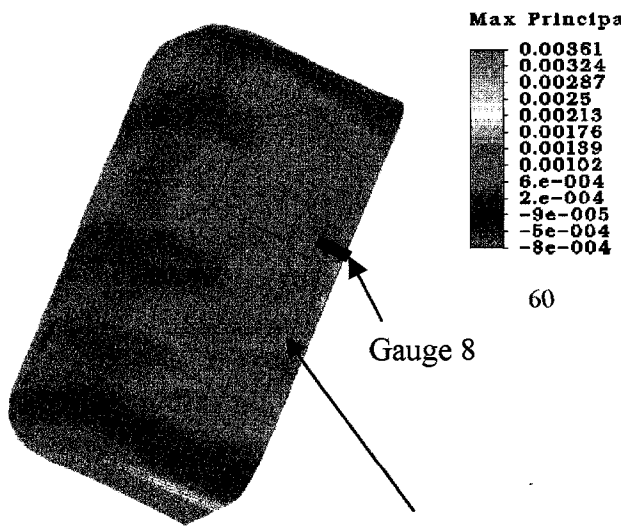

(b)

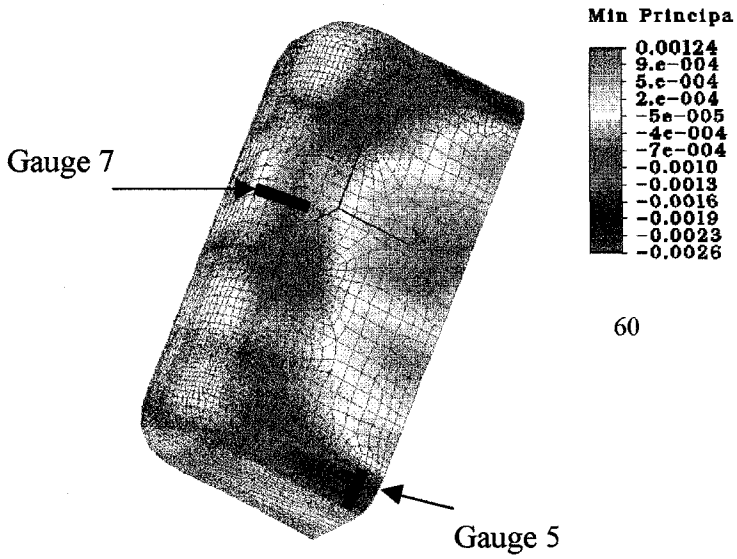

60

(c)

Figure 40. Illustration of principal strain results on prototype 3 at 414 kPa (60 PSI) (Black lines, orientated in the strain gauge direction, show location of gauges)

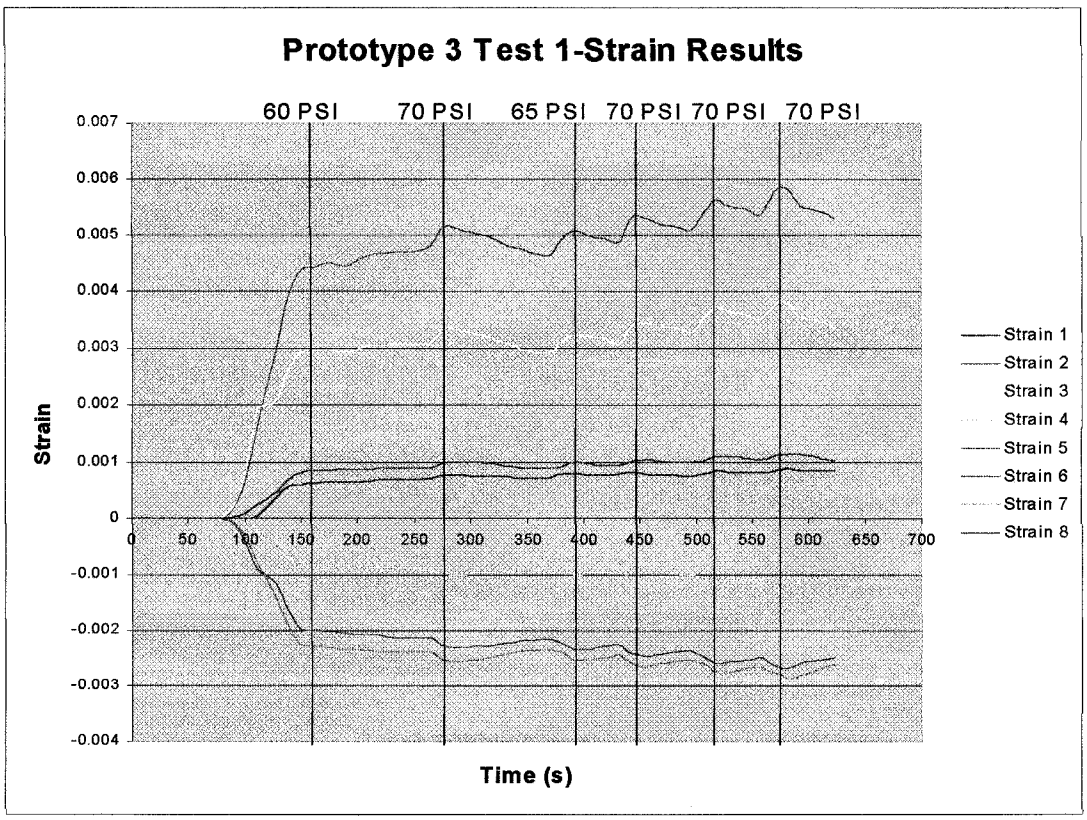

Figure 41. Strain results for first pressure test of prototype 3

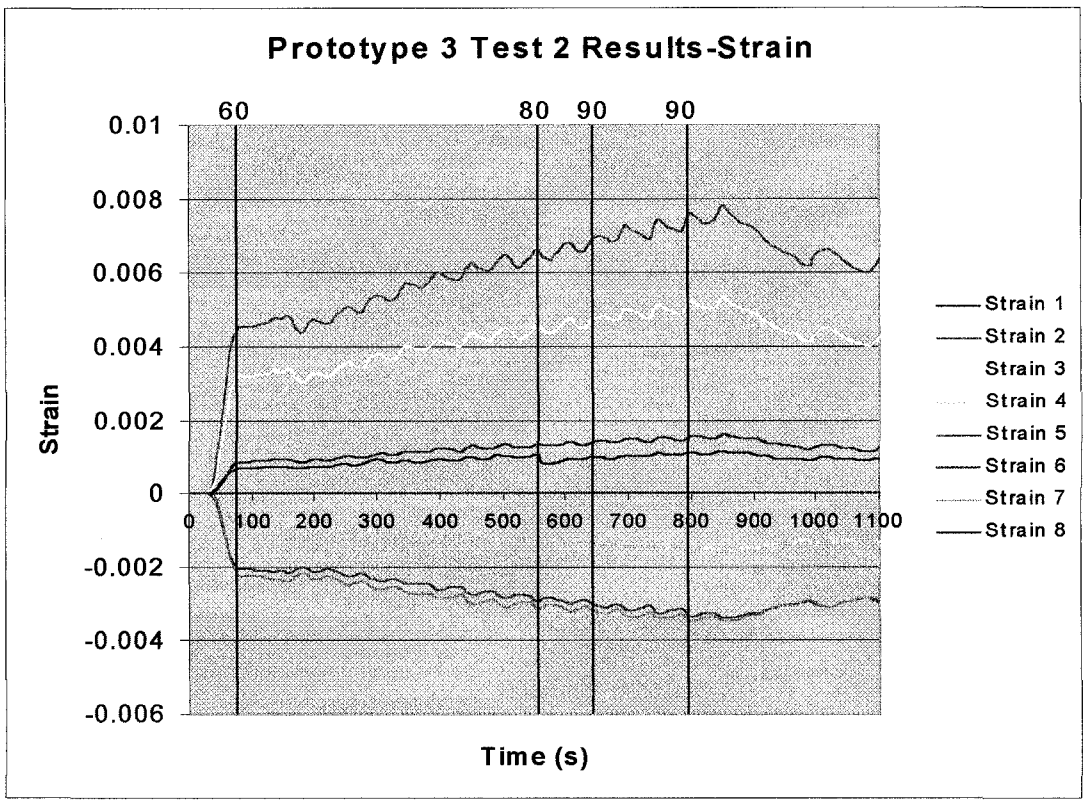

Figure 42. Strain results for second pressure test of prototype 3

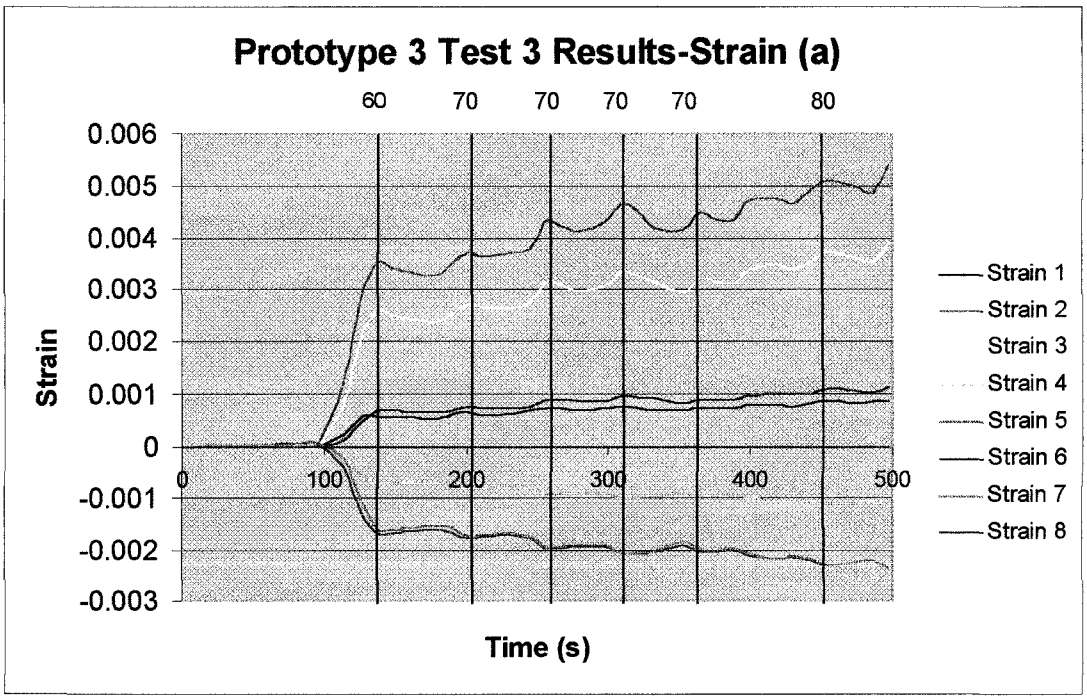

(a)

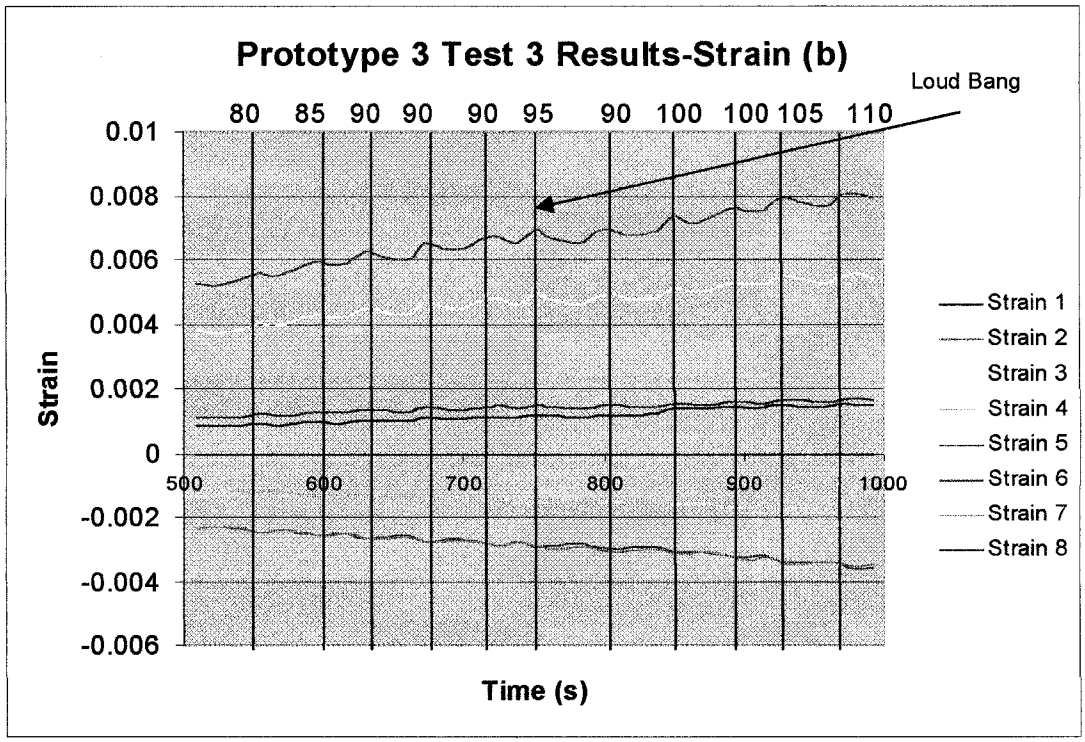

(b)

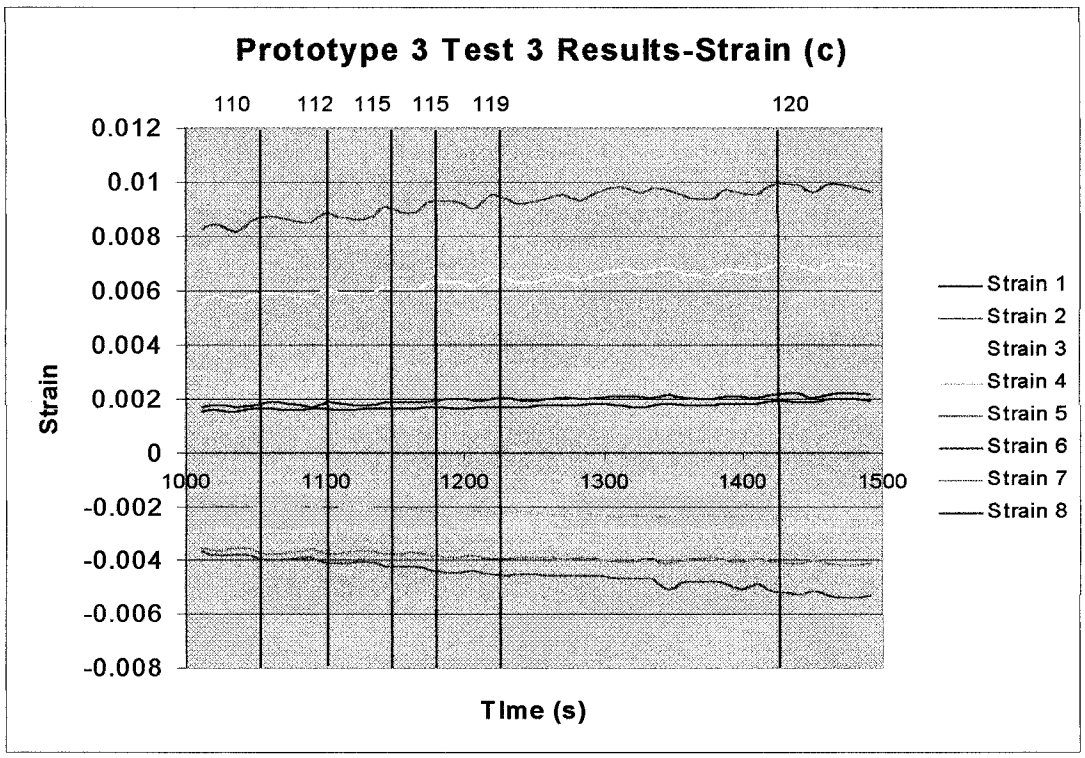

(c)

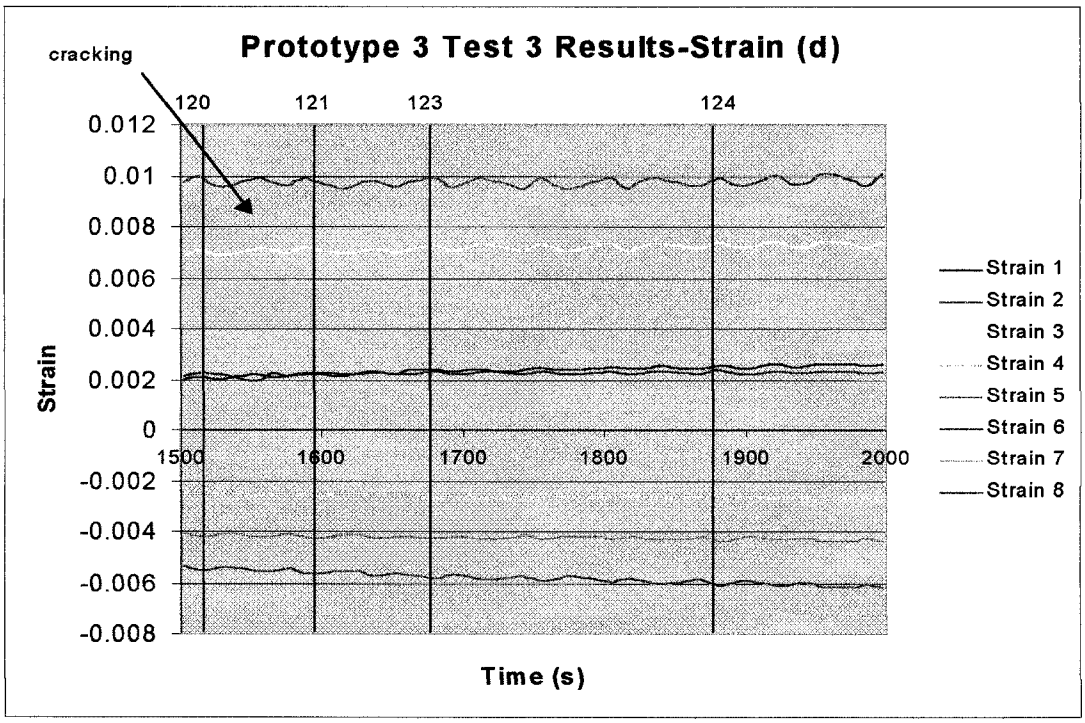

(d)

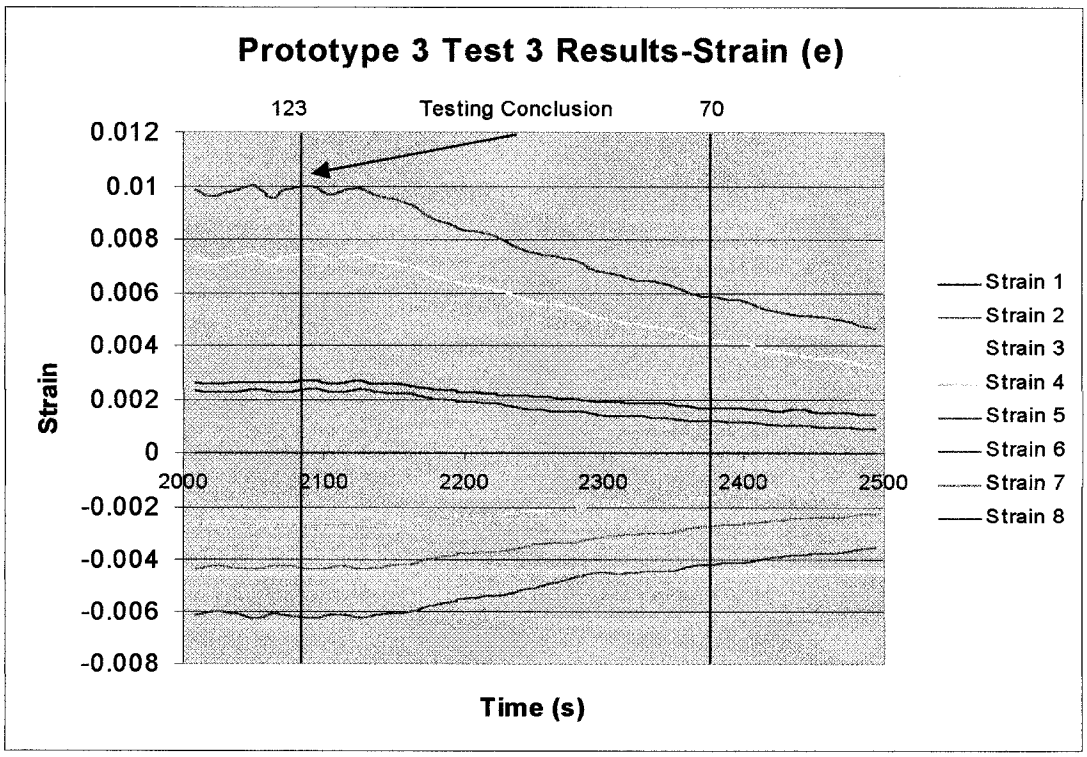

(e)

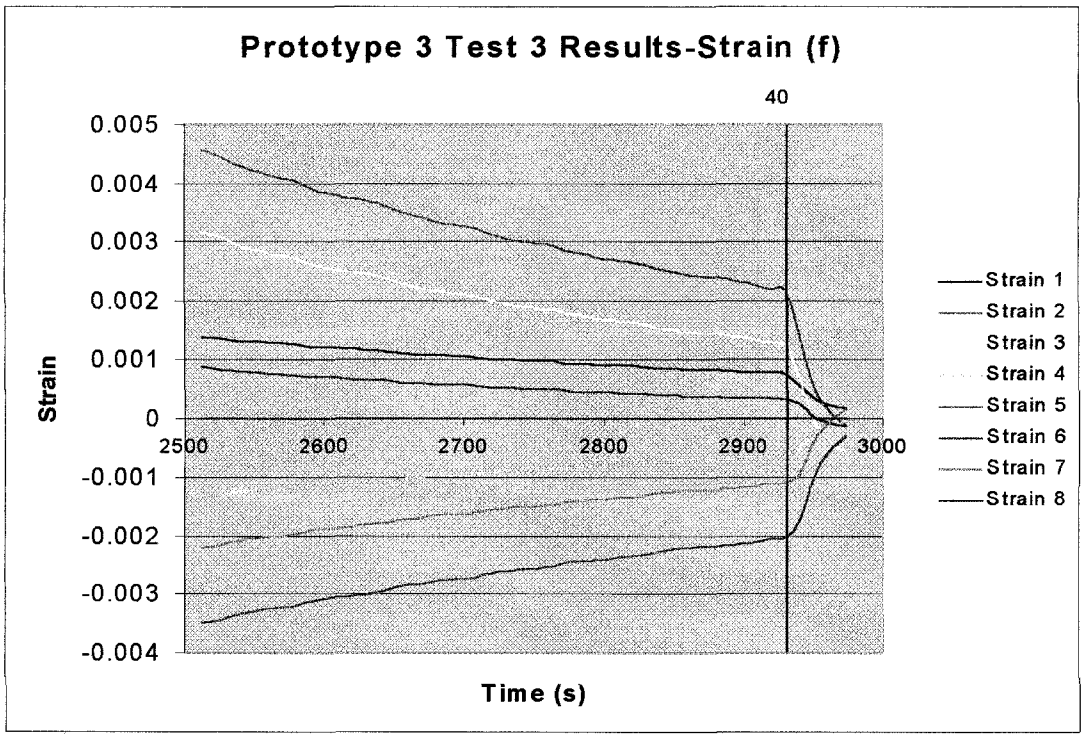

(f)

Figure 43 (a)-(f) Strain Results for Pressure Test 2
(numbers on top of graphs represent pressure in PSI)

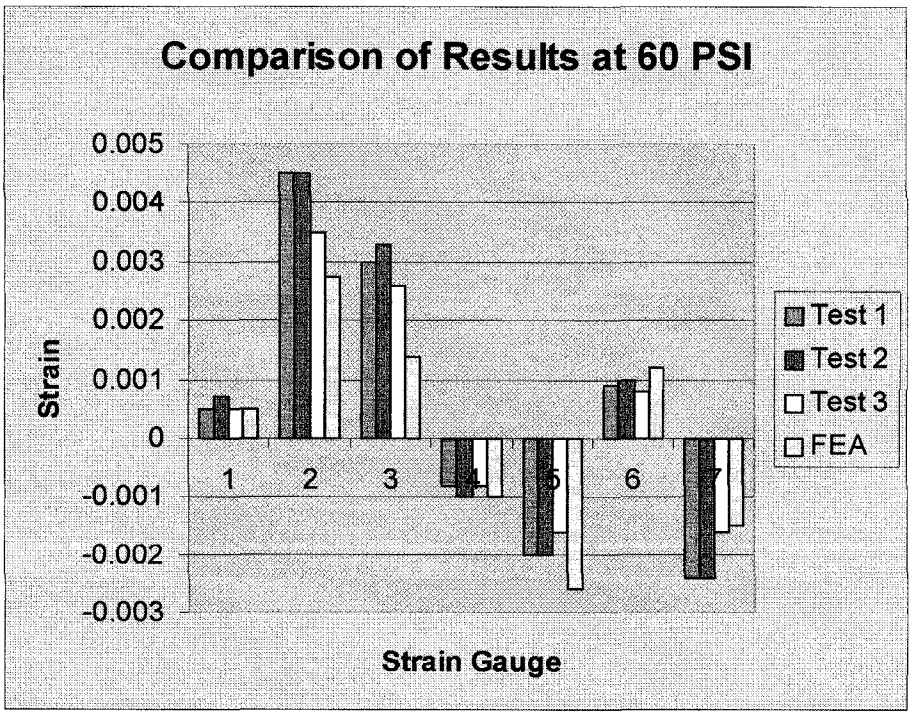

(a)

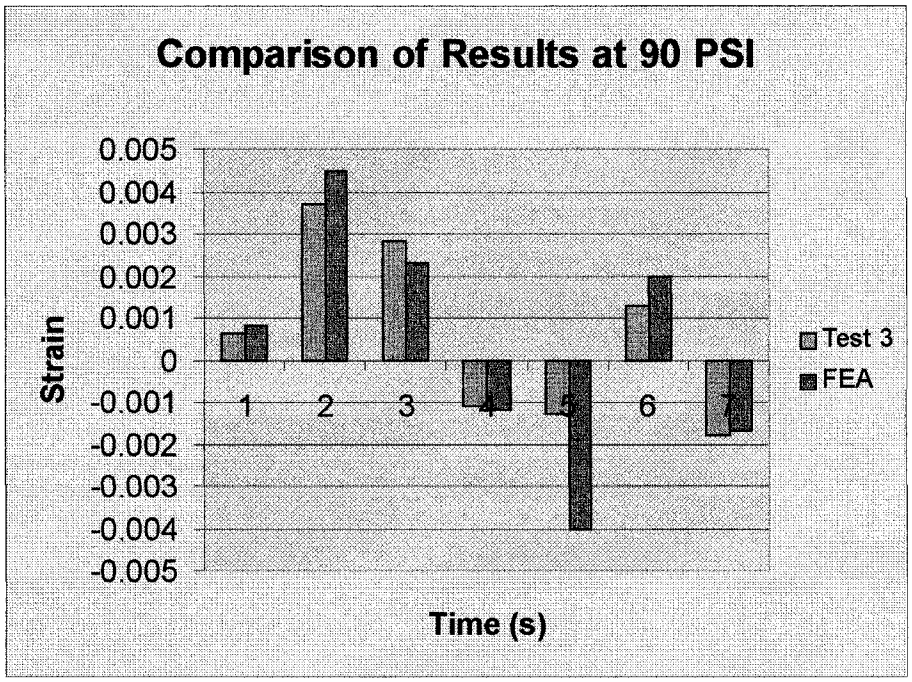

(b)

Figure 44 (a & b) Strain Comparison Between Subsequent Tests of Prototype 3

Data recorded from the experimental testing revealed behavior different from the tests performed on the second prototype. In examining data from the prototype 3 testing results, it was apparent that the strain values increased during subsequent testing. For example, the strains at 414 kPa (60 psi) between tests 1 and 2 increased. In the third test, however, the strains in the gauges decreased slightly when compared to values in the previous tests. The comparison of strain values at 414 kPa (60 psi) and 621 kPa (90 psi) between the tests are illustrated in Figure 44.

To better understand the reduction in strain in the third test, reference values were compared. Once again, the reference values are the values measured at ambient pressure before testing began. The reference values are tabulated in Table 5 below.

Reference Starting Strain				
Gauge	Test 1	Test 2	Test 3	Load Condition
1	-0.00114	-0.00133	-0.00098	Tensile
2	-0.00196	-0.00172	-0.00032	Tensile
3	-0.0013	-0.00125	-0.00047	Tensile
4	-0.0009	-0.00099	-0.00122	Compressive
5	-0.00176	-0.00201	-0.00276	Compressive
6	-0.00106	-0.00103	-0.00083	Tensile
7	-0.00165	-0.00198	-0.00252	Compressive

Table 5. Reference Strains Measured Prior to Pressurization

The load condition in Table 5 refers to the direction of strain during testing. Comparing the locations of the strain gauges on the tank, the measurements correspond to the expected directions. Gauges 4, 5 and 7 were located on the corners, where compressive strains were expected due to the outward deflection of the flat walls. Complete strain plots for the pressure tests conducted on prototype three are located in APPENDIX VII.

9.3.2 Comparison between Experimental and Predicted Values

The experimental values correlated reasonably well with the finite element analysis predicted values. To determine if better correlation could be obtained by including consideration of the differences in the reference strains, the total strain was found. Calculations of the total strain used the measured pre-strain, prior to the first test, as the reference value in all following strain calculations. The results of this comparison are illustrated in Figure 45.

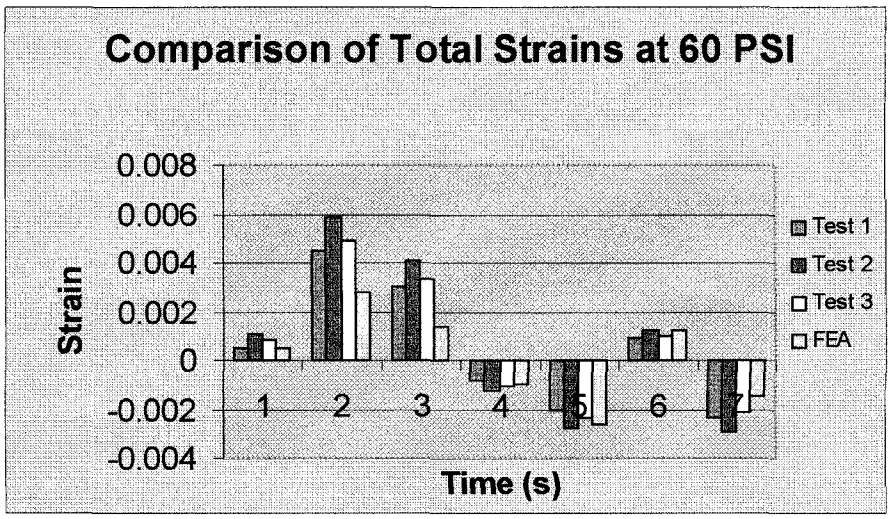

Figure 45. Comparison of results using the total strain calculations

Comparisons drawn using the total strain yielded a somewhat better correlation overall between the experimental and predicted results for gauges 5 and 6. However, in general the experimental results were very different than the predicted values. It is important to note that using the total strain values in the second prototype comparisons would yield further deviation between experimental and predicted values.

9.3.3 Summary of Results

Analysis of the measurement data obtained through pressure testing yielded results that did not correlate with FEA predictions. The strains in subsequent tests increased overall, when results were compared to values at corresponding pressures. In the third test, the values of strain appeared to decrease over the values obtained in the previous test.

During the third test of prototype 3, it was also clear that strain was increasing during re-pressurization. Careful examination of the strain plots, located in APPENDIX VII, reveals that the strain levels increased while cycling between the same pressures. The cyclic nature of the pressurization process resulted from water volume loss from the tank between strokes of the cylinder. This phenomenon appeared to level out near the end of the test when the pressure was cycled numerous times to the maximum 856 kPa (124 psi) value.

Finally comparison of the starting reference values, between each test, reveal an increase in the overall strain in the tank. It is apparent, that once pressure was released from the tank, the walls did not relax back to their initial value. This is apparent with the increase in the gauge pre-strain, at zero pressure prior to testing, between each successive test as shown in Table 5. The gages which experience compressive strains on loading have a zero pressure strain that becomes steadily more compressive. The gauges which experience a tensile load under pressure have a zero pressure compressive strain that generally gets smaller with pressure cycling. So the residual strain after each cycle is generally in the direction of the applied strains.

Chapter 10

DISCUSSION OF RESULTS

Explanations for the significant deviation in the finite element analysis predicted values and those experimentally attained were sought. Sectioning one of the prototype designs provided significant insight into reasons for the discrepancies in the results and problems with the construction method. The large wall displacements measured during pressurization, and visual observation of the sectioned prototype, indicated that the designs would fail catastrophically at pressures much lower than originally thought, even if they had incorporated an impermeable flexible liner.

10.1 Water Permeation

The first, most apparent, problem was the lack of an impermeable inner liner. During pressure testing, it was quite apparent that water leaked through the micro-cracks of the epoxy matrix. Possible consequences of this involve more than simple water permeation.

The presence of pressurized water in the epoxy micro-cracks poses potential problems. If the micro-cracks are envisioned a microscopic tubes, the pressures from the internal fluid apply expansion forces on the walls of the micro-cracks. The resulting expansion helps in opening up the crack, driving the crack tip forward. In

addition, the presence of water at the crack tip, creates surface tension effects that could aid in the further advance of the crack front.

The presence of an impermeable liner would effectively eliminate these potential problems. A liner would not only serve to prevent water permeation through the tank walls, but also reduce the risk of crack propagation by eliminating the presence of pressurized water in the micro-cracks.

10.2 Result from Tank Sectioning

Evidence suggesting problems with the construction method were first noticed in the comparison plots of predicted vs. experimental strain and displacements values. It was apparent that data correlation existed on measurements taken on the end wall of the tank. Interestingly, this wall was the only wall that did not have any type of reinforcement from filament winding. This composite wall was built solely from progressive layers of 24 oz bi-directional E-glass mat.

Sectioning the tank, across the cross-section of the ribs and corresponding unidirectional filament winding on the bottom of the tank, confirmed suspicions that problems in the filament wound reinforcement were present.

The first portion of the tank investigated was the top, ribbed wall of the tank. Discontinuities in the rib material were clearly evident, shown in Figure 46. In

examining Figure 46, two main separations in the filament windings can be seen. Parts of the windings do not join in with the general rib cross-section, but rather almost appear as individual sections in the rib. The thickness of each segment layer in the filament wound ribs, corresponds to the thickness of filament winding wound during each stage of winding. As previously mentioned, winding was done in stages to prevent the development of an exotherm during lay-up, as had previously been experienced in the winding of the first prototype.

Figure 46. Illustration of fiber separation between subsequent winding stages

Investigation of the filament winding inside of the bottom of the tank, as shown in Figure 47, revealed the same problem. Once again, the filament winding appeared, almost as sections, or independent groups of winding. Voids created between the groups of winding were significant in size.

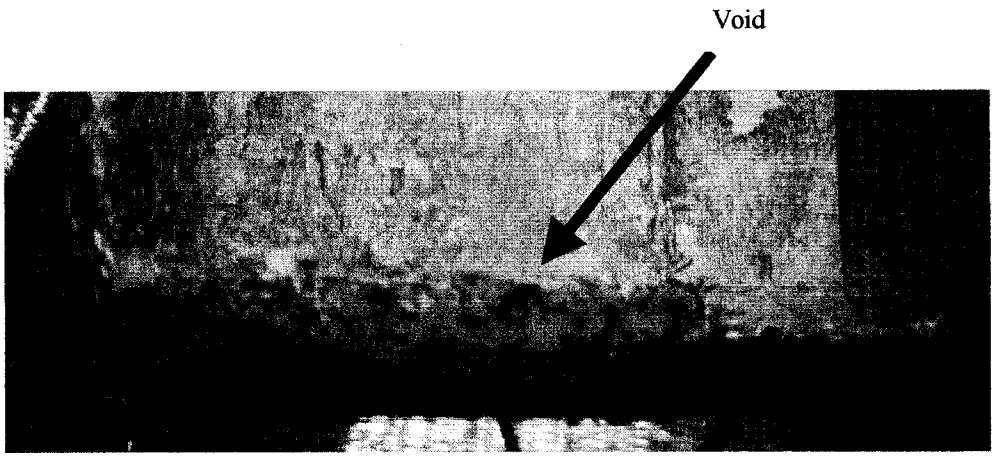

Figure 47. Illustration of voids between windings on tank bottom

It is apparent that, because the windings were not applied continuously, voids between the subsequent layers were created. Allowing the epoxy to cure between the winding stages, prevented good interaction of the epoxy between the layers. Partially cured and cured epoxy from the previous layer did not react well with the cured epoxy applied later.

Although the next layer of filament winding was applied while the previous layer was still tacky, too much curing of the earlier layer appeared to have taken place. As a result cross-linking in the epoxy between subsequent layers was poor. This ultimately led to poor adhesion between layers, and significant discontinuities in the structure.

It is also apparent, shown in Figure 47, that the material in the filament wound ribs became much more dense as it approached the top wall. This may be explained by referring to the procedure for winding the ribs. During construction, layers of thin,

bi-directional mat were applied across and into the ribs, as a means of tying the ribs to the upper wall of the tank.

A second layer of mat was applied after about 1" thickness had been attained in the ribs. This latter mat, applied at the end of one winding session, was laid into the ribs immediately after winding of the previous layer had ceased. This was done in an attempt to allow the mat to cure into shape slightly, making winding of the next layer less sloppy.

After the ribs were completely wound, voids between the individual fibers of unidirectional winding were present. In an attempt to fill these voids, epoxy was poured into the ribs until all voids appeared full. It appears that the layer of mat that was laid in at the 1" thickness, acted as a dam to the flow of epoxy into the bottom layers of filament winding. The final layer of mat, applied across the ribs, was placed into the ribs immediately before the last layer was wound on. As a result, epoxy poured into the ribs after the winding was complete, passed through this uncured layer with relative ease. The epoxy could then flow through the next layer of filament winding until the cured section of mat was encountered.

In general, reinforcement from the filament wound, internal ribs, was lower then expected. The obvious low volume fraction of the fibers and the discontinuities in the filament winding, would result in a much lower strength than originally predicted. In addition, because the rib material was dense only to about a depth of 1",

the effective area moment of inertia of the top wall, was reduced accordingly. The latter point, involving the effective rib depth, also takes into consideration the probability of water filling the voids between the fibers in the loosely packed windings.

Similar conclusions may be drawn through observation of the filament wound tank bottom. In addition to the voids, created by the multi-stage filament winding process, the interface between the filament windings and the bi-directional over-wrap was not continuous. Examination revealed that it almost appears as though the bi-directional over-wrap literally separated from the filament wound reinforcement. Effectively, once the water migrated to this location, the pressurized water would act on the wall as though the filament winding basically wasn't there. Without reinforcement from the filament winding, the deflection in the lower wall would be much greater than anticipated. The bi-directional mat itself was dense with glass uniformly distributed through it, but the unidirectional windings were very loosely attached.

In addition to the top and bottom walls, the side walls were also modeled assuming that reinforcement from the filament wound ribs would be significant. Due to the same problems mentioned earlier, the deflection in the side walls were also higher than predicted by the finite element analysis.

10.3 The Question of Fatigue

In addition to the measured values being higher than predicted, a concern over the increase in strain and stress exists. The increase in these values, during subsequent loading, raises the possible question of fatigue.

Although, the increase in measured values in each progressive test raises the question of fatigue, further thought consideration into the construction method must be given. Effects of water penetration through micro-cracks, in the epoxy matrix have been described. The possible damage that occurred, through crack propagation in the matrix, may yield some explanation into the fatigue like behavior of the testing results. Under pressure, water would flow into the cracks, but this water might not have been able to withdraw from the cracks during a lowering of the pressure. Thus the volume of water remaining in the cracks could prevent the tank from relaxing back to its original, pre-testing size. It is quite possible that the presence of water alone contributed to the increase in deflection and strain during subsequent testing.

Results of the test, however, do not provide a conclusive assessment on the possibility of fatigue. If an impermeable liner were used to prevent the introduction of water into the micro-cracks, results obtained through testing may not have exhibited the fatigue like behavior. Further investigation would be required to determine the possibility of fatigue in an impermeably inner-lined prototype.

10.4 Advantages of a liner

It is apparent that the effects of water contact with a epoxy fiberglass composite may be significant. The majority of questions in the above discussion introduce consideration into the damage incurred through this contact. In addition, water pressure acting between the filament windings, and the bi-directional mat over-wrapped walls, reduce the effect of the continuously wound reinforcement.

A second explanation for the poor structure of the unidirectional windings is that the acetone used to dissolve the foam degraded or dissolved the epoxy in the windings. An impermeable liner would eliminate this effect, preventing any degradation of the epoxy by the acetone.

If a method of constructing a tank with an impermeable liner could be devised, potential advantages are clear. A tank with an impermeable liner, could yield significantly better results than those obtained during experimentation in this project. Through the incorporation of liner into the design, water seepage through micro-cracks and the possibility of damage creation through this effect would be eliminated.

In addition, the liner would encourage better interaction between the filament wound reinforcement and the over-wrapped walls. As the internal pressure increased, the inner liner would expand outward compressing the filament windings against the

fiberglass mat. The walls could then act together to contain the expansion forces rather than being weakened by opposing pressure forces acting between the layers.

10.5 Summary of Results

From the measured results of the tests and examination of the sectioned prototype, it is clear that the method of construction was a significant factor in the lower than expected performance of the tanks. The method of filament winding led to the creation of significant voids between groups of continuous windings in the ribs and the bottom surface. Poor interaction between the bi-directional mat over-wrap, and the filament wound fibers, resulted in a significant reduction in the predicted reinforcement.

Water introduced the epoxy matrix, may have led to fatigue damage, and certainly did ultimately result in the permeation of water through the tank walls. The presence of water after unloading may have contributed to the residual strains left after pressure cycling. It appears that the future use of a liner may result in significantly better results by reducing the deleterious effects of water introduction to the composite matrix.

Chapter 11

CONCLUSIONS

The design and construction of flat sided, polymer composite pressure vessels is unique both academically and industrially. Results of the finite element modeling show the very real possibility of successful development. More importantly, significant information from the experimental realization of potential problems has contributed to further understanding, and therefore progress in the development of a shape conformable polymer composite pressure vessel.

Preliminary calculations and modeling into the effects of rib reinforcement reveal the significance of the increase in rigidity over simple flat walls. Computer models of prototypes with rib reinforcement indicate the potential for development of flat sided, conformable pressure vessels. The predicted performance of the prototypes, however, could not be conclusively validated with experimental testing because tanks were not tested to the operating and burst pressures specified for LPG tanks.

The construction method utilized posed significant problems. The first problem encountered was the threat of exotherms, occurring as a result of rapid build up of the ribs. This raises the question of the commercial viability of a high production volume tank requiring reinforcement from uni-directionally wound, fiberglass ribs.

A second problem that resulted from the filament winding process was the segmentation of the continuous fibers wound in subsequent stages. As a consequence the effective rib height was reduced, lowering the potential reinforcement from the ribs. A similar phenomenon, experienced on the bottom of the tank, verifies the possibility of segmentation between fibers wound during successive winding stages. It should be possible to develop winding processes that overcome this phenomenon.

The third problem that resulted from the construction approach was the absence of an internal, impermeable liner. A liner would have eliminated the permeation of water through the micro-cracks of the composite matrix. As a result the effects that raised the question of a fatigue situation may have been significantly reduced.

It did appear that correlation could be found between the FEA predictions and experimental results for the walls that did not rely on reinforcement from filament winding. This correlation suggests that the Finite Element Analysis better predicted results on an area of the tank that was less sensitive to material processing.

Other results determined during the course of this work include: (a) material tensile tests revealed that significant differences between the bond strengths of various thermoplastics and epoxy exist (b) the bagging type of technique for the lay-up of fiberglass mat increased the strength and modulus of the composite (c) the

inclusion of a coupling agent in the epoxy further increased the strength of the composite. As a result of the higher elongation to failure with the coupling agent, the modulus was, however, reduced.

These results confirm the possible improvement of properties through the use of a more advanced lay-up technique and a coupling agent. Development of flat-sided, polymer composite pressure vessels was advanced through the research conducted in this project. Information gained on potential problems with the construction methods, and methods in improving the properties of composites that are hand laid-up, will aid in assessing and realizing future designs. Finally, and most importantly, this research reveals the very real possibility of future successful development of a polymer composite, flat sided pressure vessel.

Chapter 12

FUTURE WORK

To provide a better assessment into the development of a commercial flat-sided polymer composite pressure vessel, additional material testing should be conducted. An important consideration should include the strength of the interfacial bond between the thermoplastic inner liner and the composite outer shell. In addition to determining the shear strength of the bonds, the pull away strength should be assessed. In order to evaluate the pull away strength, a T-test has been proposed. This test involves pulling samples that are bonded in an orthogonal, cross-like shape apart. An apparatus for conducting this test, see APPENDIX VIII, has been developed by the author and is currently under construction.

In addition, future work should involve the incorporation of an impermeable liner in designs. The use of an impermeable liner will result in the reduction of the damaging effects encountered during testing of the existing prototypes. Further work, should also investigate other materials for use as rib reinforcement due to the inherent problems with the current filament winding of the ribs.

The weight efficiency of the prototype designs was quite poor. Future work should also include further research into designs that can be made through the use of lower-weight composites. In addition, the design of a liner to provide reinforcement,

rather than the use of filament wound ribs, could result in significant reductions in the overall weight.

Finally, future work should include a cost assessment of the manufacturing process or materials proposed for production. It was quite clear that designs that require more than one continuous day to manufacture, will not be viable commercially. Further attempts to reduce the cost and weight, while increasing the volumetric efficiency, should be made in the future.

REFERENCES

1. Bain, Douglass, M.A.Sc. Thesis, Design of a Modular Polymer Composite LPG Fuel Tank, University of Windsor, 1999.

2. Mc.Crum, N.G. et al., Principles of Polymer Engineering, Oxford Science Publications, New York, 1997.

3. Azimi, H.R. et al., "Fatigue of High Epoxy Composites: Epoxies Containing Rubber and Hollow Glass Spheres", Polymer Engineering and Science, Sept. 1996, Vol. 36, No 18.

4. Smith, W.S. et al., "Properties of Constituent Materials", Engineering Handbook: Composites, ASM International, 1987.

5. Callister, W.D., Materials Science and Engineering, John Wiley and Sons, 1991.

6. Hull, D., Clyne, T.W., An Introduction to Composite Materials: Second Edition, Cambridge Solid State Science Series, 1996.

7. XU, X.Q., Doctoral Thesis, University of Windsor, 1994.

8. Mallick, P.K., Fiber Reinforced Composites, Marcel Dekker, INC., New York, 1988.

9. Chrysler Canada Internal Report, dated 05/01/95

10. Thiokol Industries and Industrial Technologies, "Low-Cost Conformable Storage to Maximize Vehicle Range", January 1998.

11. Timoshenko, S, and Young, D.H., Elements of Strength of Materials, 5th ed., Van Nostrand, Princeton, N.J., 1968.

12. http://www.searay.com/dreambuilders/page10.html

13. Thoikol Corporation, "Thiokol Takes its Rocket Motor Technology on the Road", Thiokol Magazine, 1996.

14. Witt van Moort, internal research report, 1997.

APPENDIX I

FINITE ELEMENT ANALYSIS MODELS

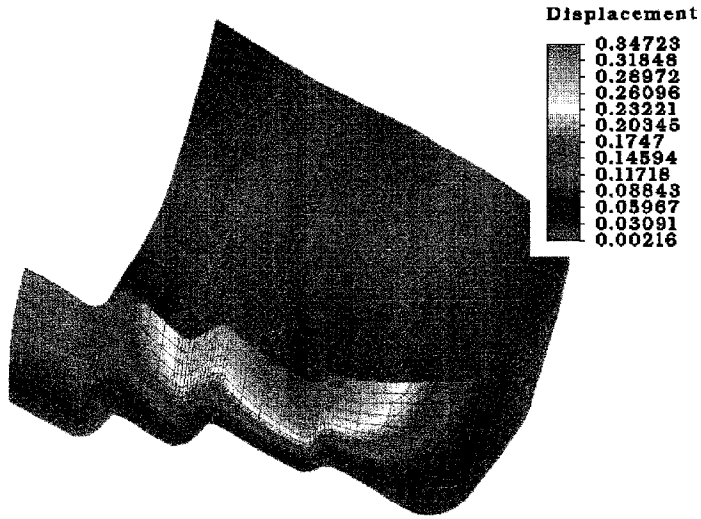

Displacements in inches

Stresses in psi

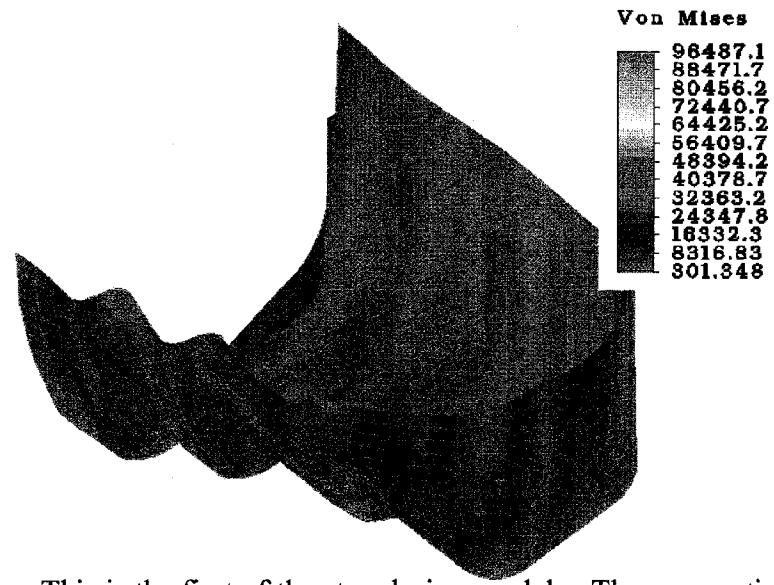

This is the first of the step design models. The assumptions made here were on the conservative side with a moduli of 1.5 e6 on the walls and 4.0 e6 on the ribs. Also note the variable step height. The first step was 3 inches high, the second 2 inches, the third 1 inch. The maximum displacement was shifted to the location of the shortest rib depth. Additionally, the over flow of uni-directional ribs was left unaccounted for on the bottom of the tank.

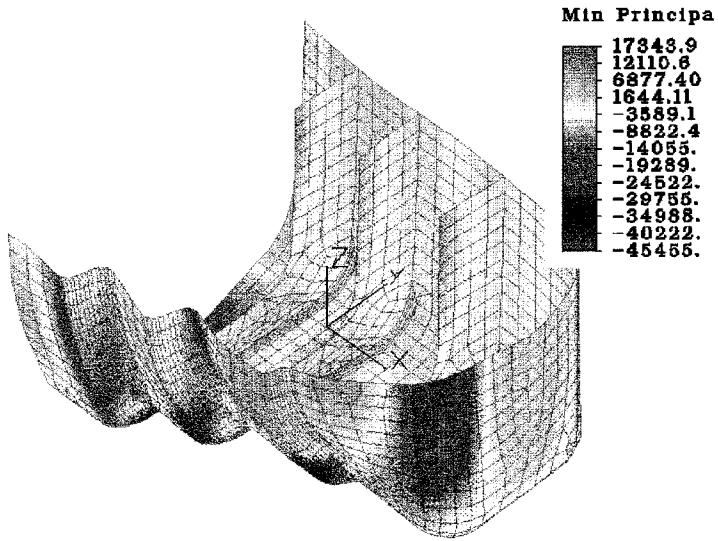

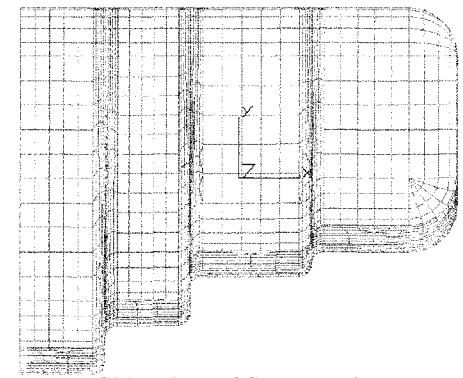

Side View of Step Profile

FEA Design of First Model

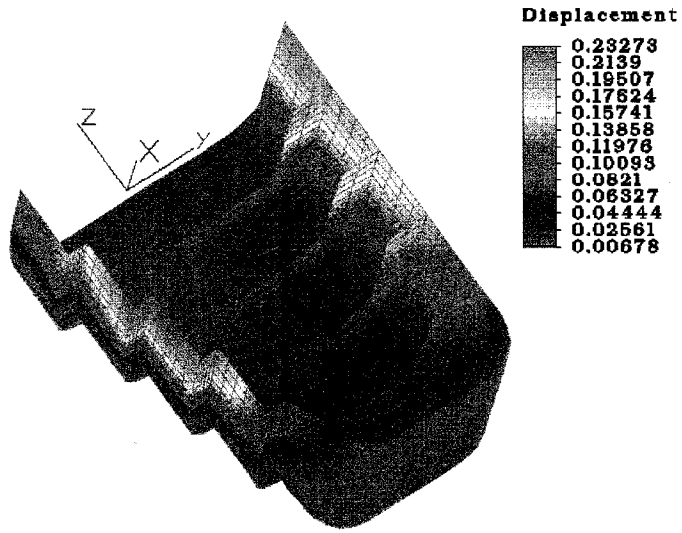

Displacements in inches

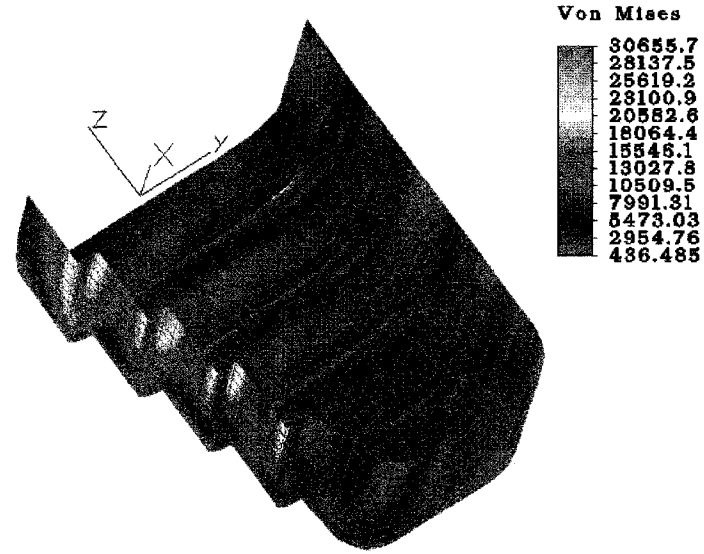

Stresses in psi

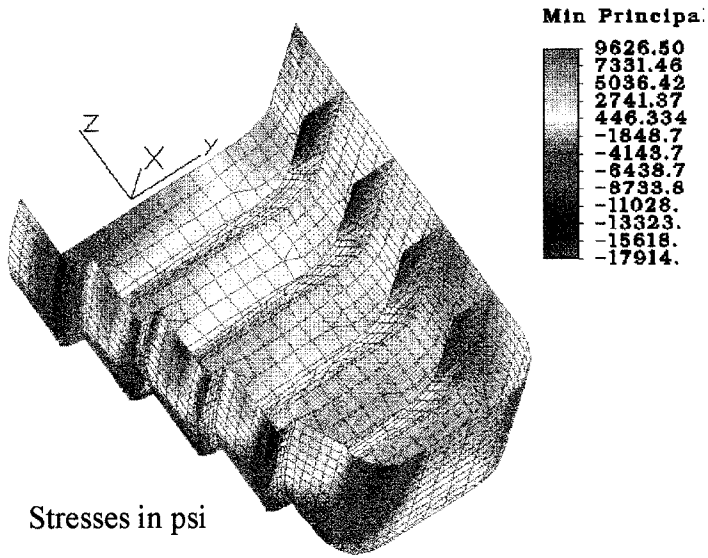

Stresses in psi

This is the second iteration of the stepped profile. Results from the previous model revealed that a possible additional step was required to tighten up the deflection. All steps were 2 inches deep, ribs were 4 inches deep. Spacing between the steps with the greatest displacement were 1/2 inch further apart.

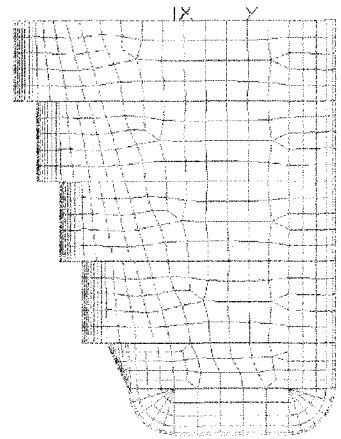

FEA Design of Second Model

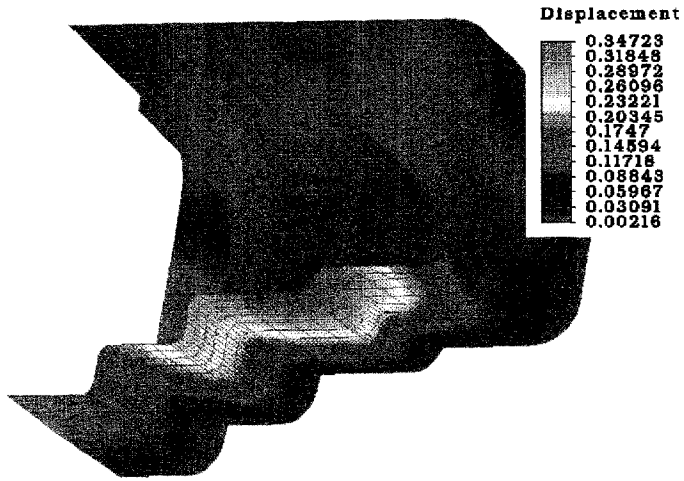

Displacements in inches

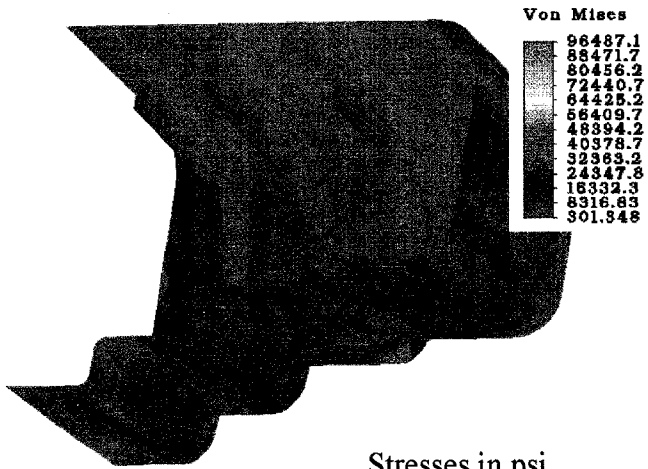

Stresses in psi

250 psig

STEP/RIB FEA OF FIRST DESIGN (Full Scale)

This was the first design that was modeled with both a step profile with curvature on the bottom of the tank. The depth of the first two steps is 3 inches, the remaining step has a depth of 2 inches. The unsupported span length was also increased between the second and third steps to allow for more fuel volume.

Results:

Finite Element Analysis results illustrate the importance of rib/step depth and spacing. The maximum deflection in this tank moved away from the center of the tank to the location of the largest unsupported span and smallest step depth. The high values of the Von-Mises stress were located at the tank wall/rib interface. To reduce processing time and simplify the model, the ribs were modeled to meet the tank walls at a square 90 degree angle. The final models and prototypes will incorporate filleted intersections that will reduce the stress concentrations. Note that the stress in the remainder of the tank approaches the maximum 20 000 psi stress limit.

Assumptions:

Young's Modulus- 4.0 e6 psi

Rib thickness and Depth- 1X4 inches

Wall Thickness- 1/2 inches

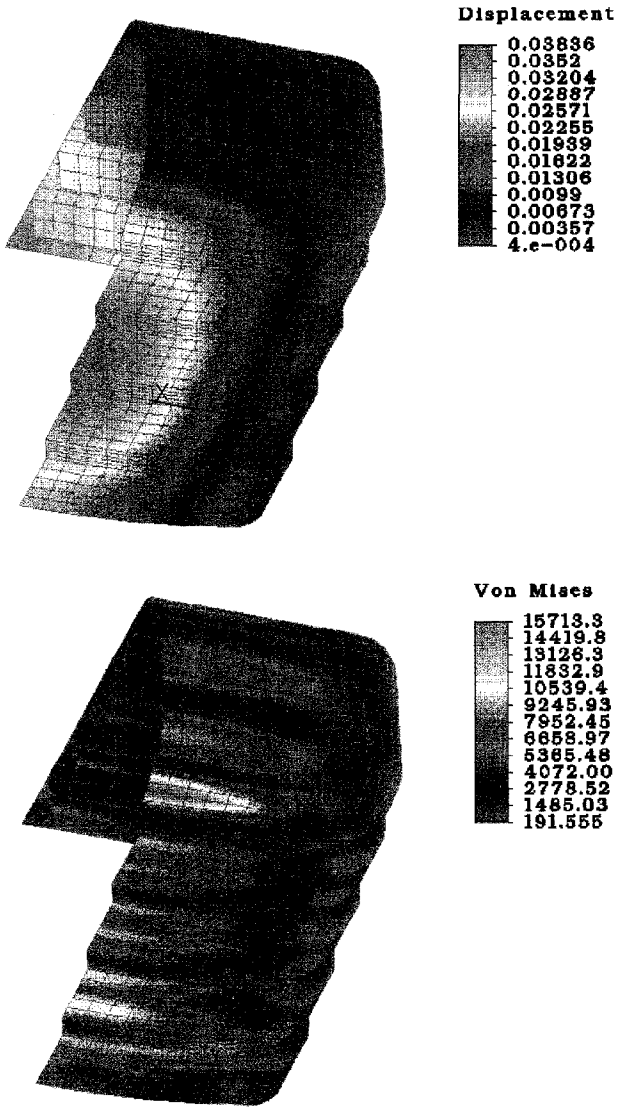

250 psig

Step/Rib FEA of First Prototype Design (1/2) Scale of Full

Results from the first step rib design revealed the need to incorporate an additional step to reduce the length of the unsupported spans. Volume loss was a concern that arose from having deep steps on the bottom of tank in the first design. To resolve this the step depth was reduced to 1/2 inch. The intention was to build a suitable prototype to experimentally compare the accuracy of the FEA deflection results with a real model. This comparison would determine how feasible it would be to accurately model a full scale design using finite element analysis software.

Results

Results from this analysis appeared very promising. The tank was modeled in exactly half scale dimensions of the full scale 36X23X14" tank. Here the maximum deflection was less than 0.04" everywhere. Additionally the maximum Von Mises Stress was less than the 20000 psi limit everywhere including the stress concentrated areas.

Assumptions

Young's Modulus- 4.0 e6 psi

Rib Thickness and depth- 0.8X2 inches

Wall Thickness- 0.35 inches

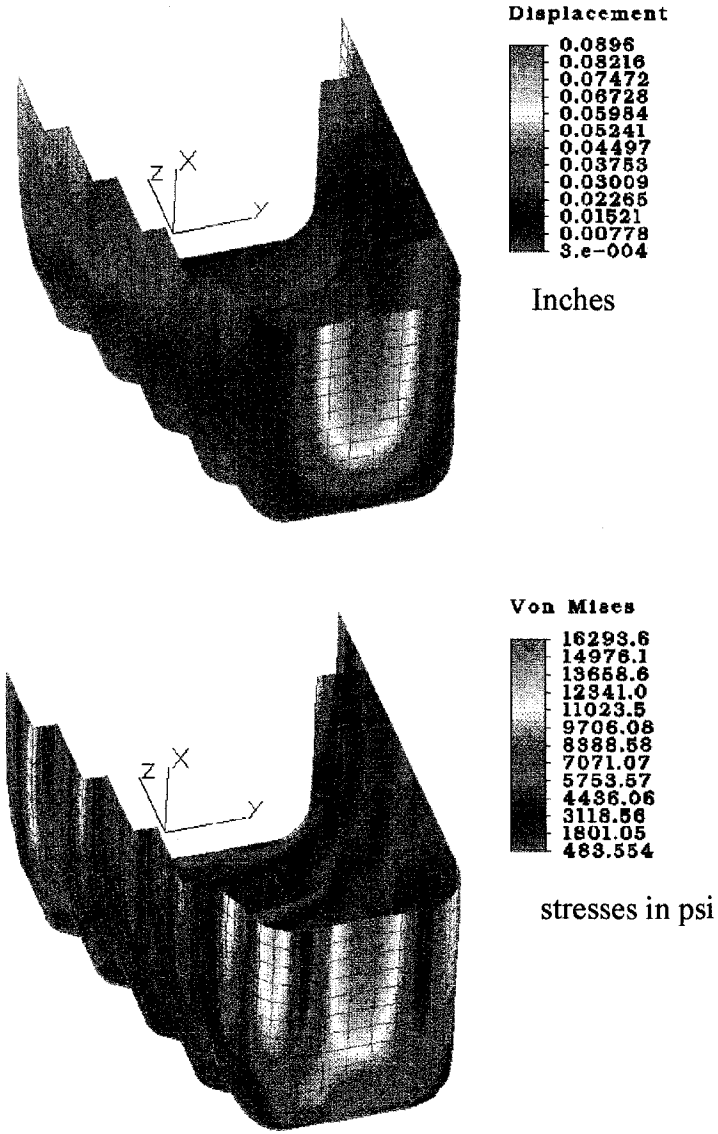

Inches

stresses in psi

250 psig

FEA of Final Prototype Design 1/2 Scale Dimensions

This model is identical to the previous models with a two major differences. The first is that the modulus of the fiberglass over-wrap was taken to be 1.5e6 psi, rather than the published values of approximately 4.0e6. Additionally, the thickness of the walls and ribs were exact half scales of the proposed full scale tank. The FEA results are at 250 psi.

Results

The results from this model illustrate the difference changing the wall thickness, rib thickness and modulus reduction will have on the tank. Even with more realistic values for dimensions and modulus, the tank still performed well at 250 psi. The maximum displacement in this case was still less than 1/10 of an inch. The stress levels were still significantly below 20 000 psi at 16295 in the most stressed regions. This prototype model is proposed for immediate construction and testing.

Assumptions

Young's Modulus	Walls-1.5e6
	Ribs-4.0e6
Rib Thickness and Depth	***0.5X2 inches***
Wall Thickness	***0.25 inches***

Final Prototype Performance at Elevated Pressures

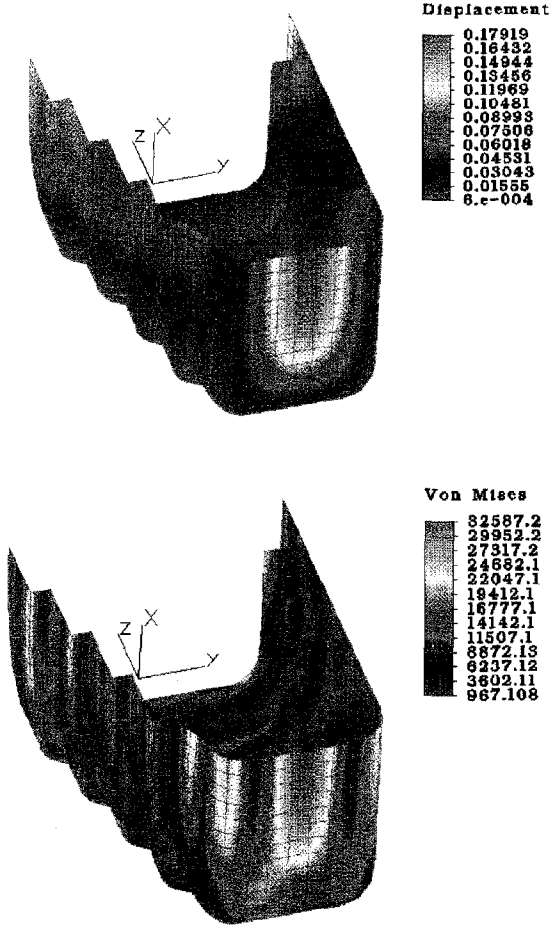

500 psig

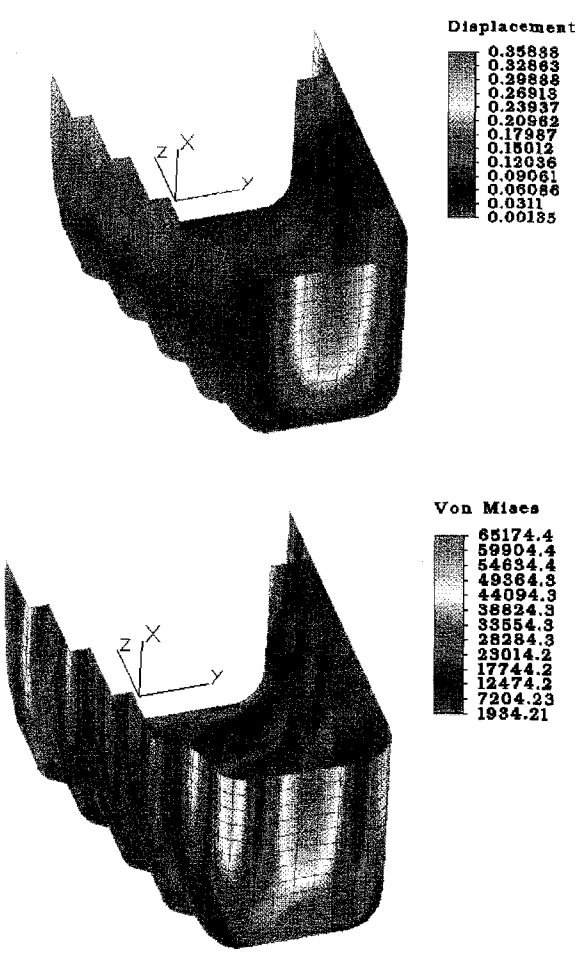

1000 psig

Performance of Full Scale Prototype Design at 250 psig

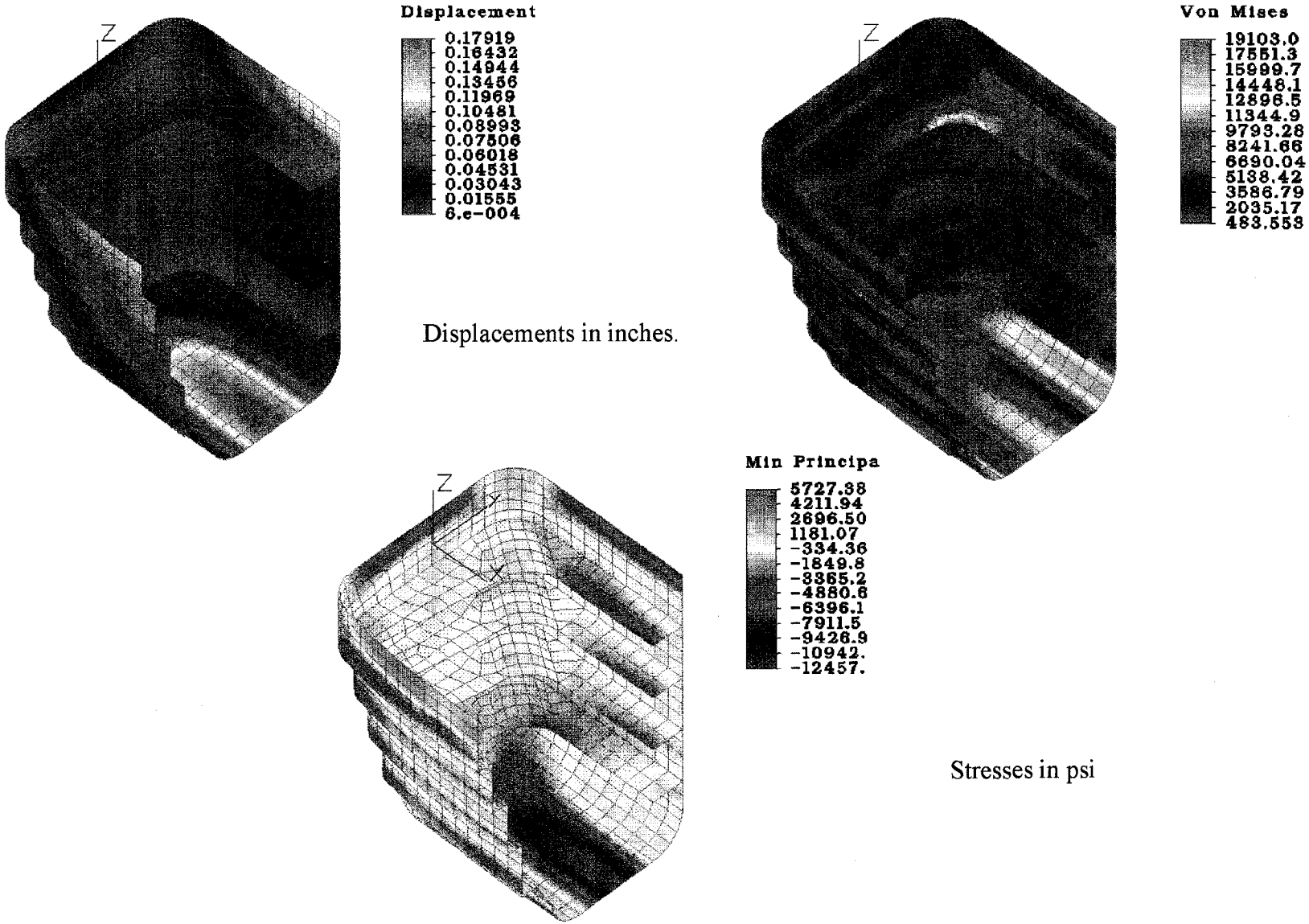

Displacements in inches.

Stresses in psi

CONTINUOUS RIB DESIGN FEA ANALYSIS OF THIRD PROTOTYPE

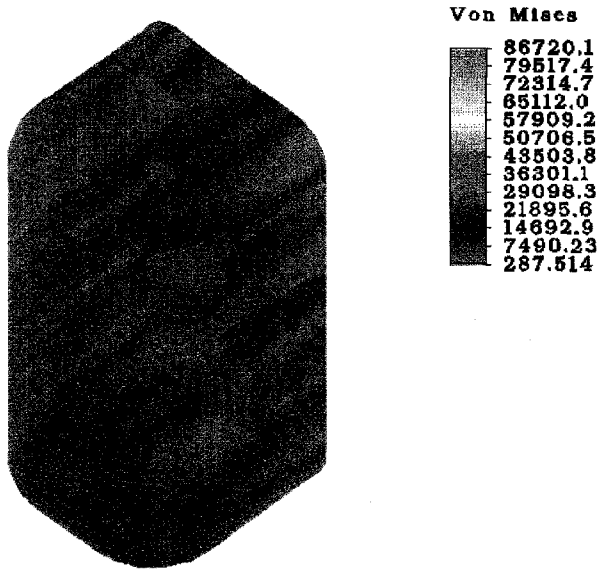

Stresses in psi

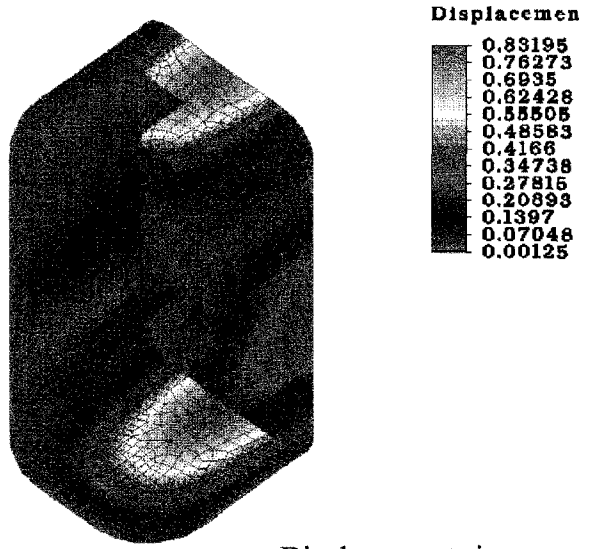

Displacements in inches

This tank was designed based on earlier full scale designs of step/rib designs. It was hoped that the spacing between the ribs and steps on the bottom of the tank could be reworked to increase the volumetric efficiency of the tank. The dimensions of this model are nearly identical in two dimensions to the dimensions allowable in the storage envelope of the B-van. The tank measures 22"X22"X12. This permits a 1/2 over-wrap around the tank and an approximate inch thick bottom, while remaining within the set dimensional design constraints. This model accounted for the dispersion of the toe on either side of the shallower bottom ribs. Ribs had a depth of 3" and a width of 1" on the top and sides of the tank. The bottom of the tank had a rib 1" deep with a width of 1". Elements on either side, approximately 1 inch width on both sides, of the bottom ribs were assigned a thickness of 1", with a modulus averaging between that of the filament wound ribs and the flat walls.

Results:

Finite element analysis of this model revealed significantly high deflections on the largest unsupported spans. Stress concentrations were located at the rib/wall intersections. The stresses in the remainder of the tank, away from stress concentrated areas, blue shaded regions, appeared to lie within the design limit of 20000 psi for the provision of the design factor of four. In addition, highest displace regions were localized on the ends and bottoms.

Assumptions:

Young's Modulus Walls- 1.5e6

Ribs- 4.0e6

Wall Thickness- 0.6 inches

Rib Dimensions (Top and Sides)- 3X1 inches

APPENDIX II

MATERIAL TESTING RESULTS

Shear Lap Test Results

Results of shear lap testing, based on ASTM Designation D 1002-94, are presented on the following page. Please note that only one test on the High-Density Polyethylene-Epoxy bond was possible. While tightening down the grips for testing, the prior three samples broke from the transmitted mounting forces. Sample 3 of the ABS bond tests broke when an attempt to correct the alignment, on the cross-head of the INSTRON, was made. Failure in the HIPS-Epoxy bond testing occurred in the cross-section of the HIPS. The shear strength of the bond exceeded that of the HIPS material, with the exception of one sample.

Shear Lap Test of ABS/EPOXY Bond

Shear Area				Failure	Failure Shear
ABS #	b (inches)	w (inches)	A (inches	Load (lbs)	Stress (PSI)
A1	1.59	1.178	1.87302	498	265.881
A2	1.58	1.172	1.85176	Nil	Nil
A3	1.55	1.165	1.80575	510	282.431
A4	1.57	1.182	1.85574	507	273.206

Average Failure Stress
273.8 PSI

Shear Lap Test of High Density Polyethylene/EPOXY Bond

Shear Area				Failure	Failure Shear
HDPE	b (inches)	w (inches)	A (inches	Load (lbs)	Stress (PSI)
H1	1.31	0.995	1.30345	66	50.635
H2	1.29	1.025	1.32225	Nil	Nil
H3	1.33	1.012	1.34596	Nil	Nil
H4	1.28	0.983	1.25824	Nil	Nil

Average Failure Stress
50.6 PSI

Shear Lap Test of High Impact Polystyrene/EPOXY Bond

Shear Area				Failure	Failure Shear	Failure Tensile
HIPS	b (inches)	w (inches)	A (inches	Load (lbs)	Stress (PSI)	Stress (PSI)
HP1	1.13	0.987	1.110375	236	212.541	1700.326
HP2	1.13	0.991	1.114875	240	215.271	Nil
HP3	1.12	0.993	1.115139	180	161.415	1291.319
HP4	1.13	1.012	1.14356	248	216.867	1734.933
HP5	1.13	0.996	1.121496	215	191.708	1533.666
HP6	1.13	0.983	1.11079	240	216.062	1728.500

Average Exceeded Shear Stress
202.3 PSI

Note: The shear stresses actually exceed these values. Failure occurred across the cross-section of the HIPS. Values stated in Failure Shear Stress are maximum values attained before failure in the ABS occurred.

Table AVII-1 Tabulation of Calculations to determine Shear Strength of Bonds

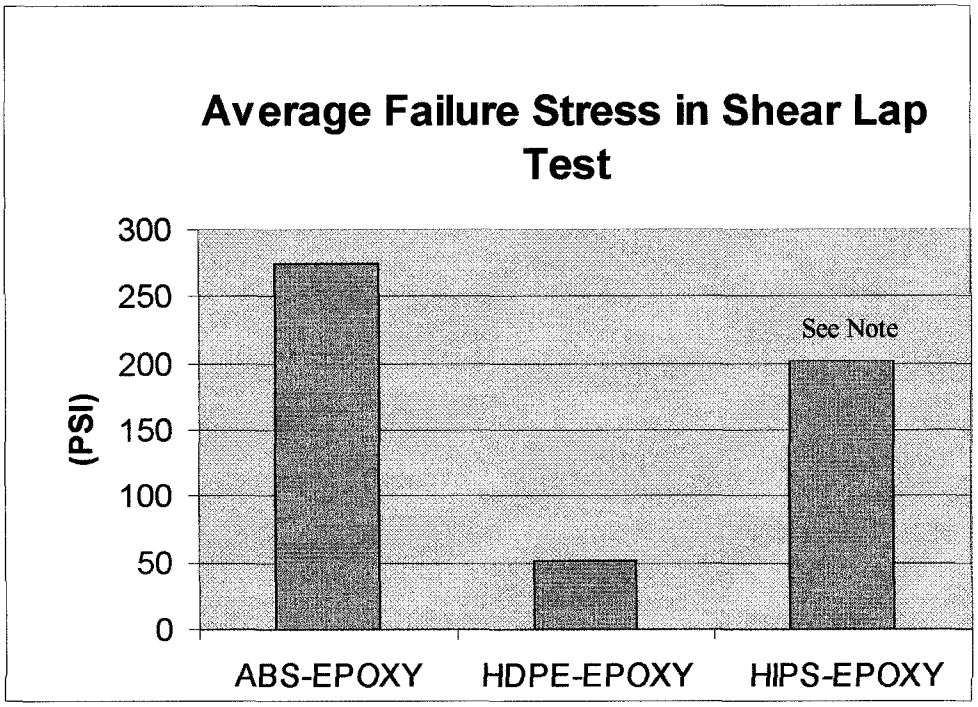

Figure AVII-1 Average Failure Shear Stress

	Average Failure Shear Stress
ABS-EPOXY	273.8 (PSI)
HDPE-EPOXY	50.6 (PSI)
HIPS-EPOXY	202.3 (PSI)

Table AVII-2 Average Failure Shear Stress in Bond Strength

Tensile Testing Results of Varied Lay-up Techniques

Tensile testing of samples was conducted using a INSTRON™ testing machine. The 20000lb load-cell was selected for tensile testing. Strain measurements were made using INSTRON™ extensiometers designed for use with the tensile testing machine. Results presented in the following tables and figures, were obtained from calibrated stress and elongation plots of the test. Note that two different extensiometers were used; one with a 1" gauge-length, the other with a 2" gauge-length. This was a result of a failure in the 1" gauge-length extensiometer early in the testing. Prior to using the 2" gauge-length extensiometer, the extensiometer was re-calibrated prior to subsequent testing.

Results from Samples With No Coupling Agent Added to Epoxy

Sample	Impregnation Method	Width (inches)	Thickness (inches)	Area (square inches)	Failure Load (lbs)	Failure Stress (PSI)	Failure Elongation (inches)	Gauge Length (inches)	Strain	Modulus (PSI)
LAI	1	0.99	0.11	0.1089	2980	27364.55	0.03	2	0.015	1824304
LAII	1	1.01	0.1	0.101	2800	27722.77	0.03	2	0.015	1848185
LAIII	1	0.98	0.11	0.1078	2570	23840.45	0.028	2	0.014	1702889
LAIV	1	0.99	0.098	0.09702	2880	29684.6	0.034	2	0.017	1746153
LAV	1-2	0.99	0.075	0.07425	2900	39057.24	0.021	1	0.021	1859869
LAVI	2	0.995	0.075	0.074625	2190	29346.73	0.028	2	0.014	2096195
LAVII	2	0.99	0.07	0.0693	2290	33044.73	0.028	2	0.014	2360338
LAVIII	2	0.99	0.07	0.0693	2380	34343.43	nil	nil	nil	nil
LAIX	2	0.95	0.075	0.07125	2060	28912.28	0.028	2	0.014	2065163
LAX	2-3	0.99	0.09	0.0891	2150	24130.19	0.012	1	0.012	2010849
LAXI	3	0.99	0.07	0.0693	1910	27561.33	0.028	2	0.014	1968666
LAXII	3	0.99	0.07	0.0693	2480	35786.44	0.033	2	0.0165	2168875
LAXIII	3	0.98	0.07	0.0686	2675	38994.17	0.014	1	0.014	2785298
LAXIV	3	0.99	0.07	0.0693	2350	33910.53	0.021	2	0.0105	3229575

Results from Samples With Coupling Agent Added to Epoxy

Sample	Impegnation Method	Width (inches)	Thickness (inches)	Area (square inches)	Failure Load (lbs)	Failure Stress (PSI)	Failure Elongation (inches)	Gauge Length (inches)	Strain	Modulus (PSI)
LBI	1	0.99	0.109	0.10791	2180	20202.02	0.035	2	0.0175	1154401
LBII	1	0.99	0.1	0.099	3390	34242.42	0.042	2	0.021	1630592
LBIII	1	0.98	0.105	0.1029	2590	25170.07	0.031	2	0.0155	1623875
LBIV	1	0.98	0.106	0.10388	3390	32633.81	0.044	2	0.022	1483355
LBV	1-2	0.99	0.1005	0.099495	2400	24121.82	0.025	2	0.0125	1929745
LBVI	2	0.99	0.098	0.09702	3180	32776.75	0.042	2	0.021	1560797
LBVII	2	0.98	0.09	0.0882	3170	35941.04	0.046	2	0.023	1562654
LBVIII	2	0.99	0.08	0.0792	2310	29166.67	0.028	2	0.014	2083333
LBIX	2	0.98	0.08	0.0784	2890	36862.24	0.034	2	0.017	2168367
LBX	2-3	0.98	0.09	0.0882	2660	30158.73	0.033	2	0.0165	1827802
LBXI	3	0.99	0.075	0.07425	2500	33670.03	0.032	2	0.016	2104377
LBXII	3	0.99	0.083	0.08217	3100	37726.66	0.014	1	0.014	2694762
LBXIII	3	1	0.08	0.08	3300	41250	0.014	1	0.014	2946429
LBXIV	3	0.99	0.09	0.0891	3010	33782.27	0.036	2	0.018	1876793

Table VII-3 Tabulation of Results from Testing of Varying Lay-up Techniques

Results from the testing are also illustrated graphically in the following figures. As clarification the following will be used as reference:

Sample#'s

1 thru 4	Samples laid-up using method 1 as the impregnation method
5	Sample bordering impregnation methods 1 and 2
6 thru 9	Samples laid-up using method 2 as the impregnation method
10	Sample bordering impregnation methods 2 and 3
11-14	Samples laid-up using method 3 as the impregnation method

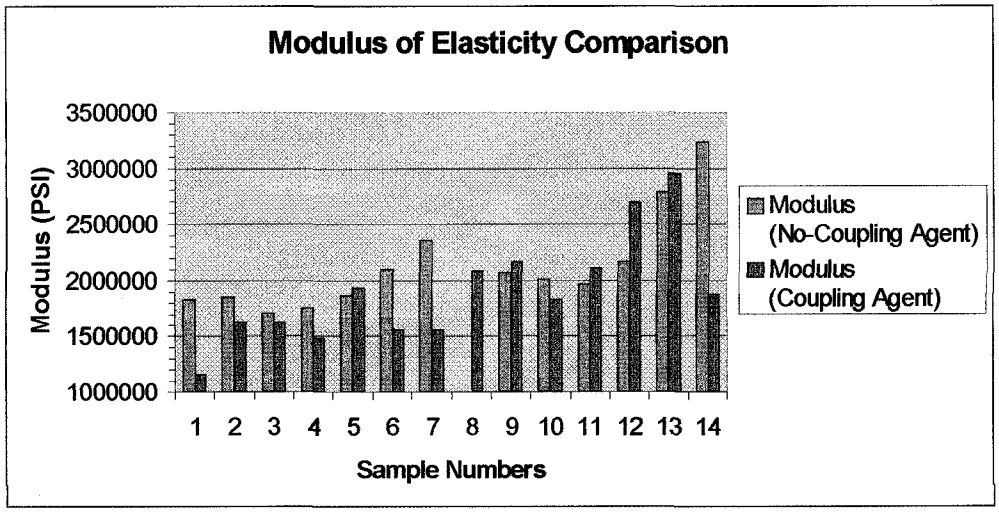

Figure AVII-2 Comparison of Modulus of Elasticity

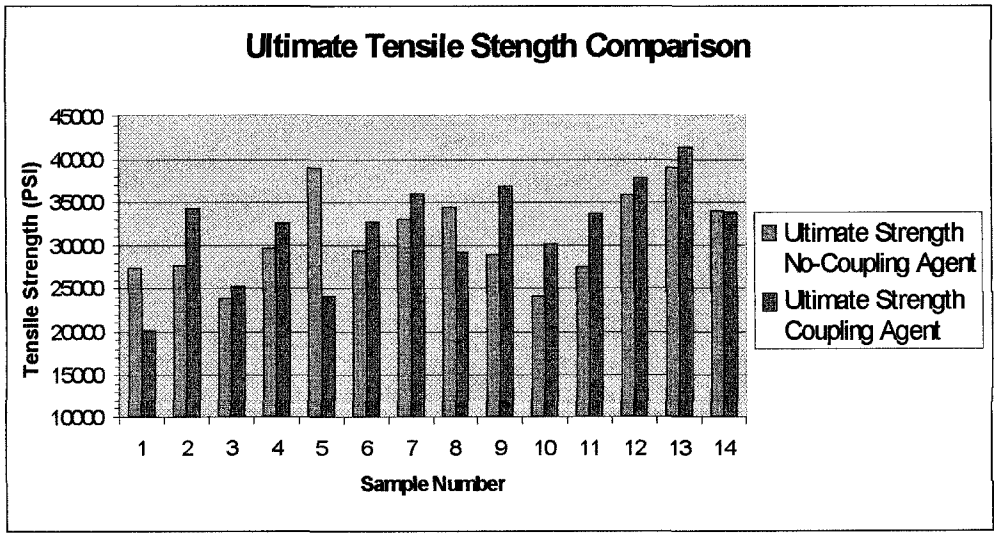

Figure AVII-3 Comparison of Ultimate Tensile Strength

As a final step, the mean values for strength and modulus were calculated. The results of the calculations are shown in Table AVII-3

Mean Modulus Values		
Method	No Coupling Agent	Coupling Agent
1	1.780E+06	1.473E+06
2	2.174E+06	1.844E+06
3	2.538E+06	2.406E+06

Mean Ultmate Strength Values		
Method	No Coupling Agent	Coupling Agent
1	2.715E+04	2.806E+04
2	3.141E+04	3.369E+04
3	3.406E+04	3.661E+04

Table AVII-3 Mean Values of Ultimate Strength and Modulus

APPENDIX III

VIEWS OF PROTOTYPE CONSTRUCTION AND PATTERN DESIGNS

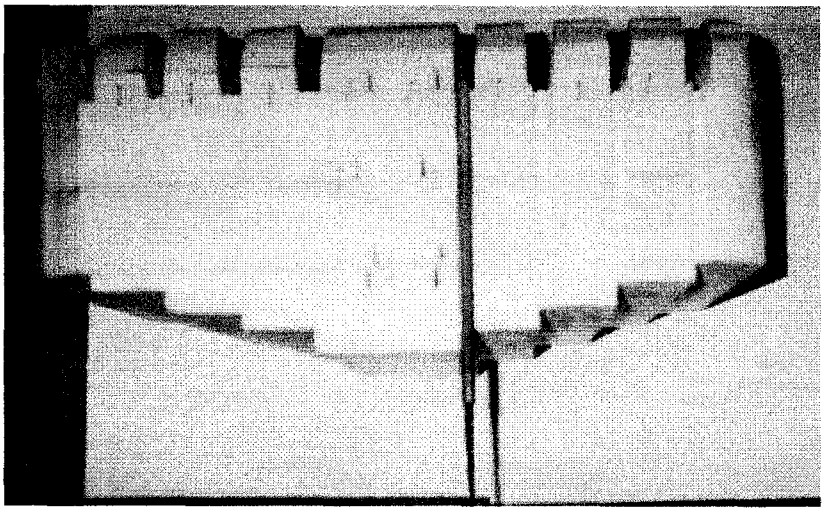

Figure AII-1 Front View of Prototype 2 Under Construction

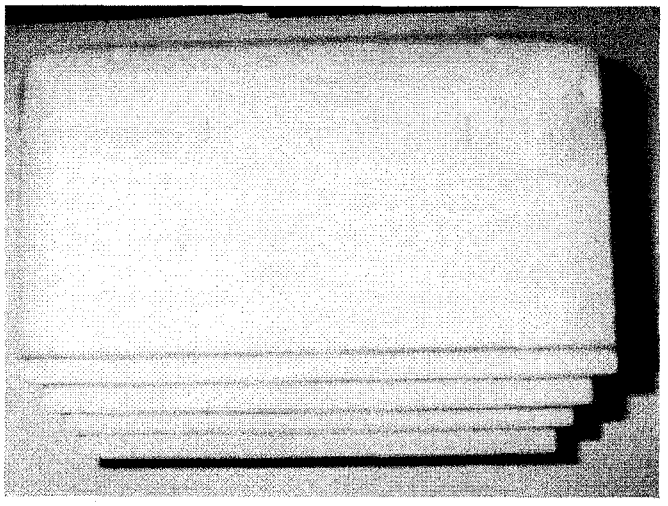

Figure AII-2 Side View of Prototype 2 Under Construction

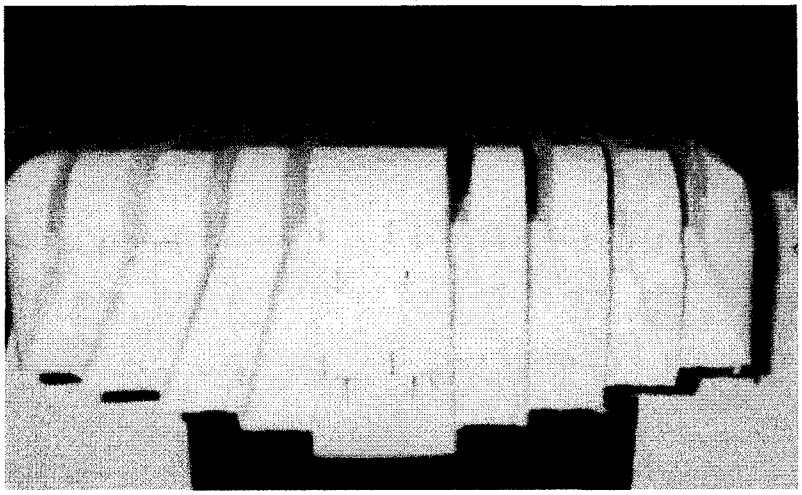

Figure AII-3 Side View of Prototype 2 After Completion
(note the tapering out of ribs to the bottom of the tank)

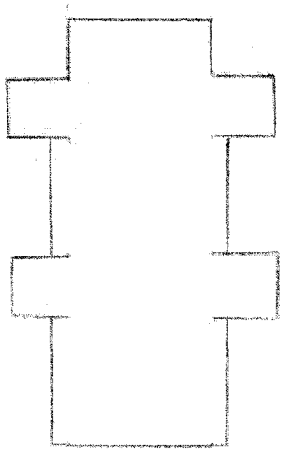

1

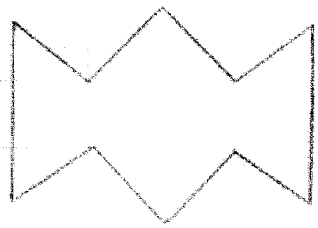

2

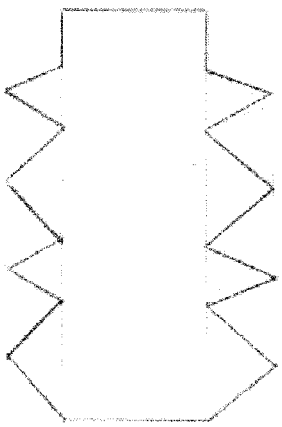

3

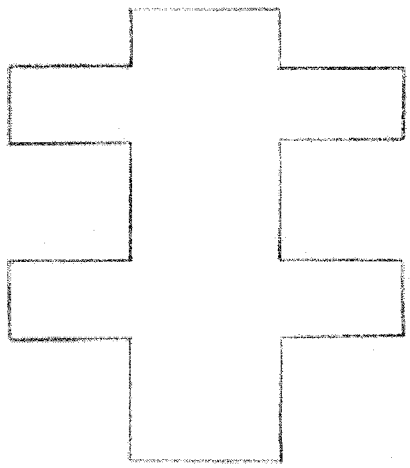

4

5

PATTERNS USED IN THE LAY UP OF PROTOTYPES

APPENDIX IV

DATA ACQUISITION SYSTEM USER MANUAL

GEN200™ DATA ACQUISITION SOFTWARE

Introduction

An introductory operating procedure manual has been developed to aid new users in the use of the Sciemetric GEN200™ data acquisition software. The development of this manual is based on the anticipated use of the software with the Sciemetric System200™ data acquisition system.

Inputs and Tasks

Inputs are used to designate the measurement of any analog, digital or counter signal. In the case of the current static measurement set-up, the system 200 will provide analog measurement signals for measure. Signals from the acquisition of strain and deflection measurement voltages will be routed through a PC interface card located within the IBM XT.

The definition of an input does not result in the automatic measurement of the assigned quantity. Rather defining an input tells the software how to interpret the information it is receiving from the data acquisition system. To make use of the desired inputs, the inputs must be assigned as a task within the software. It is important to note that inputs must be assigned names of no more than 8-alphanumeric characters.

A task is a collection of commands that instruct the software on which channels to scan, the frequency at which they are scanned and the method of storing information in a file. The user must ensure that the quantities they want to have measured are included as tasks within the software.

GEN200 Menus

Gen200 is driven entirely through the use of menus. Menus within the software are fairly self-explanatory. The Gen200 opening menu is illustrated in Figure AV-1, on the following page. It will be useful to consider this menu when following the sequence of instruction presented in the following pages.

The current system does not facilitate the use of a mouse. All selections must be made using cursor arrows or function keys. Typically, carefully reading the instructions on the bottom of the screen with prevent pushing keys erroneously, leading the user to undesired menus, or accidentally exiting the program. Typically, the Esc key can be used to return the user to a main menu. However, in some cases a function key is required to return to the previous menu. Care must be taken until the user becomes familiar with the software package.

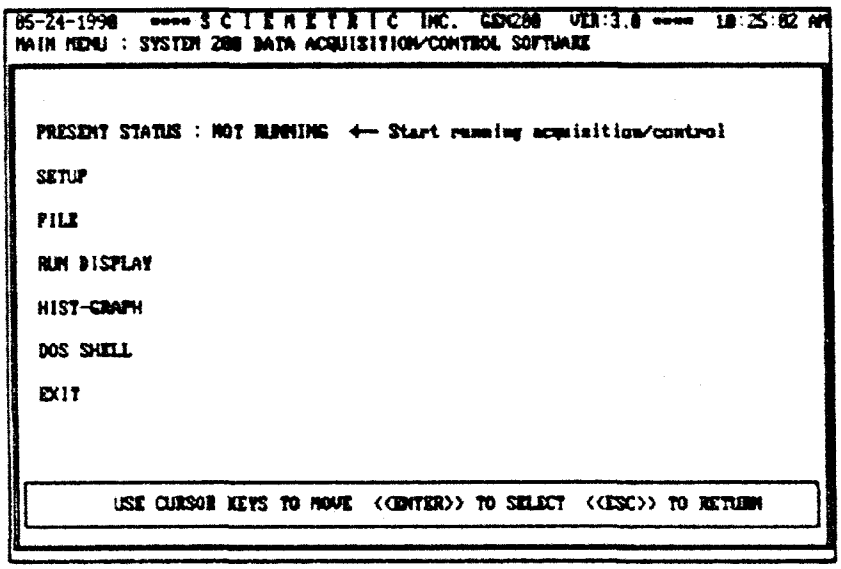

Figure AV-1. Reproduction of GEN200 Opening Screen

Each menu on the opening screen will now be desribed

PRESENT STATUS: Toggling the cursor over this menu, and hitting enter, will either start data acquisition or stop the acquisition process.

SETUP — This is perhaps the most important menu to the user. Within the setup menu, tasks and inputs are assigned.

FILE — This is the menu from which configuration files are created, saved or retrieved.

RUN DISPLAY — The run display menu allows the user to view the acquired results as they are received in the data acquisition system. Prior to viewing graphical plots of the incoming results, graphs must be defined and curves of the variable measured must be assigned to the graphs.

HIST-GRAPH — This menu allows for the viewing of the analysis results after data acquisition has ceased.

DOS SHELL — This self-explanatory menu, allows the user to work within DOS without exiting the program.

EXIT	This menu allows the user to exit the software. The user should make sure any work is saved through the use of the FILE menu. NO AUTOSAVE feature is present in the program.

Getting Started

The existing software on the IBM XT used, for data acquisition in experimental measurement of strains and deflection, is located within the GEN directory on the C drive. The assumption is made that the user can get from the root C: drive to the GEN directory by utilizing the C: cd GEN command.

Step by step instruction of setting up and running the software will now be described.

Step 1.

Start the GEN200 program by typing GEN200 on the command line prompt. (C:\gen\GEN200)

Step 2.

Toggle down to the FILE menu and press enter. If a previous configuration file is known, type the file name in after toggling on LOAD command. Otherwise a file may be located by toggling down to the DIRECTORY command and pressing enter. Any files named filename.gen are previously developed configuration files. As an example, loading any version of the gammag#.gen configuration files may be useful. If the user so desire, a file may be developed by scratch by toggling on the SAVE command and entering the filename wanted.

Step 3.

Toggle back to the main menu by pressing the Esc key. At this time toggle down to the SETUP menu and press enter. The SETUP menu will appear, Figure AV-2.

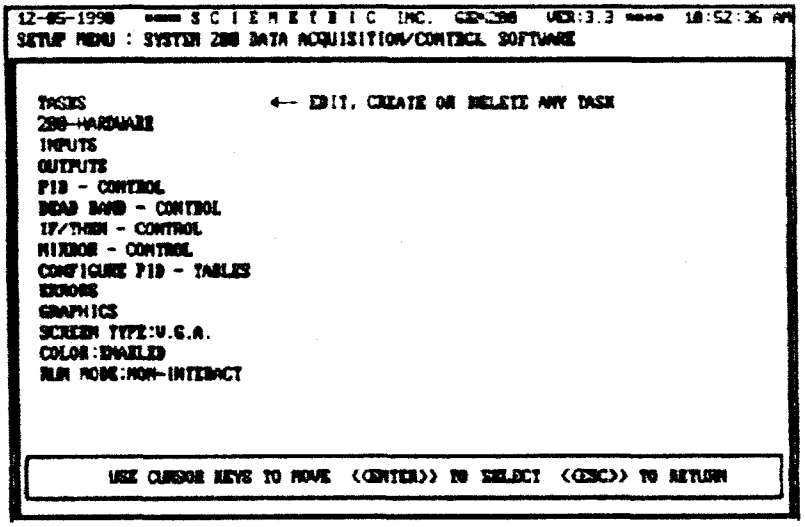

Figure AV-2. GEN200 INPUT SETUP MENU

STEP4

Toggle to the INPUTS menu and press enter. Press the F3 key and assign a name to the input function to be created. Press Esc. The name of the input will be present on the screen, and should be highlighted. Press the F1 key to edit the input. If a previous input requires modification, this may be accomplished by simply toggling over to the desired input (if more than one has been named) and pressing the F1 key.

STEP5

A variety of menus should appear on the screen. Every menu has to be addressed in the definition stage. Toggle over to the Module (HW) command and press enter. If the input is a strain gauge measurement, the module number is 1, the linear potentiometers use module 2. Next toggle over to the CHANS (CH) command and press enter. Strain gauges utilize channels 0 through 7, number in order of there left to right position on the 206A bridge/strain gauge conditioning board. When defining potentiometers, channel numbers start at 8. This corresponds to the starting position of location 8 on the 32-channel expansion module (channels 0-7 are reserved for 206A).

Next toggle over to the FNC: menu. Toggling over to the range (RNG) menu, select auto range for the strain gauge measurement or ±10V if the potentiometer measurement is being defined in the input channel. Here if strain gauges are used, select DCV (direct current voltage) or if linear potentiometers are used DCVHG for selection of the High pin to ground (corresponds to settings on 32-channel expansion module).

It is possible to define one of the inputs to convert the output voltage to strains. This is accomplished through the selection of MTH. This command allows a user to use information from another input. This is useful for strain calculations. Once again MATH must be selected in the FNC menu must be selected to accomplish this task.

Step6

If the MTH function is selected the line menu on the bottom of the screen changes to include UNITS and EQ: The unit typically selected if strains are to be calculated is E. This unit is a convenient way of representing strain due to the limited availability of symbols for unit representation. Conversion of the measured input voltage to a strain may be accomplished using an appropriate strain conversion equation. In the case of the current quarter bridge configuration, the calculation may be accomplished by toggling over to EQ: menu and typing the equation in the exact manner of the following.

-4*({name of input channel}/5)/(GF*(1+2*{name of input channel}/5))

The type of brackets, around the name of the input channel referred to, must be identical to the ones shown. If other brackets are used, the reference to an input channel will not be recognized. The value of 5 is the supply voltage. Currently the Bridge power supply is set at 5 volts. Changing the power supply voltage will result in the need to change this

value in the equation. The value for Gauge Factor, GF, is supplied with the strain gauges used.

If the MATH function was not selected in the FNC menu, the next menu will once again be MTH. The MTH function allows the input channel to be mathematically processed based on the following equation:

$$Y = A + B(X - D) + C(X - D)^2 + E * 10^{(X-D)*F}$$

Ensuring that values of A,C, D, E, and F are all 0, results in the mathematically processed signal to be a multiple of the output signal value, X. If raw data is required, assign a value of 1 to B. If the signal is linearly expanded, multiply the value by the appropriate multiplication factor.

The next command to select is the FMT line menu. Here the values of the input signals are assigned a number format to be saved under. Typically, strain gauges are formatted by using #.##### in the command line. This is due to the fact that, unless the input signal is multiplied by increasing the B value, strain values are in the milli-range. The same approach should be used for the potentiometer inputs, except one more # should be placed before the decimal if the 10V power supply is used.

UNITS (U), this command assigns units to values if the MATH command was not selected under the function menu. The selection of Volts in both the case of the linear potentiometers and strain gauges will be correct under the current configuration.

The FTR command was not utilized. This command allows the set-up of the averaging filter. A low value of 3 out of a scale of 1 to 999 was used. Lowering the filtering increased the rate at which data acquisition occurred. Additionally, due to the slow, static nature of the test, filtering of the signal was not necessary. Leave RLY set off and press Esc.

STEP 7

Selecting the task is the next step in the progression of setting up the data acquisition software. When the TASK menu is selected from the Set Up menu, a vertical set of numbers, starting at 1, appears. To create the first task, toggle the cursor keys so the number 1 is highlighted. Next press F1 to create a task. If the user wants to delete a task, toggling over and highlighting the desired task, and pressing the F2 key will delete the task.

If the F1 key is pressed, a line menu will appear at the bottom of the screen. The first step is to set the scan rate. This is accomplished by toggling over to SCAN and pressing enter. Press enter again to select Constant. The scan rate is measured in seconds. Depending on how frequently the user wants to scan the channels, a value in seconds is

type in. For example, if channels are to be scanned every 10 seconds, a value of 10 is entered. More frequent scanning is accomplished by lowering the scan number.

Next the CHANS menu has to be selected. All the defined input channels should appear on the screen. This command allows the assignment of input channels to a task. To assign a input channel to the task, highlight the desired input function and perform the following. Hitting the space bar will remove the input from the task, this is used if assigned input channels aren't being utilized for acquisition. Reducing the number of unused inputs in the task, will speed up the processing of data. However, if the channel is being used for the acquisition, utilize one of the following function keys:

F1- Scans the channel but does not record the data
F2- Scans the channel and saves the last scanned value during each save period
F3- Scans the channel and saves the average scanned value during each save period
F4- Scans the channel and saves the maximum scanned value during the save period
F5- Scans the channel and saves the minimum scanned value during the save period
F6- Scans the channel and saves the total of the scans during each period.

Either the F2 or F3 command are typically the most useful for the data acquisition required with the strain gauges and potentiometers.

Selection of the MODE menu allows the user to decide between the available saving methods. The options are NO-SAVE, CLOSE OR OPEN. The first option is self-explanatory. Close saving runs slower than open mode, this is because the save file is closed after each time data is written to it. In the event of a power failure, the close command would ensure that data during the test would be safely saved in the file up to the last data acquisition scan. The open saving method may result in lost information, if power is lost while the data saving file is open.

STATE turns the task ON and OFF

The SAVE menu assigns the frequency, in seconds, at which the scanned data is saved. Press enter on Constant. Assigning a save value the same as that of the scan value will result in data being saved each time a scan takes place.

Finally the FILE command allows the user to assign a name to the data file to which the data is written to.

Step8

The next step is to set up the graphics menu. This is accomplished by toggling down to GRAPHICS in the SETUP menu. Hitting enter on the graphic menu will result in two additional menus: GRAPHS and CURVES. First select the GRAPH menu. In the following menus, selecting MODIFY; NEW_GRAPH will allow the user to define

parameters such as titles and scales to the graphs. After selecting NEW_GRAPH, the software requires that a name be entered for the new graph.

At this Graphs Set-up will appear. The selection of REAL-TIME, from the TYPE menu will result in the acquired input channels being plotted against time. This is most suitable in all cases. Within the following menus, the selection and formatting of axis is permitted

Hitting the escape key until the choice between GRAPHS and CURVES appears again is the starting point for the next operation. Toggle over to curve and hit enter. Press enter over Select Modify. Next assign the curve an individual number. A new line menu should appear, following instructions on the bottom of the screen will allow the user to select the channel the curve is going to represent and the graph (assigned previously) to which the curve will be plotted on.

STEP 9

At this point the software is setup for the acquisition of data. It is important that throughout the previous process, that data was saved occasionally by using the FILE:SAVE command. If this task had not been done to this point, it should be done as part of this step.

STEP 10

This is the last step that requires setup of the data acquisition system. Assuming strain gauges have been applied, the next step is connecting the gauges to the 206A bridge/strain conditioning module. The use of three colour (black, white and red) wire strands would be useful at this point. Strip the ends of the wires so that the plastic covering is remove. Next, tightly twist the ends of the black and white wires together. At this point solder one of the strain gauge terminals to the black/white wire twisted end and the other to the red wire. At the 206A board, splice the other ends of the wires so that the plastic coating is removed from the other end. Connect each of the color-coded wires to the terminals that match the wire colors on the connectors. Repeat this process for the remaining gauges, using connectors for the consecutive bridge circuits utilized for each strain gauge.

Connect the positive and negative power supply wires to the positive and negative terminals on the potentiometers. Run the signal wire from the potentiometer back to the 32-channel expansion module, and connect the signal wire to the bottom terminals on the three terminal connectors. As a check make sure the connections correspond to the H marking on the board.

STEP 11

With all setup complete toggle onto the PRESENT STATUS menu and hit enter to start data acquisition. To view data as it is acquired, toggle down to RUN DISPLAY. Within the RUN DISPLAY screen, press F2 to see graphical plots of the data. To toggle between graphs, use the up and down cursor arrows and hit enter when the name of the desired graph is displayed.

STEP 12

Stop data acquisition by pressing F6 or escape.

STEP 13

All experimental data, written to the data file, may be re-opened in any spreadsheet. The data file is space delimited, so appropriate selections for importing the file must be made.

Comments

It is important to mention that this introductory operating procedure is intended to be used as a method of allowing users to gain familiarity with the software. The capabilities of the data acquisition system are not limited to the strain and deflection measurements. The current acquisition system, however, is configured for this type of measurement.

APPENDIX V

FINAL FEA MODELING RESULTS OF PROTOTYPES 2 & 3

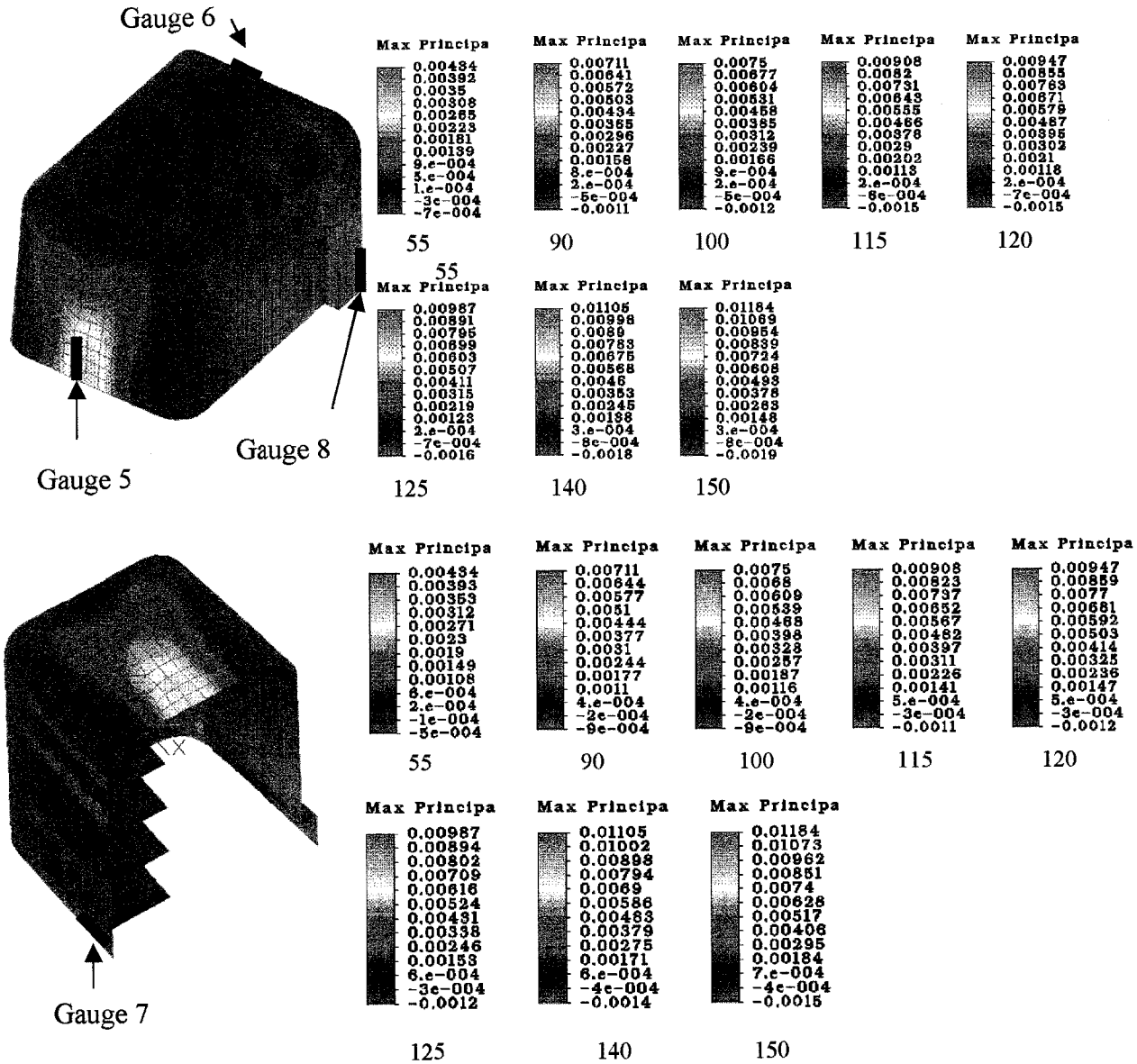

Figure AV-1 Strain predictions from finite element analysis. Strains used in comparison for experimental strain measurements on gauges illustrated use maximum principal strain. Black lines indicate orientation and locations of strain gauges. Numbers under strain predictions indicate the internal pressure in pounds per square inch.

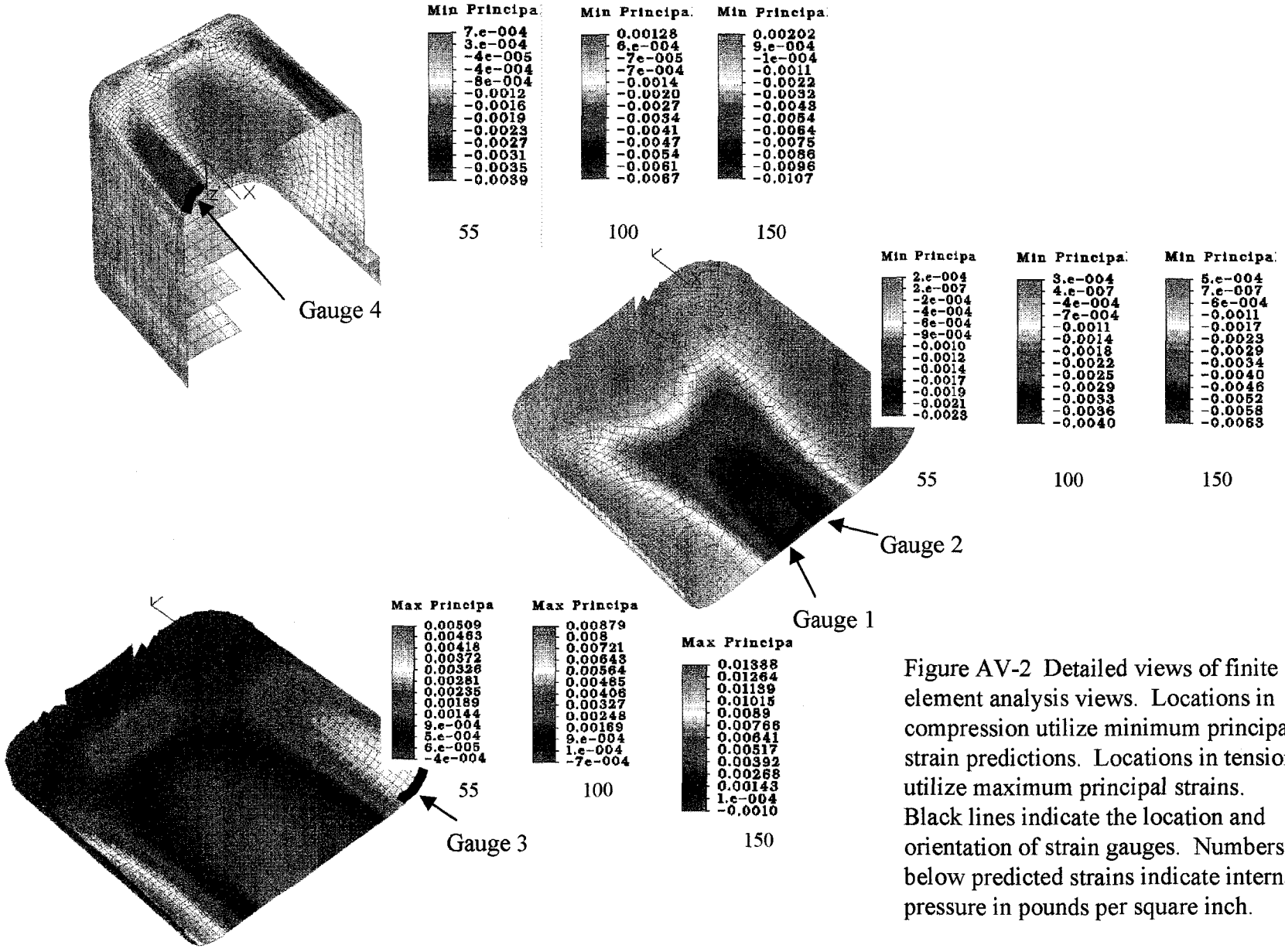

Figure AV-2 Detailed views of finite element analysis views. Locations in compression utilize minimum principal strain predictions. Locations in tension utilize maximum principal strains. Black lines indicate the location and orientation of strain gauges. Numbers below predicted strains indicate internal pressure in pounds per square inch.

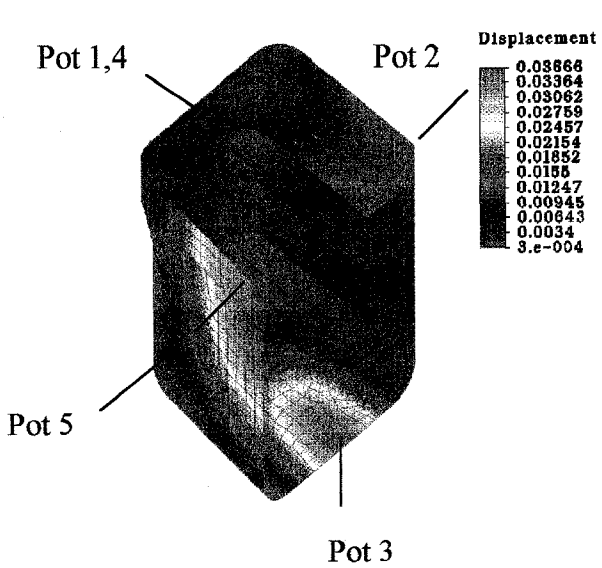

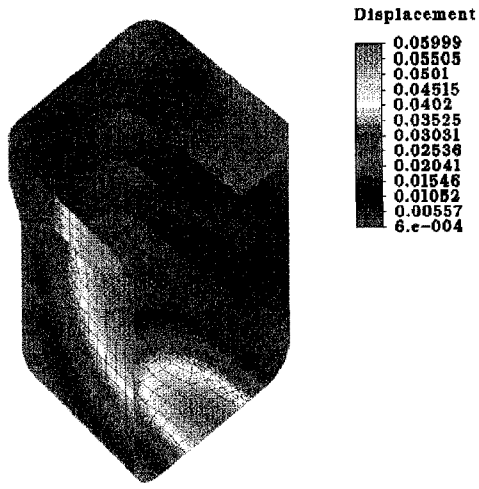

55 PSI

90 PSI

Displacements in inches

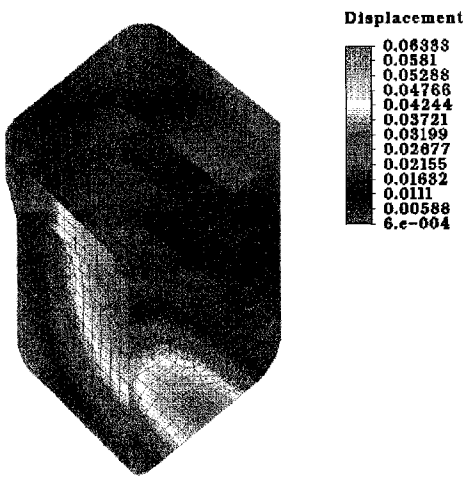

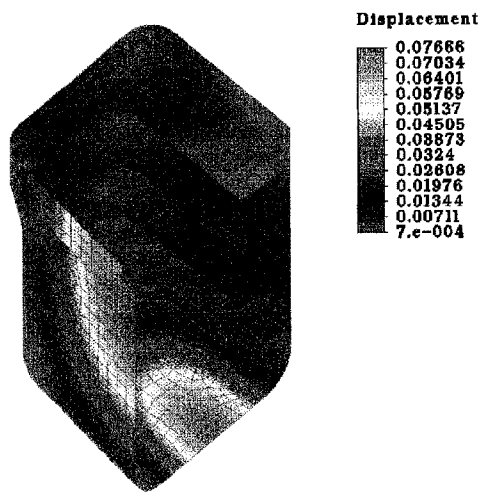

95 PSI

115 PSI

ALGOR FEA Deflection Predictions of Prototype Tank 2

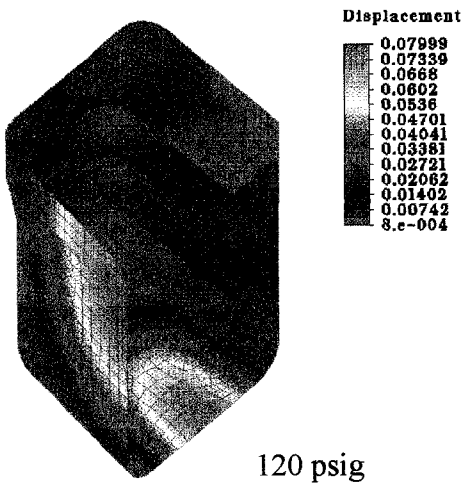

120 psig

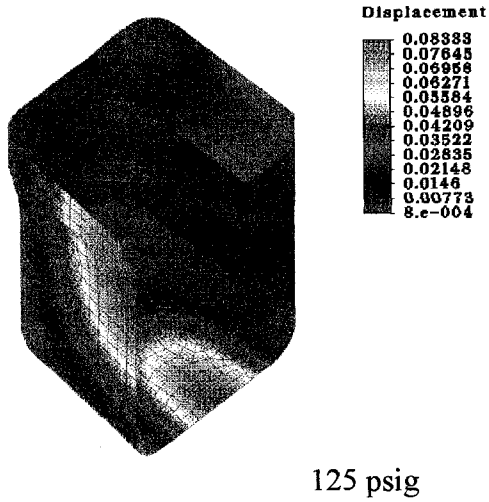

125 psig

Displacements in inches

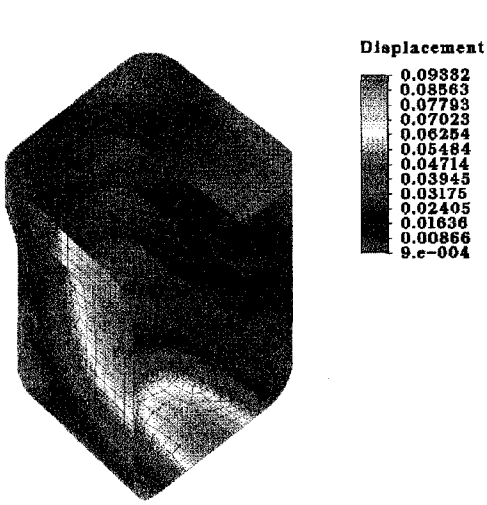

140 psig

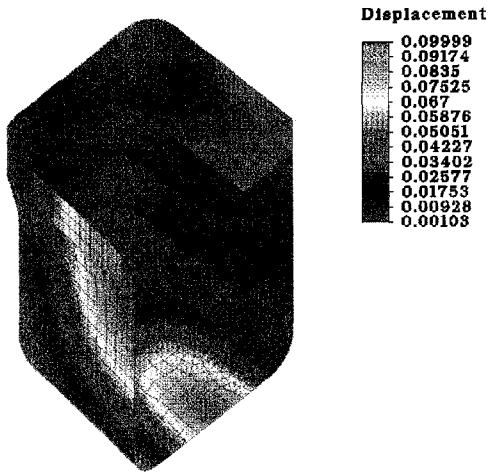

150 psig

FINITE ELEMENT ANALYSIS OF PROTOTYPE 3

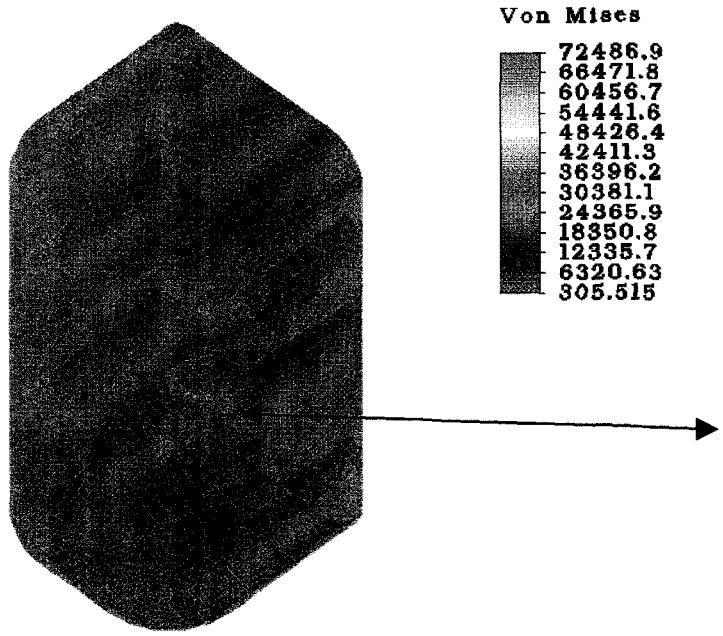

Close-up View of stress concentrations at bottom rib fillets

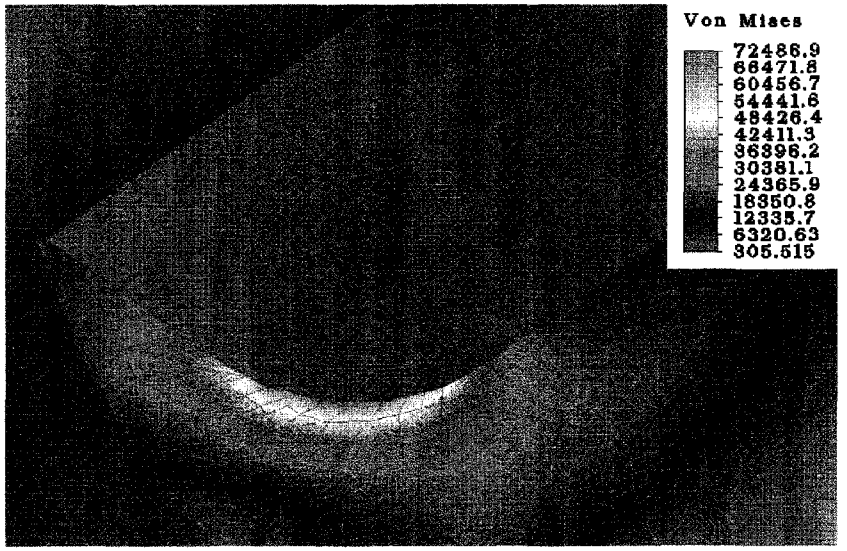

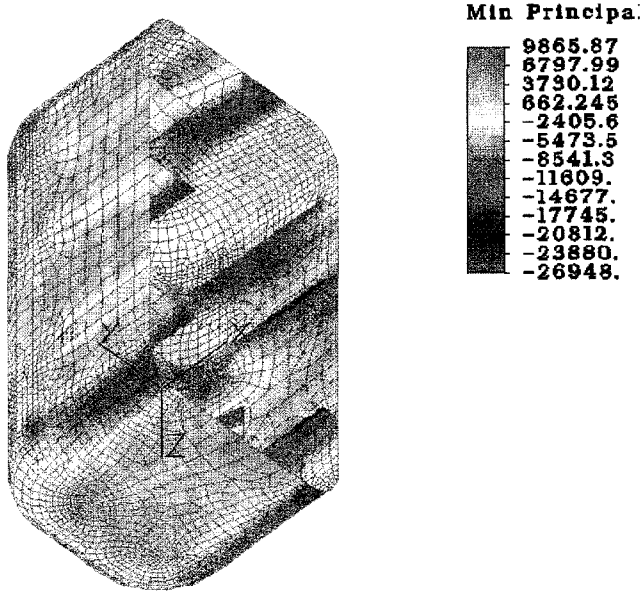

Analysis results of minimum principal (maximum compressive) stresses in the third prototype tank. Stresses in psi.

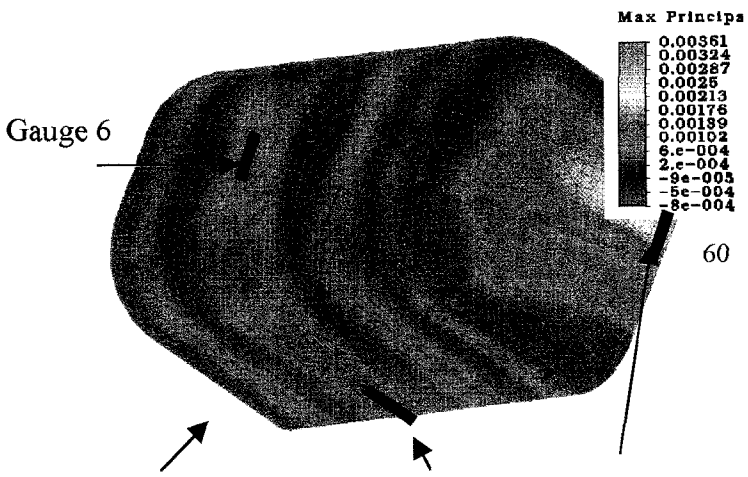

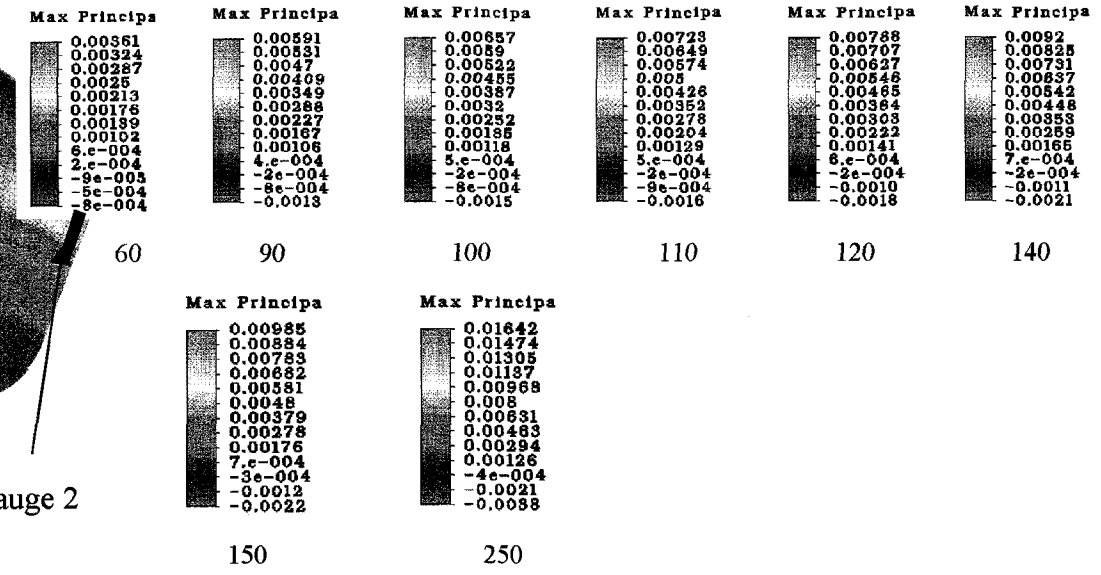

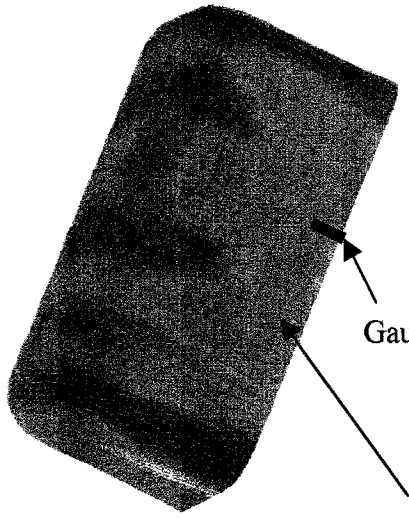

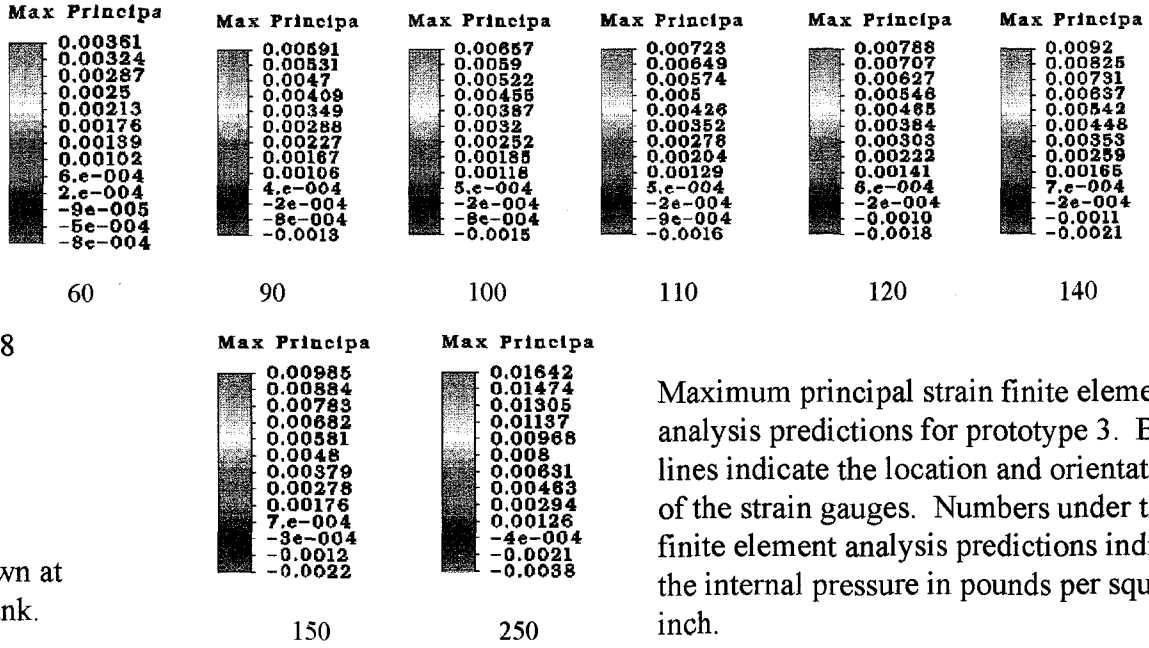

Maximum principal strain finite element analysis predictions for prototype 3. Black lines indicate the location and orientation of the strain gauges. Numbers under the finite element analysis predictions indicate the internal pressure in pounds per square inch.

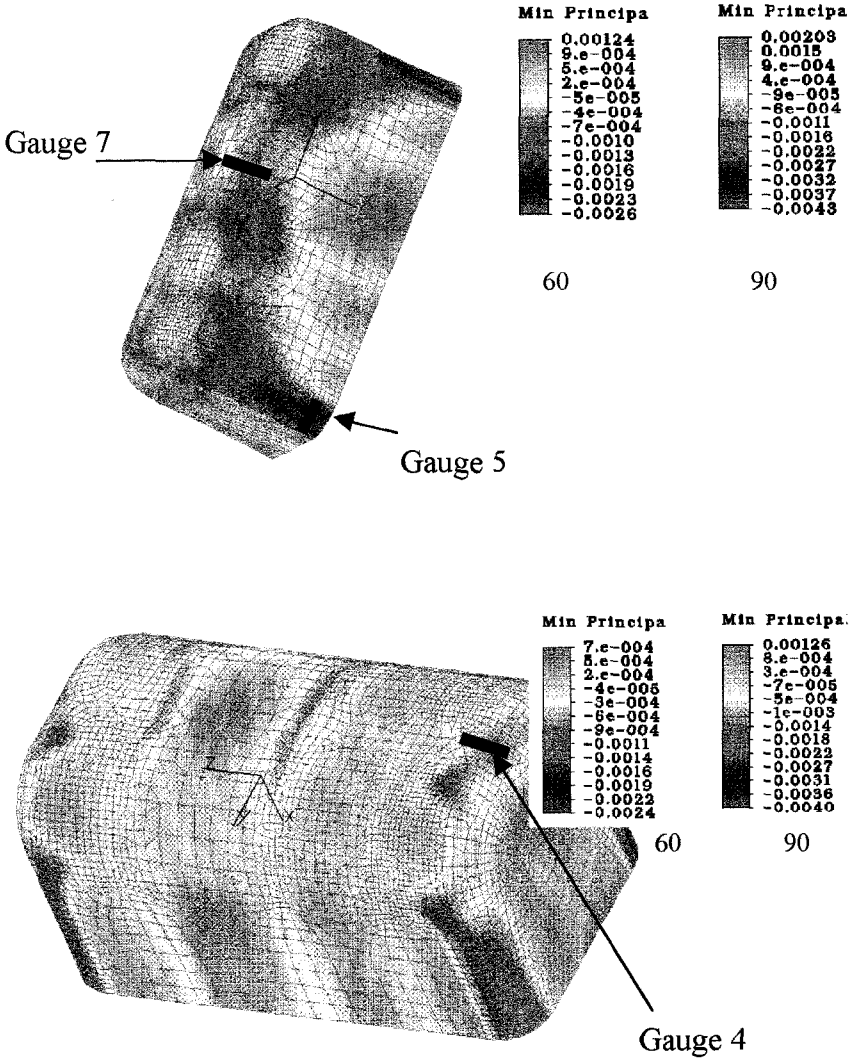

Strain predictions for locations measured experimentally. Black lines indicate the location and orientation of strain gauges. Numbers under finite element analysis predictions indicate the internal pressure in pounds per square inch. Minimum principle strains are used for comparison of locations in compression. In the case of comparisons for gauge 1, strains in the 11 (x-direction) were used to differentiate between the finite element analysis predictions for strain gauge 2.

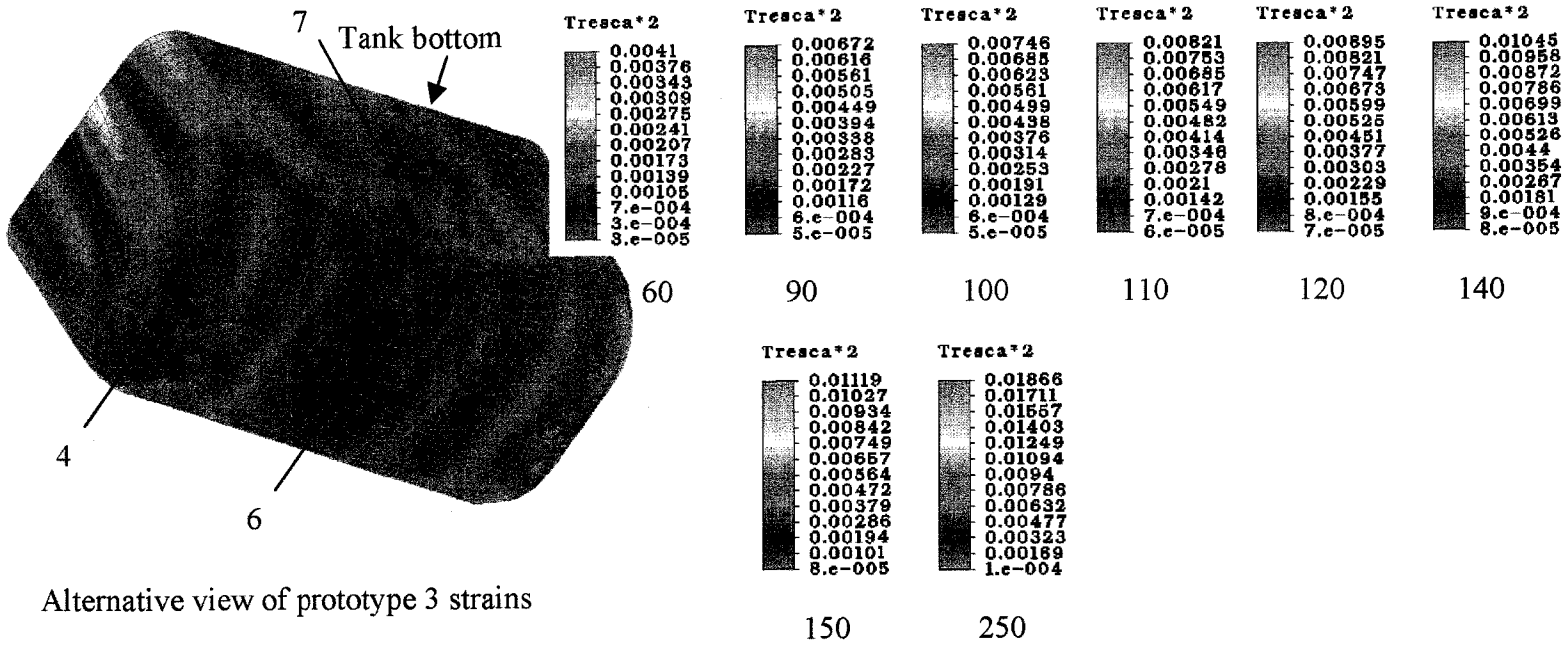

Alternative view of prototype 3 strains

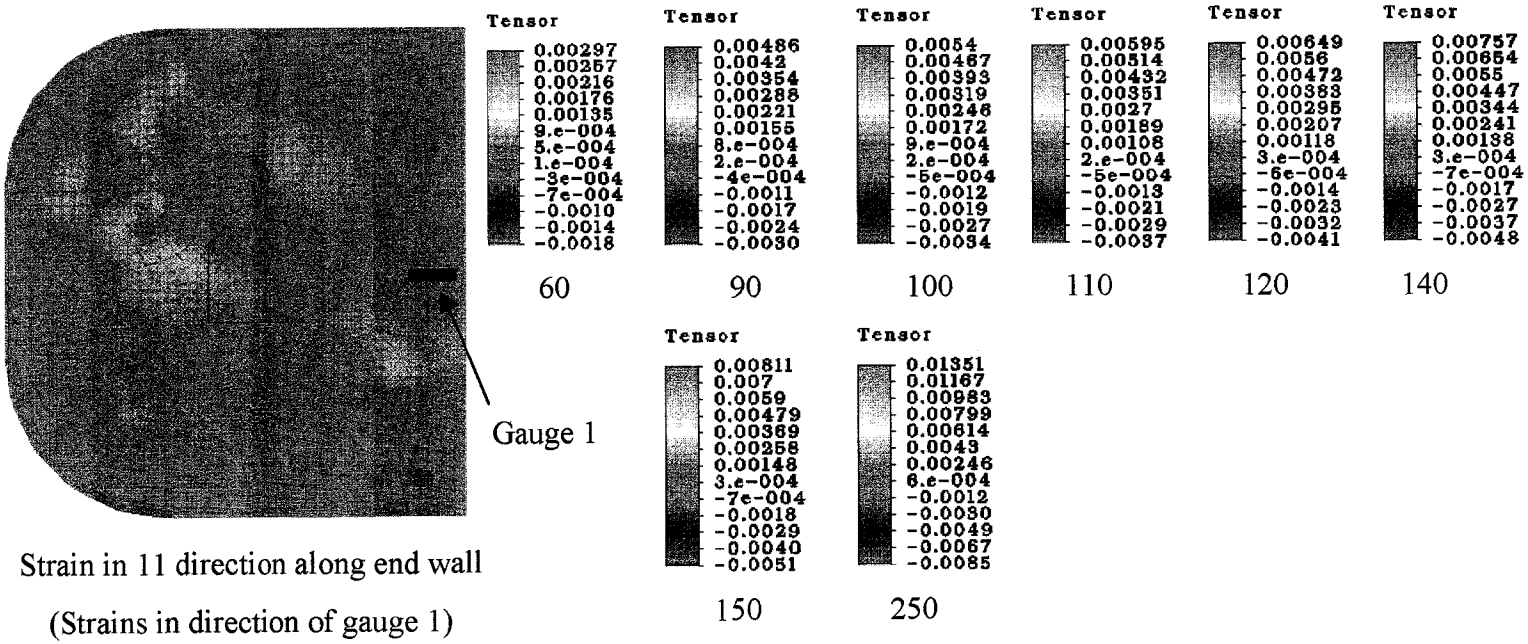

Strain in 11 direction along end wall

(Strains in direction of gauge 1)

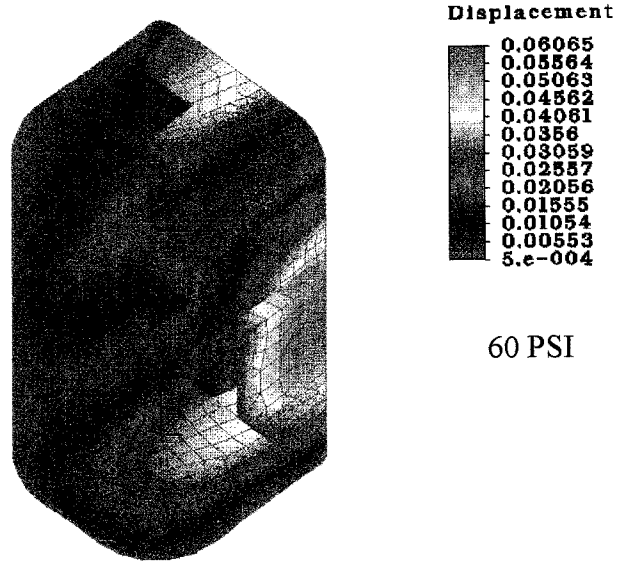

60 PSI

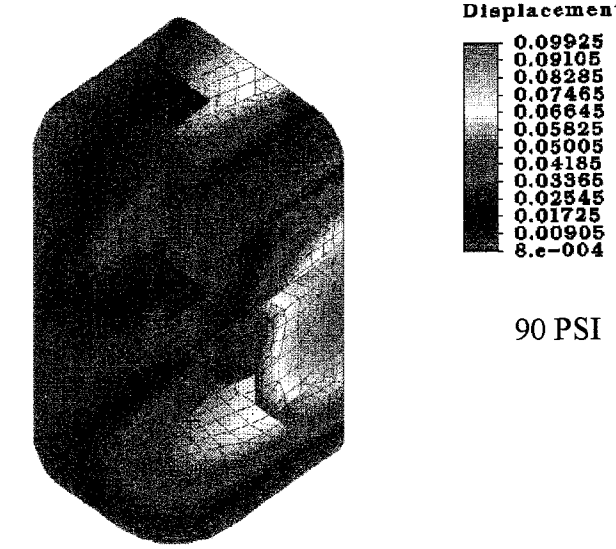

90 PSI

Displacements in inches

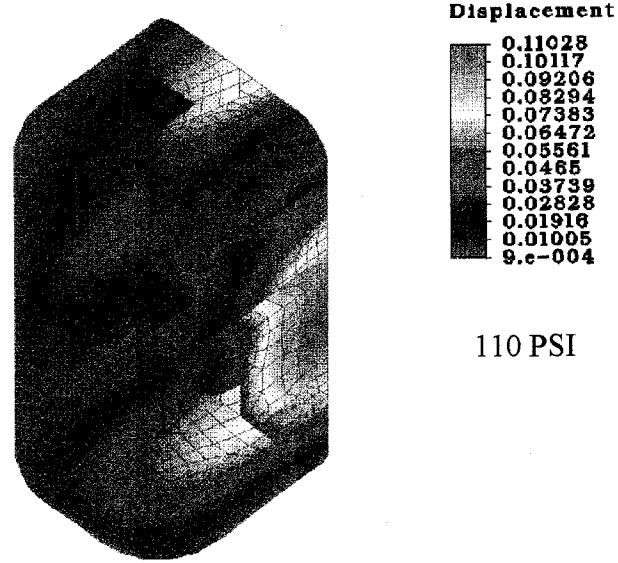

110 PSI

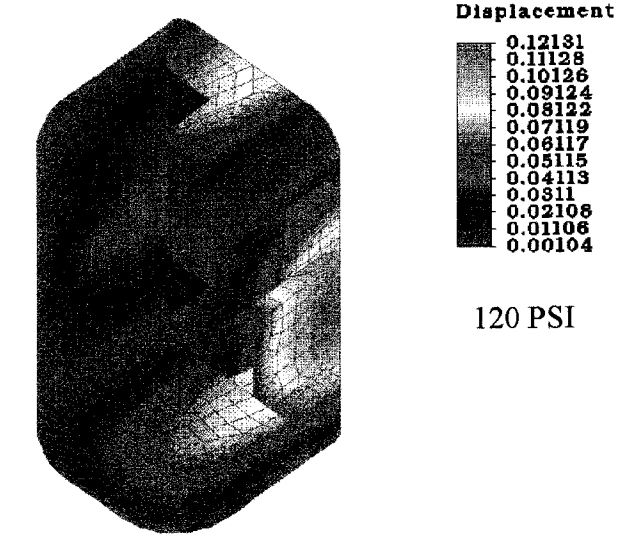

120 PSI

ALGOR FEA Deflection Predictions for Prototype Tank 3 (1-4)

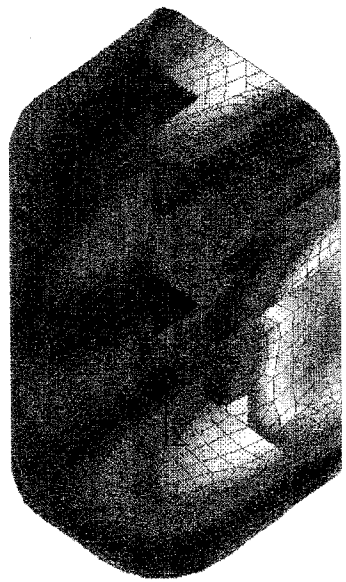

140 PSI

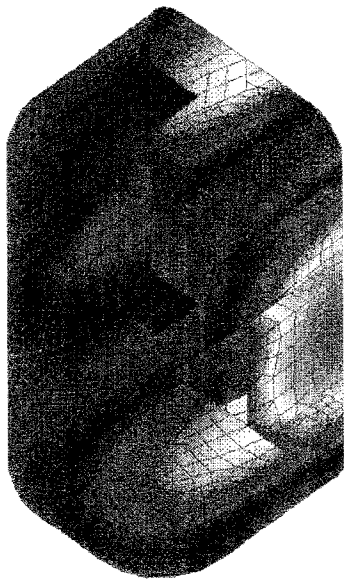

150 PSI

Displacements in inches

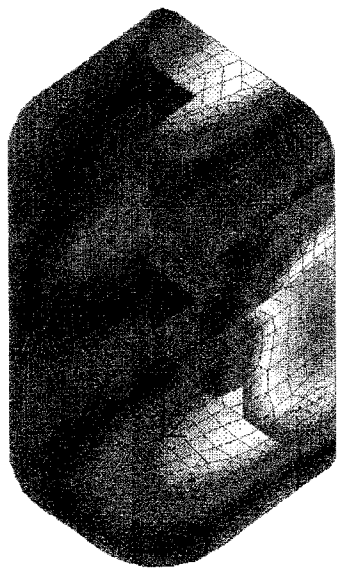

250 PSI

APPENDIX VI

ANALYSIS OF RESULTS FOR PROTOTYPE 2

DISPLACEMENT RESULTS

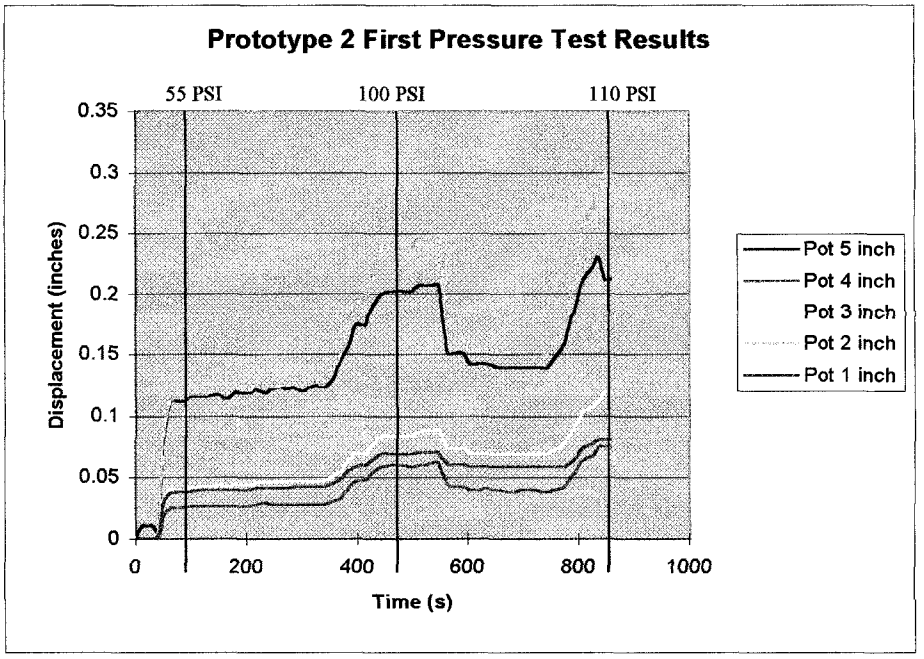

Figure AVI-1 Displacement Results for Pressure Test 1

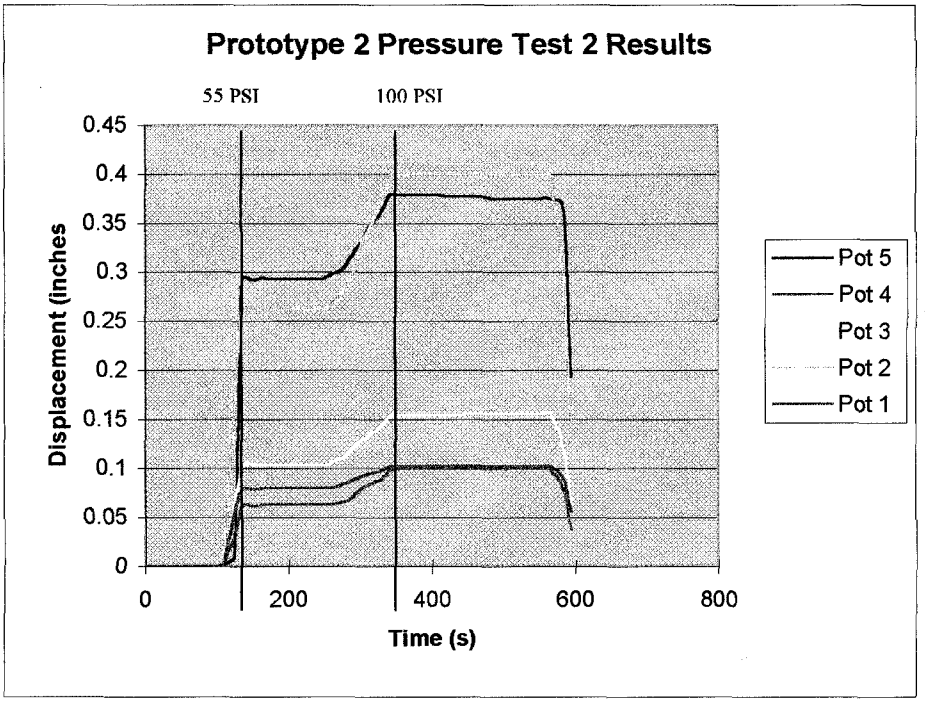

Figure AVI-2 Displacement Results for Pressure Test 2

STRAIN RESULTS

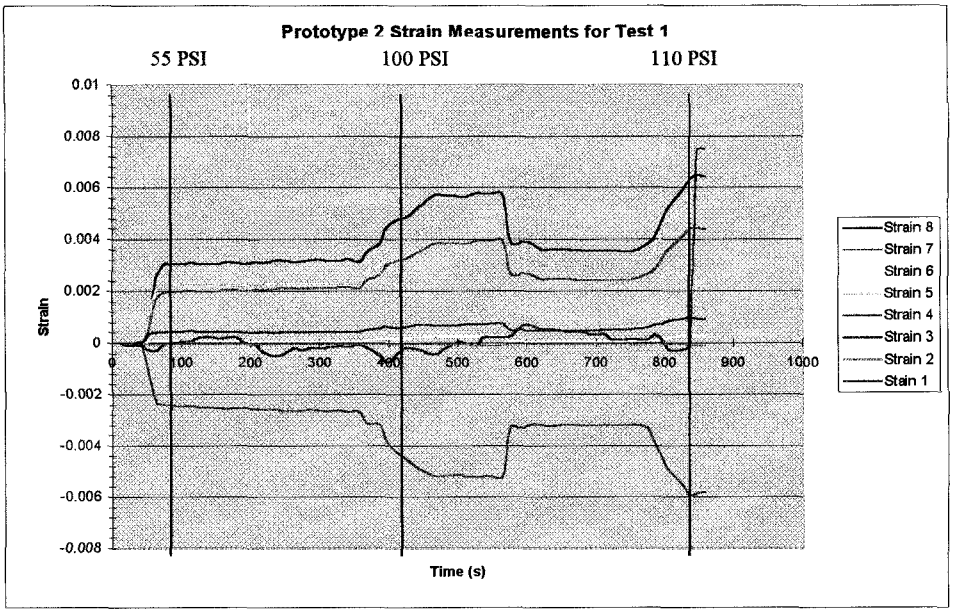

Figure AVI-3 Strain Results for Pressure Test 1

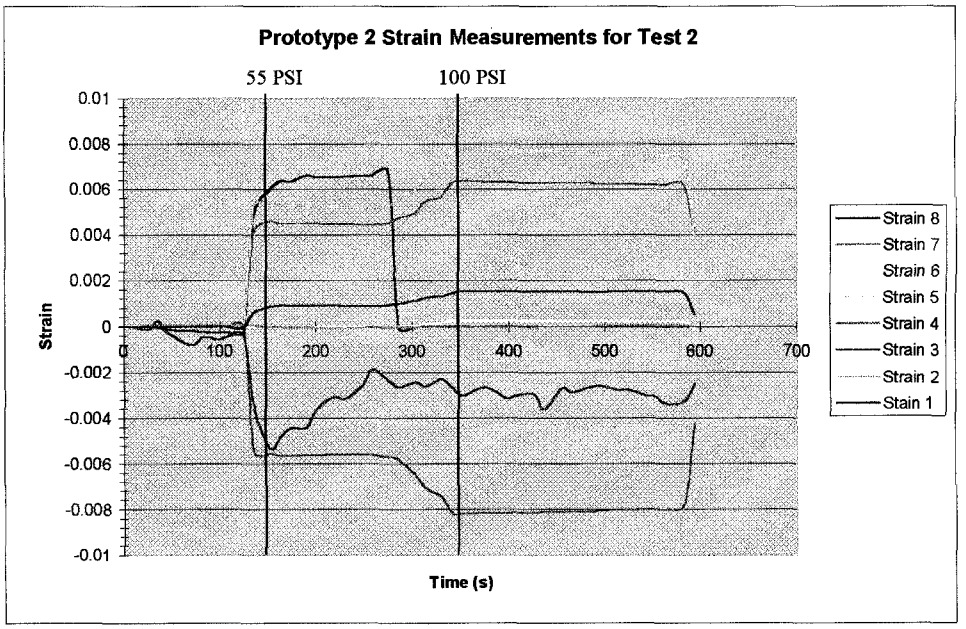

Figure AVI-4 Strain Results for Pressure Test 2

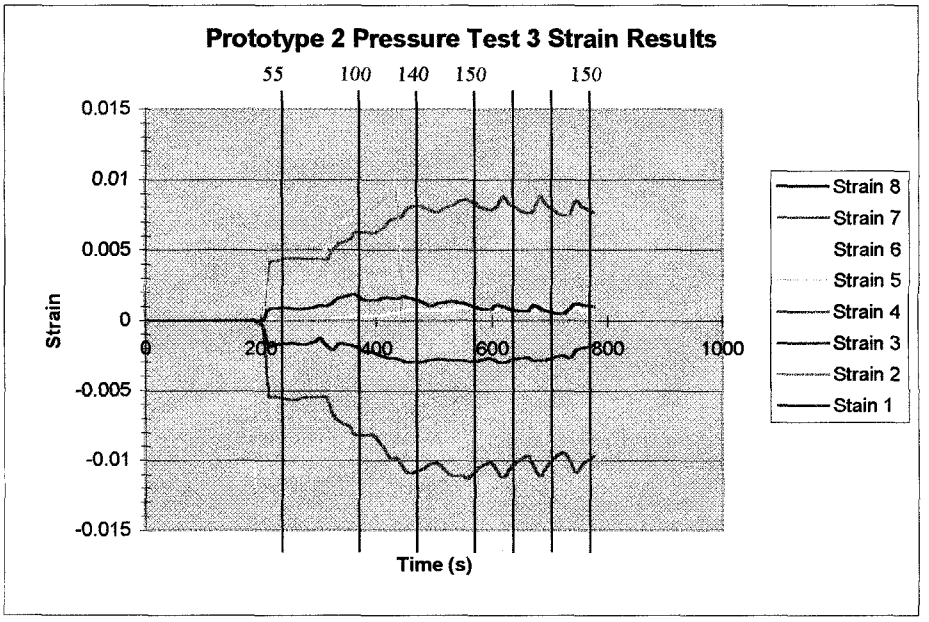

Figure AVI-5 Strain Results for Pressure Test 3

COMPARISON OF RESULTS-DISPLACEMENT

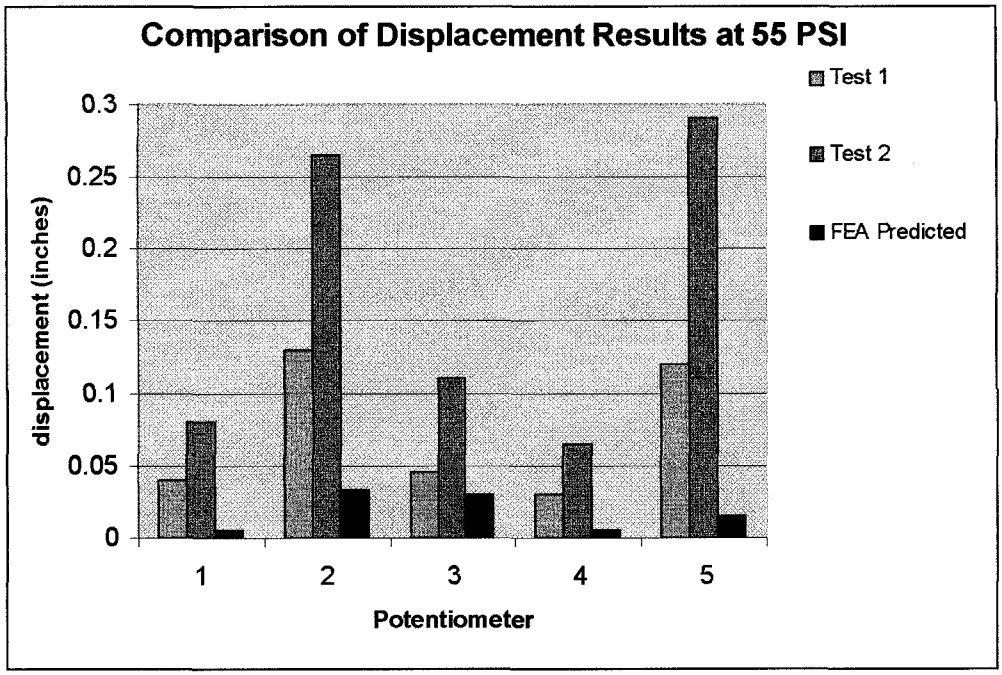

Figure AVI-6 Comparison of Displacement Results at 55 PSI

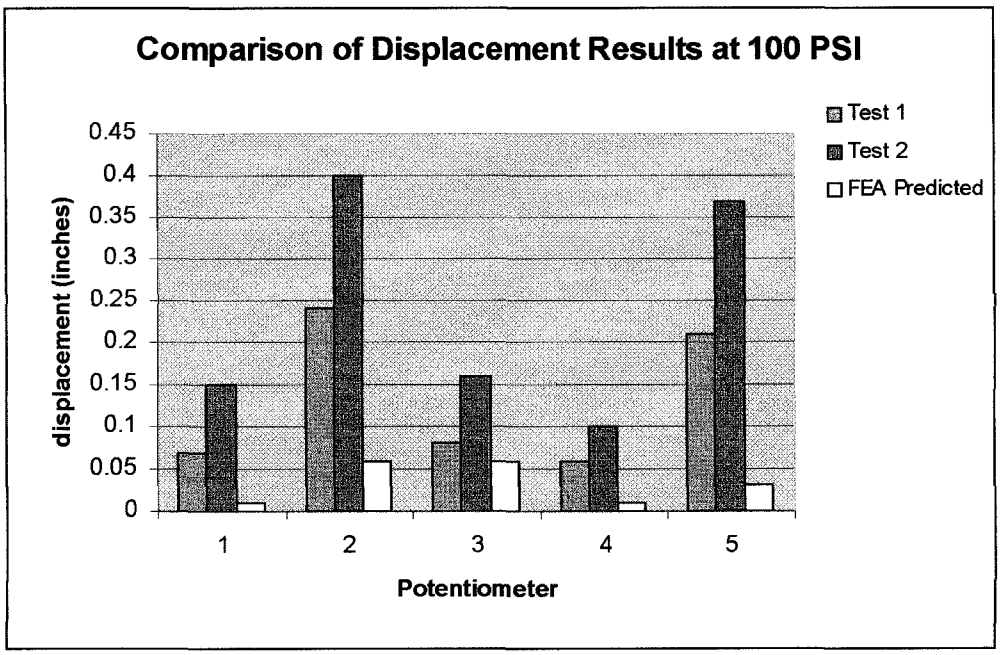

Figure AVI-7 Comparison of Displacement Results at 100 PSI

COMPARISON OF RESULTS-STRAIN

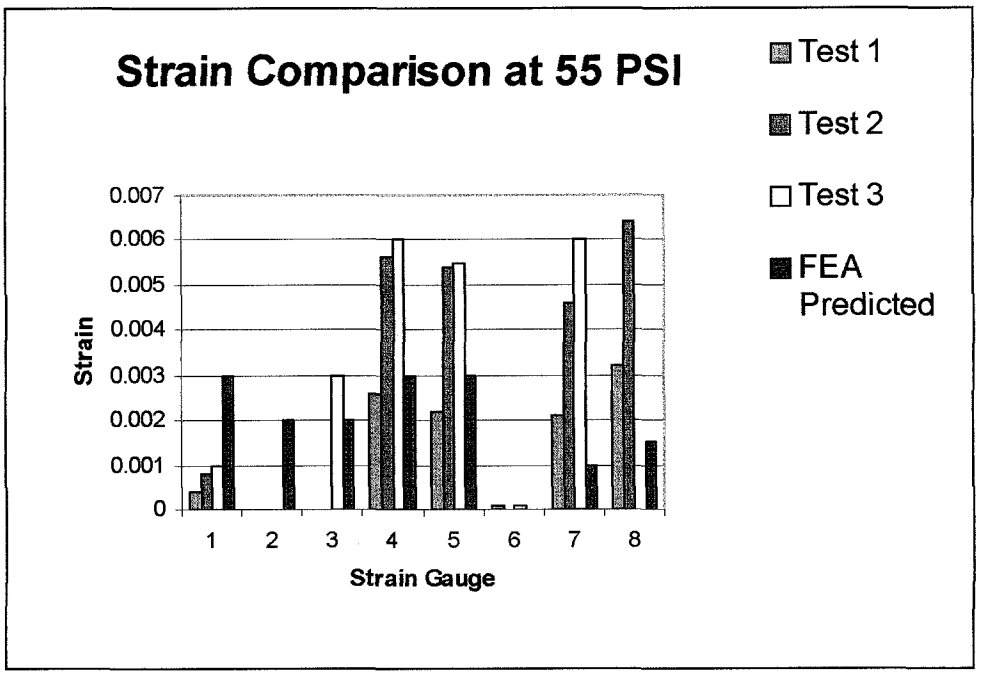

Figure AVI-8 Comparison of Strain Results at 55 PSI

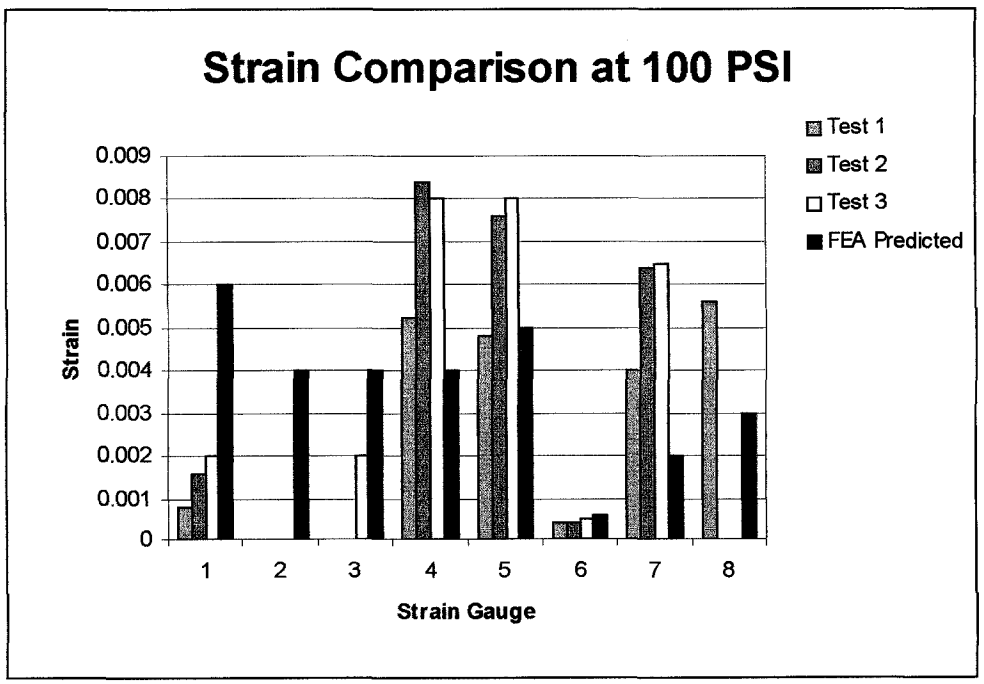

Figure AVI-9 Comparison of Strain Results at 100 PSI

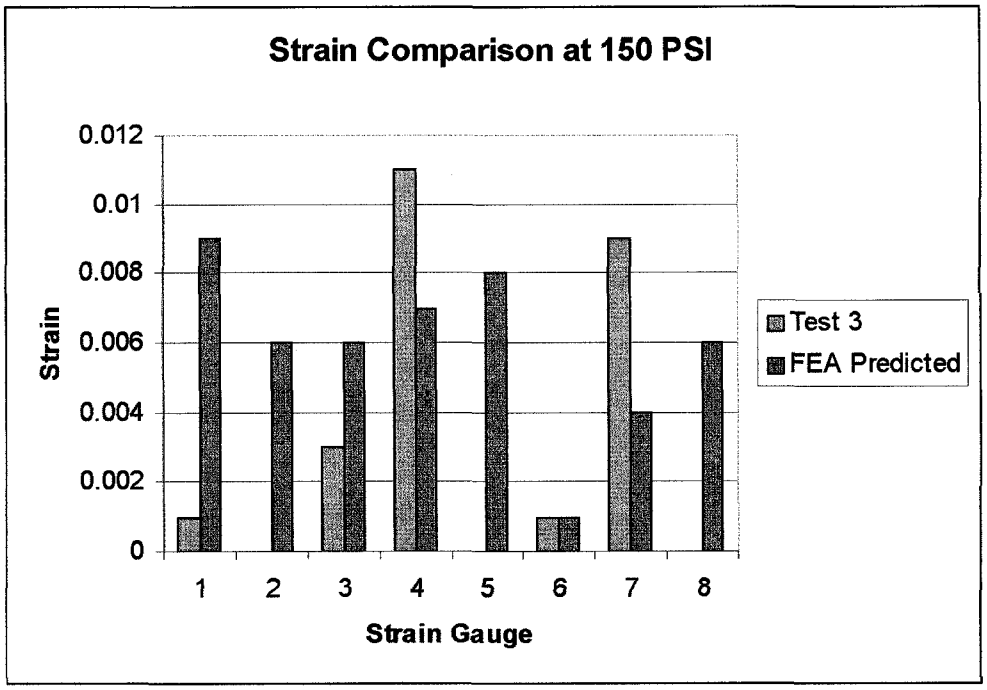

Figure AVI-10 Comparison of Strain Results at 150 PSI

Comparison of Reference Strain

Gauge	Test 1	Test 2	Test 3
1	-0.000966	-0.00046	-0.00016
2	nil	nil	nil
3	-0.020348	-0.01506	0.00448
4	-0.004071	-0.00161	-0.00152
5	0.00176	0.0008	0.000405
6	-0.001386	-0.00138	-0.00135
7	-0.001435	-0.00062	-0.00055
8	-0.002011	-0.00128	nil

Table AVI-1 Comparison of Reference Strains in Prototype 2 Testing

APPENDIX VII

ANALYSIS OF RESULTS FOR PROTOTYPE 3

STRAIN RESULTS

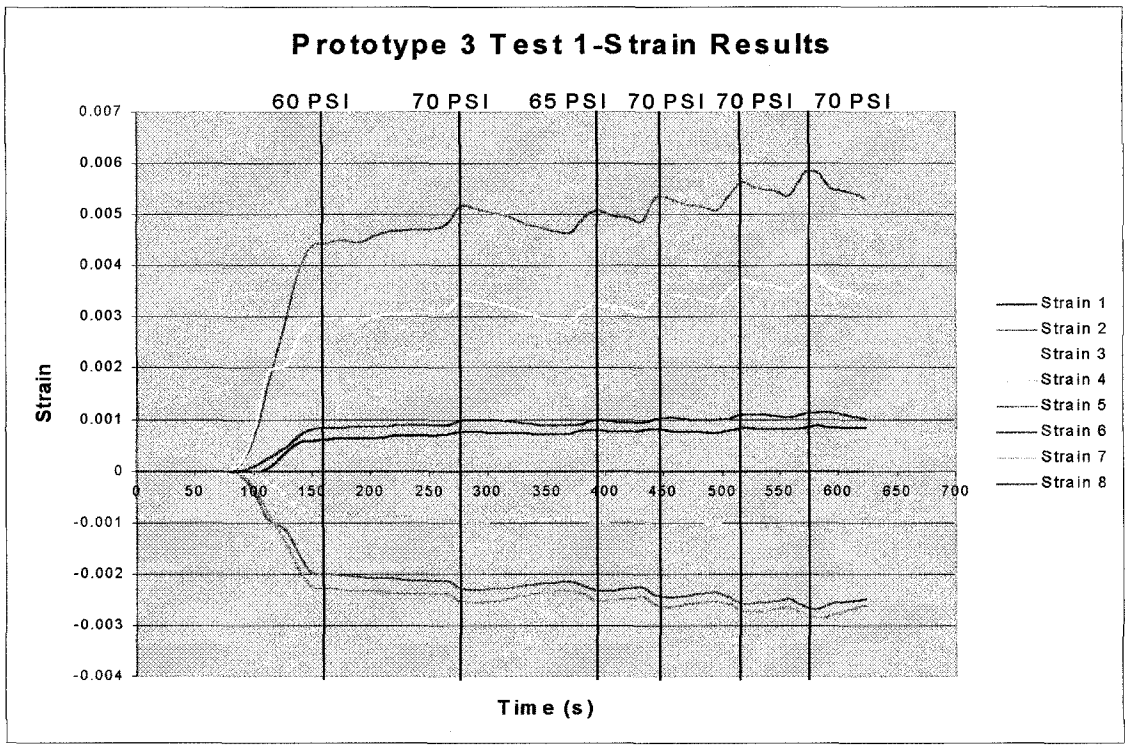

Figure AVII-1 Strain Results for Pressure Test 1

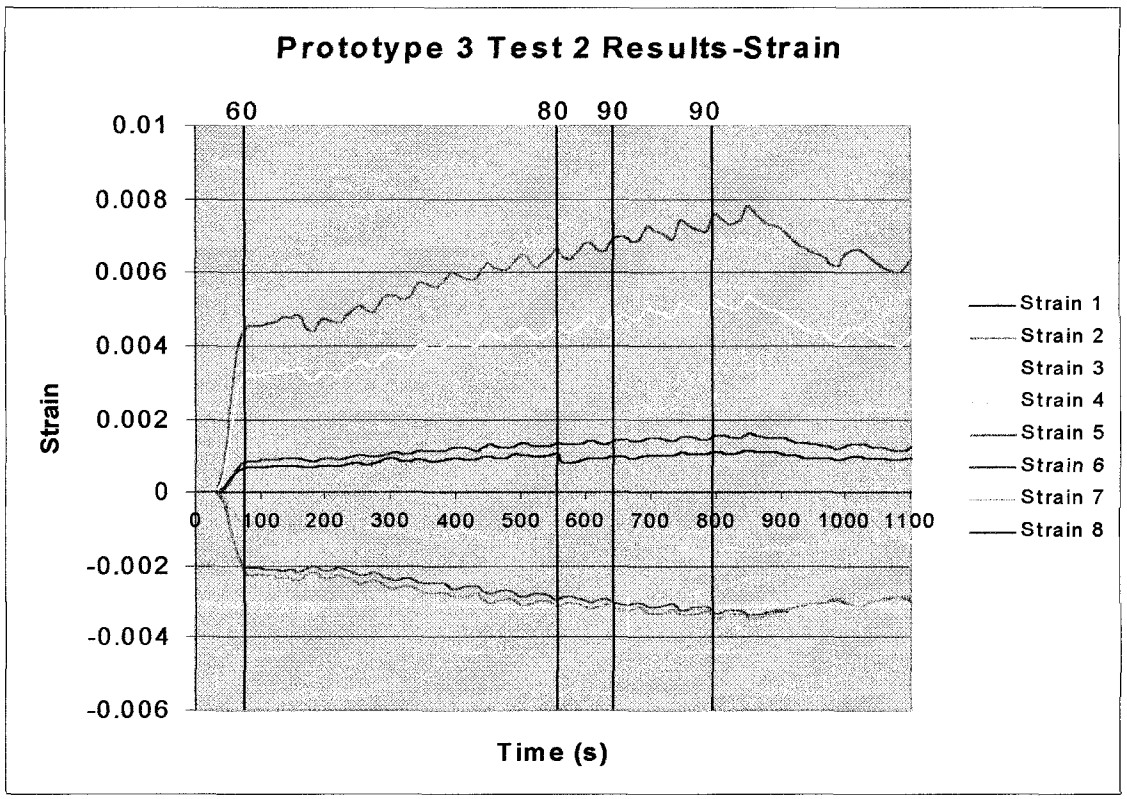

Figure AVII-2 Strain Results for Pressure Test 2

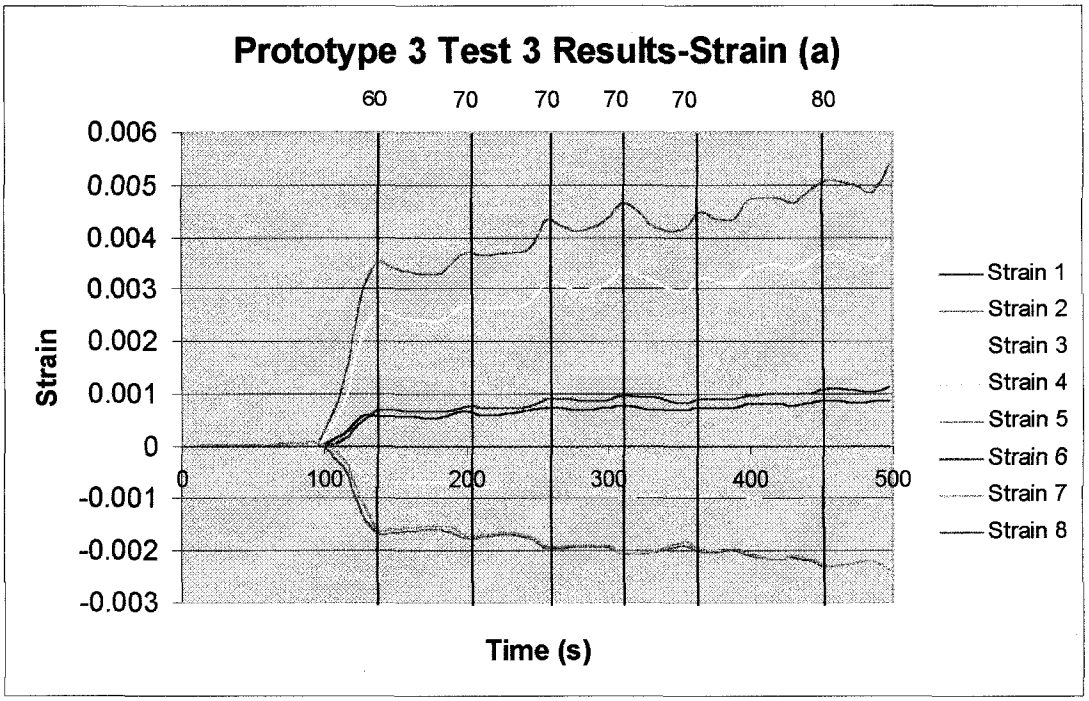

(a)

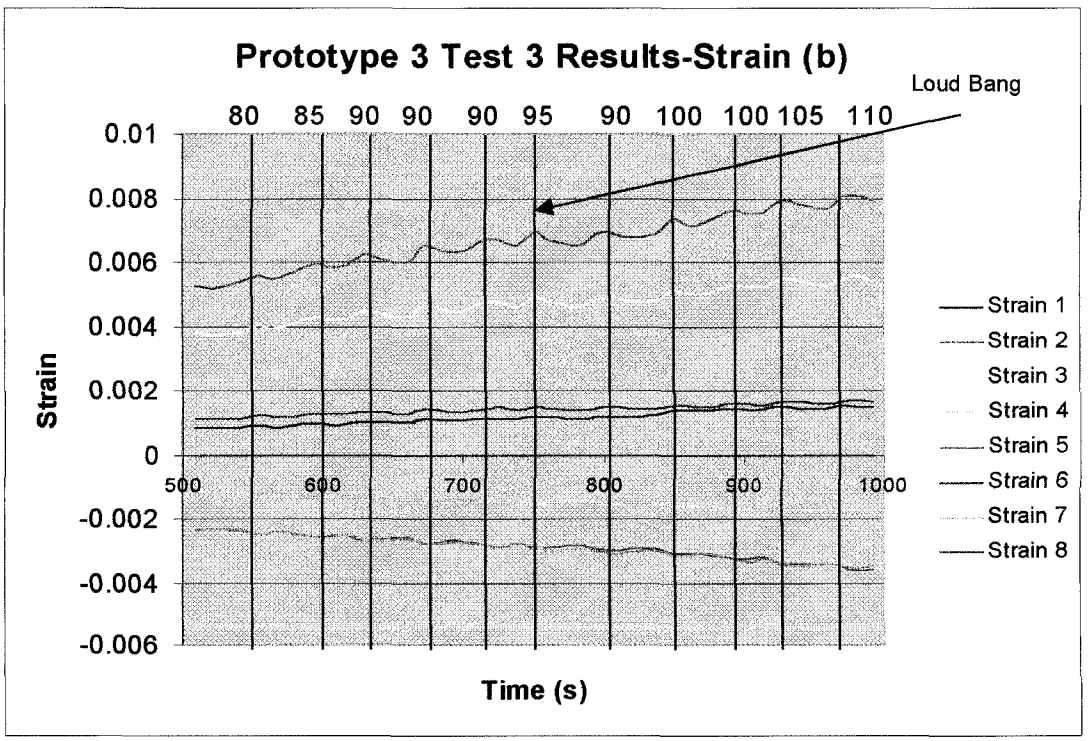

(b)

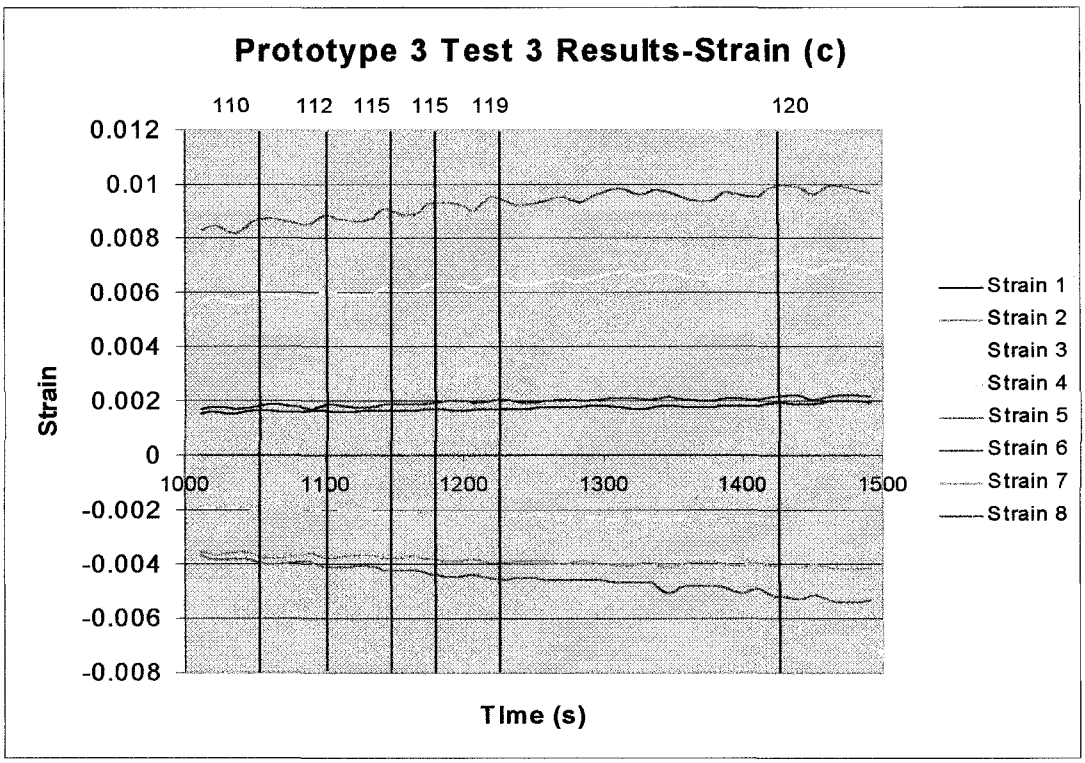

(c)

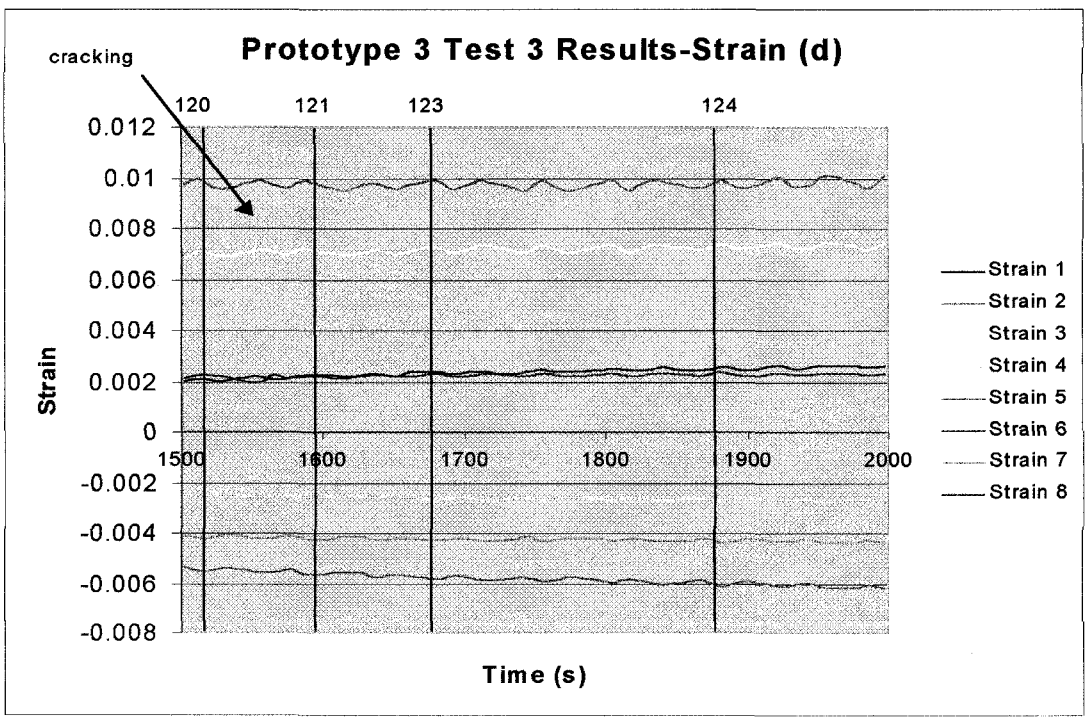

(d)

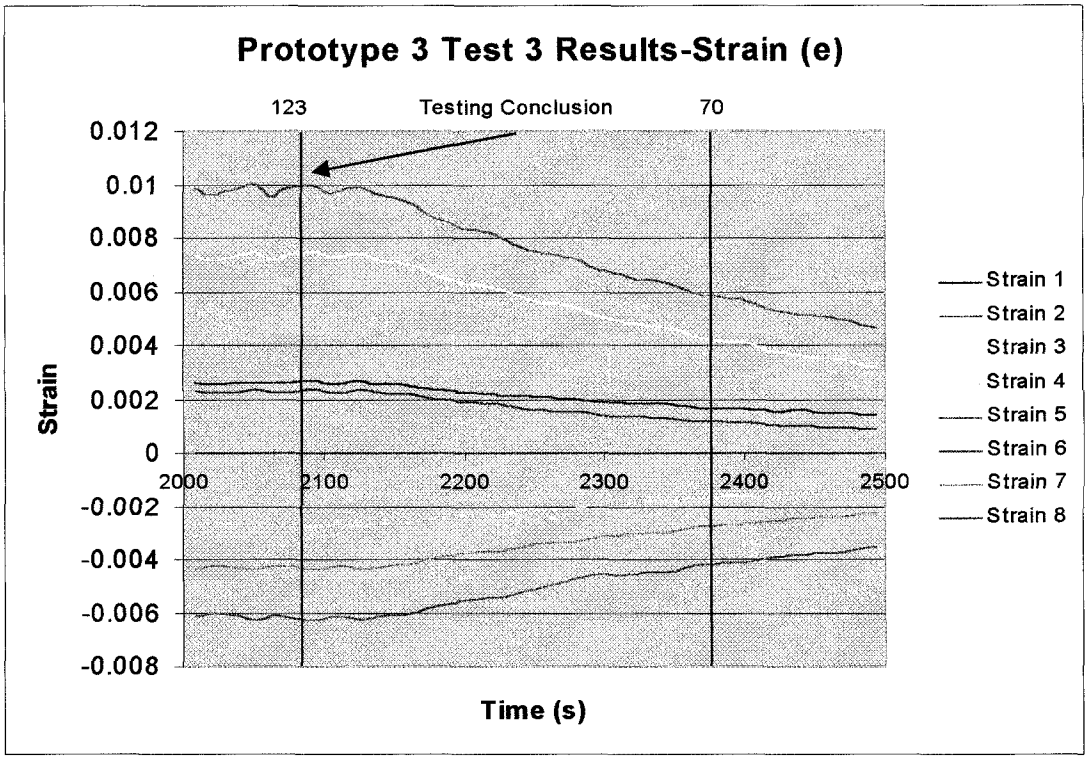

(e)

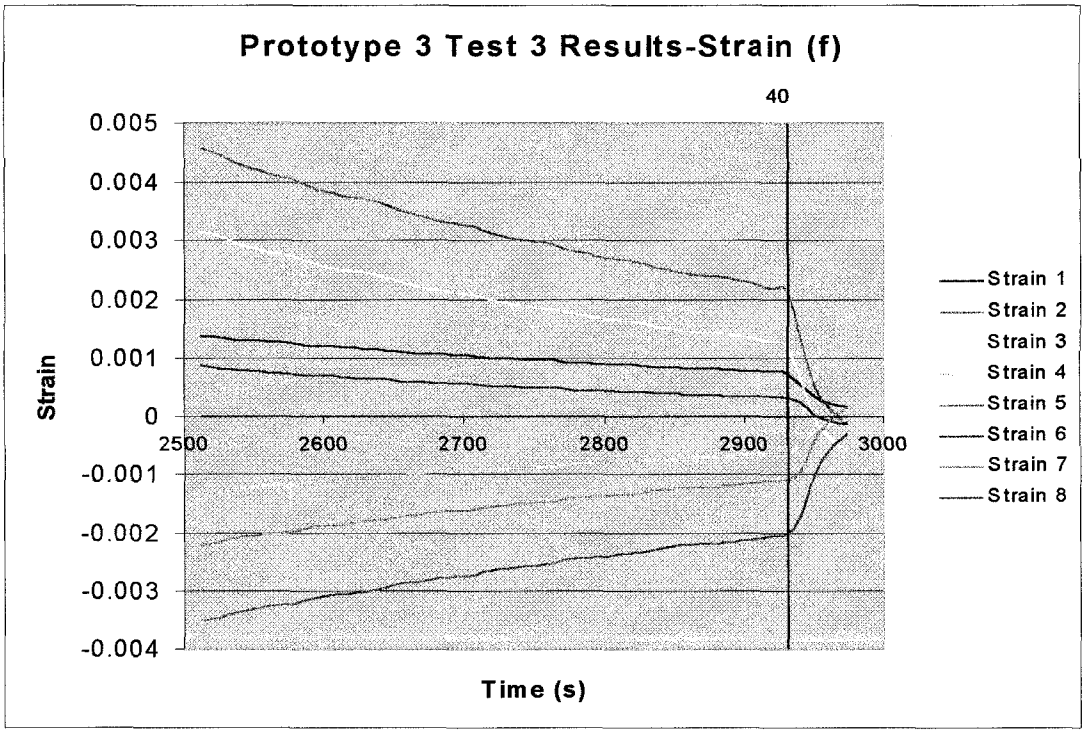

(f)

Figure AVII-3 (a)-(f) Strain Results for Pressure Test 2
(numbers on top of graphs represent pressure in PSI)

COMPARISONS OF RESULTS-STRAIN

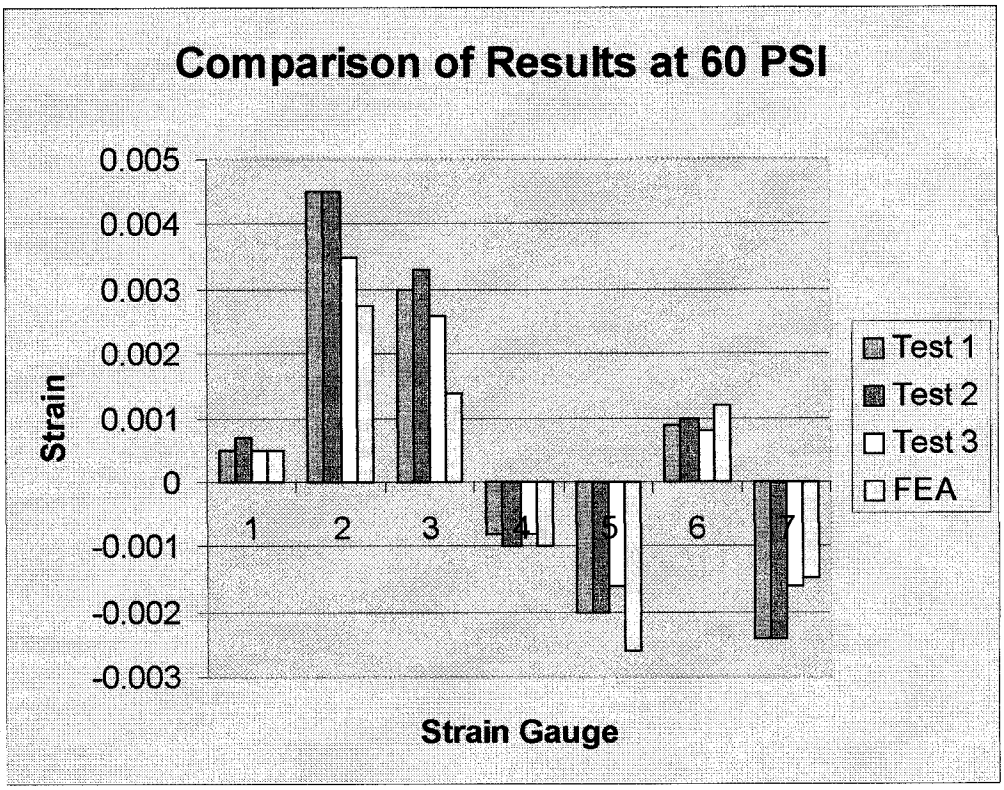

Figure AVII-4 Comparison of Strain Results at 60 PSI

Comparison at 60 PSI-Strain

Gauge	Test 1	Test 2	Test 3	FEA
1	0.0005	0.0007	0.0005	0.0005
2	0.0045	0.0045	0.0035	0.00275
3	0.003	0.0033	0.0026	0.00139
4	-0.0008	-0.001	-0.0008	-0.001
5	-0.002	-0.002	-0.0016	-0.0026
6	0.0009	0.001	0.0008	0.0012
7	-0.0024	-0.0024	-0.0016	-0.0015

Table AVII-1 Comparison of Results at 60 PSI

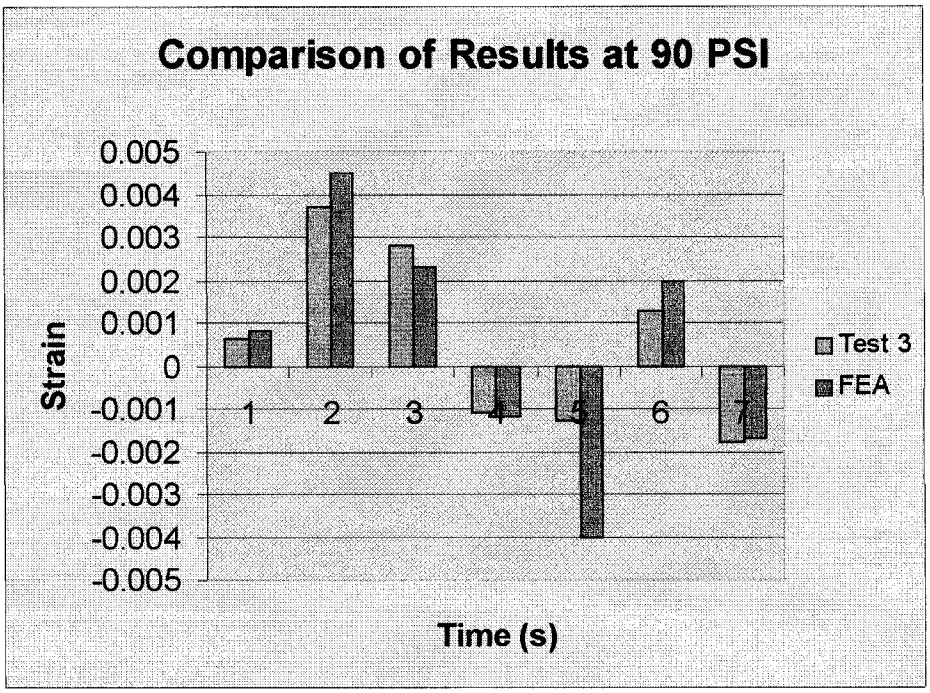

Figure AVII-5 Comparison of Results at 90 PSI

Comparison at 90 PSI-Strain

Gauge	Test 3	FEA
1	0.00062	0.0008
2	0.0037	0.0045
3	0.0028	0.0023
4	-0.0011	-0.0012
5	-0.0013	-0.004
6	0.0013	0.002
7	-0.0018	-0.0017

Note: Accurate comparison could not be performed on data from test 2 due to pressure gauge "spiking" problem.

Table AVII-2 Comparison of Results at 90 PSI

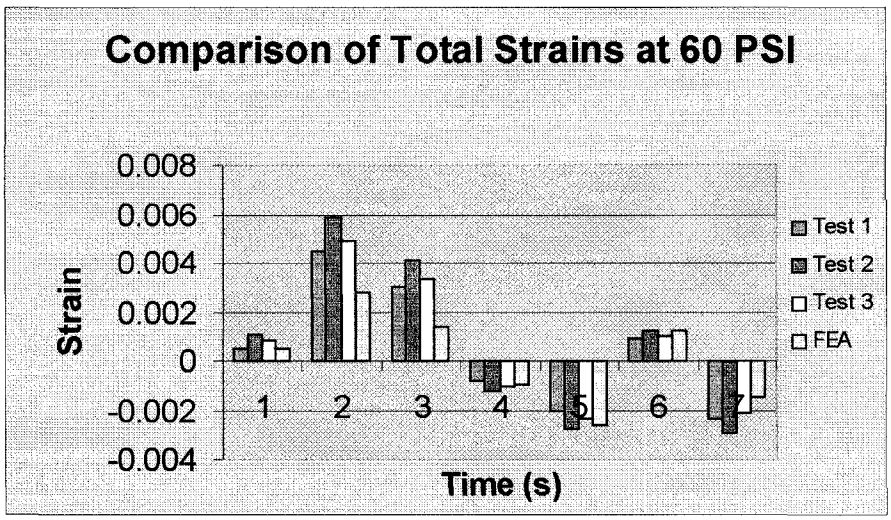

Figure AVII-6 Comparison of total strains at 60 PSI
(Strains referenced from original strain in gauge prior to pressure testing)

Comparison at 60 PSI-Total Strain

Gauge	Test 1	Test 2	Test 3	FEA
1	0.0005	0.00105	0.00085	0.0005
2	0.0045	0.0059	0.0049	0.00275
3	0.003	0.00408	0.00338	0.00139
4	-0.0008	-0.00123	-0.00103	-0.001
5	-0.002	-0.00275	-0.00235	-0.0026
6	0.0009	0.0012	0.001	0.0012
7	-0.0024	-0.00294	-0.00214	-0.0015

Table AVII-3 Comparison of Total Strains at 60 PSI

Reference Starting Strain

Gauge	Test 1	Test 2	Test 3	Load Condition
1	-0.00114	-0.00133	-0.00098	Tensile
2	-0.00196	-0.00172	-0.00032	Tensile
3	-0.0013	-0.00125	-0.00047	Tensile
4	-0.0009	-0.00099	-0.00122	Compressive
5	-0.00176	-0.00201	-0.00276	Compressive
6	-0.00106	-0.00103	-0.00083	Tensile
7	-0.00165	-0.00198	-0.00252	Compressive

Table AVII-4 Reference Starting Strains for Each Pressure Test

APPENDIX VIII

PROPOSED "T" TESTER

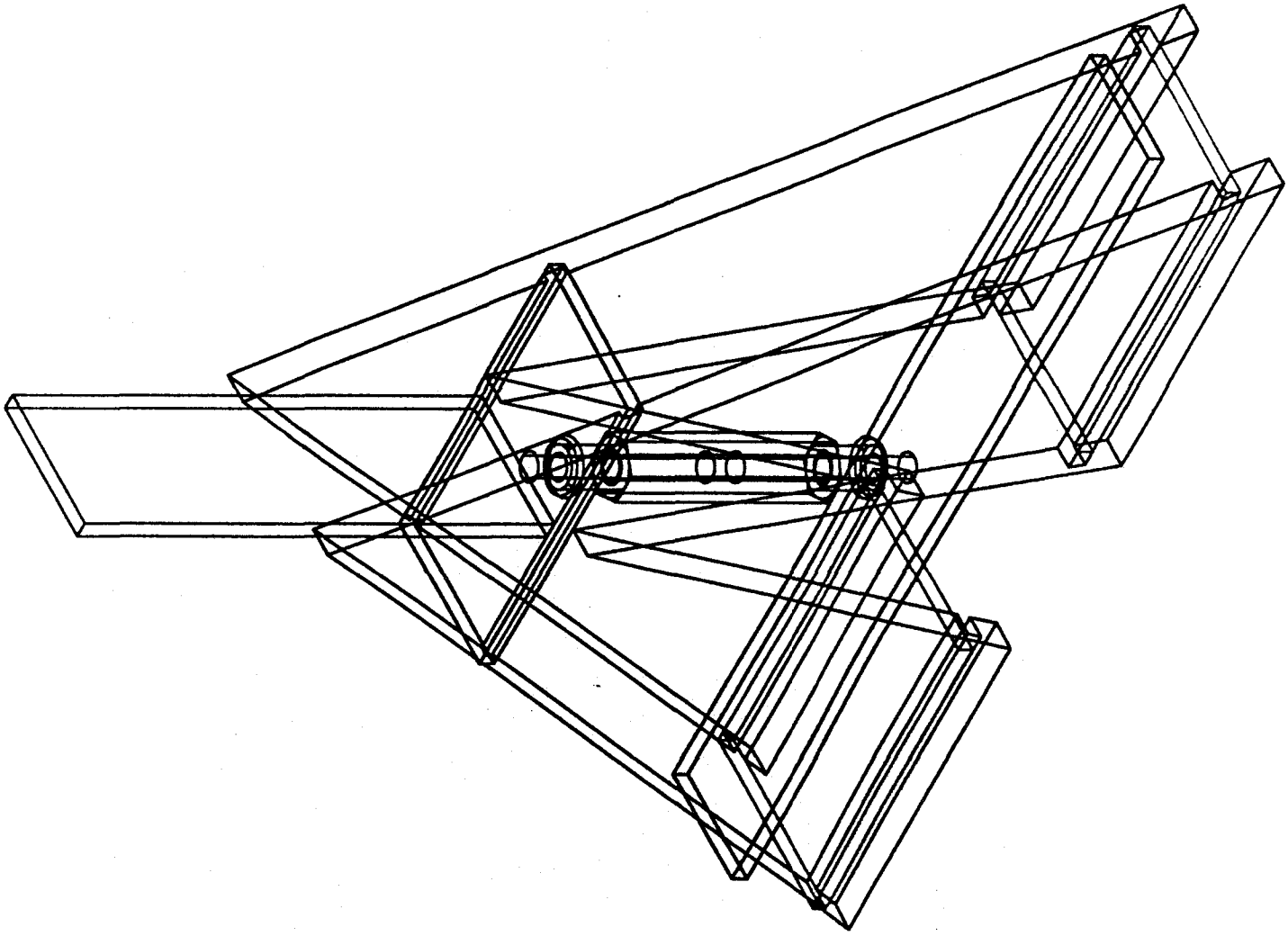

2 ONLY
STEEL

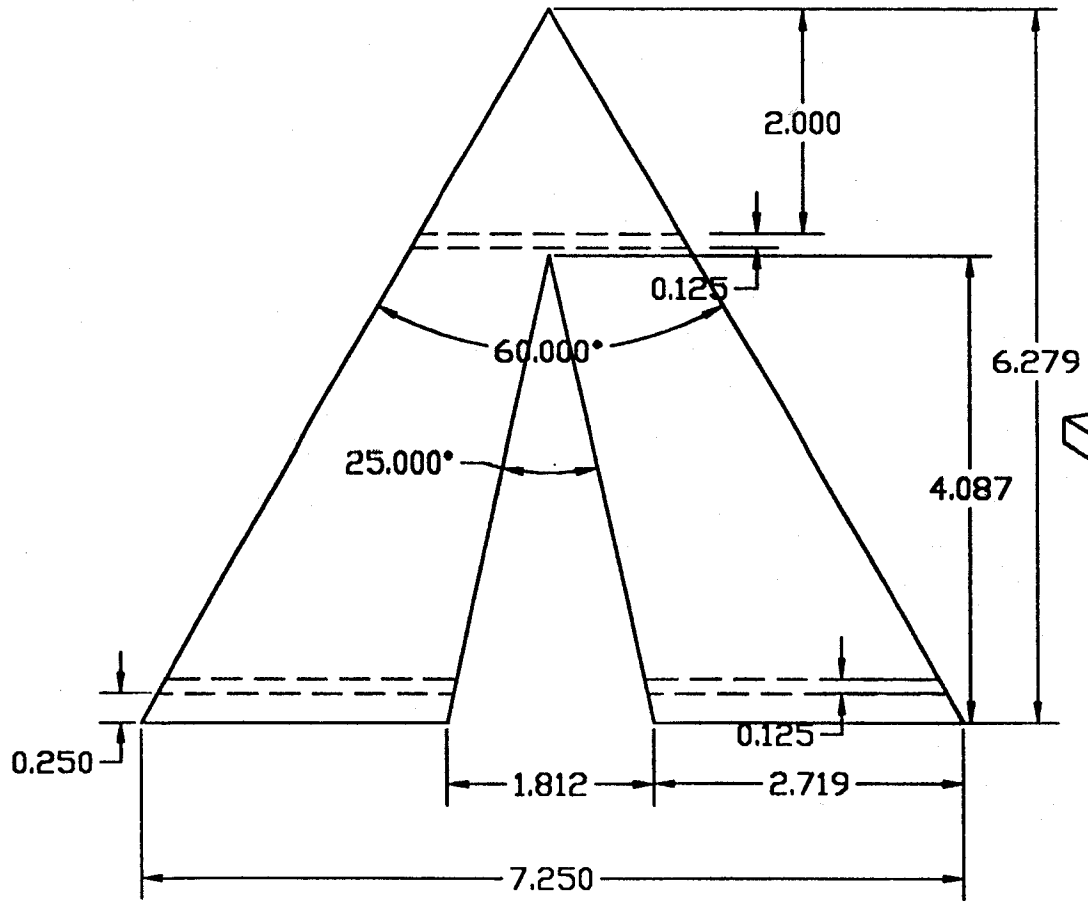

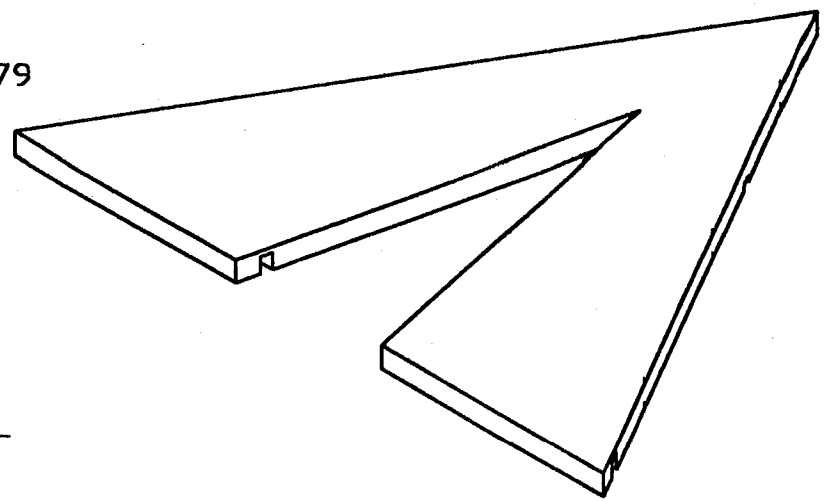

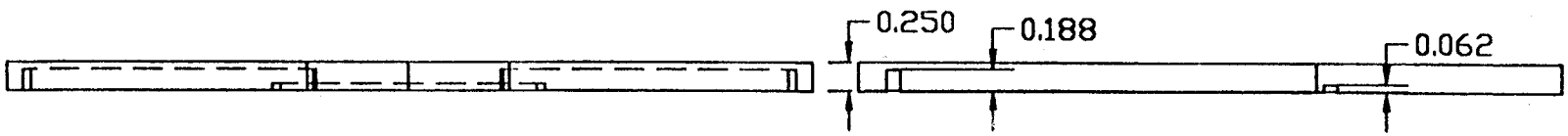

APPENDIX IX

WHEAT STONE BRIDGE CIRCUIT FUNDAMENTALS

Wheatstone Bridge Circuit Fundamentals

Sir Charles Wheatstone (1802-1875), an English scientist, discovered a method of accurately measuring changes in resistance in 1842 [16]. The bridge circuit he developed for the measurement of resistance became known as the Wheatstone bridge. His circuit is useful, for both the determination of the absolute value of resistance, in addition to the measurement of changes in resistance.

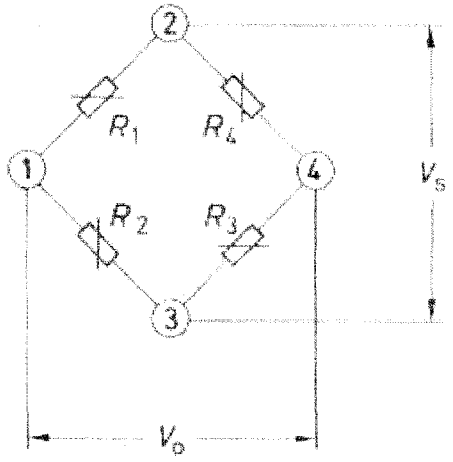

Figure 32 Schematic of Wheatstone Bridge

The principles of the Wheatstone bridge, illustrated in Figure 32, are based largely on the relationship between the supply voltage, V_s, between points 2 and 3 and the output

$$V_1 = \frac{R_1}{R_1 + R_2}$$

voltage, V_o, between points 1 and 4. With a voltage supplied to the circuit, the partial voltage across resistor 1, R_1, is a product of the supply voltage multiplied by the ratio of resistance of R_1 over the total resistance of the arm.

If the partial voltage is similarity calculated across resistor 4, R_4, the difference between the two partial voltages is:

$$V_o = V_s\left(\frac{R_1}{R_1+R_2} - \frac{R_4}{R_3+R_4}\right)$$

If the values of resistance are all equal, the bridge is perfectly balanced, $V_0=0$. Changing the resistance in any one of the resistors, result in a measurable output voltage from the bridge circuit.